A MULTI-FIDELITY FRAMEWORK FOR PHYSICS BASED ROTOR BLADE SIMULATION AND OPTIMIZATION

A Dissertation
Presented to
The Academic Faculty

by

Kyle Brian Collins

In Partial Fulfillment
of the Requirements for the Degree
Doctor of Philosophy in the
School of Aerospace Engineering

Georgia Institute of Technology
December 2008

A MULTI-FIDELITY FRAMEWORK FOR PHYSICS BASED ROTOR BLADE SIMULATION AND OPTIMIZATION

Approved by:

Dr. Dimitri Mavris, Co Advisor
School of Aerospace Engineering
Georgia Institute of Technology

Dr. Lakshmi Sankar, Co Advisor
School of Aerospace Engineering
Georgia Institute of Technology

Dr. Daniel P. Schrage
School of Aerospace Engineering
Georgia Institute of Technology

Dr. Kenneth S. Brentner
Department of Aerospace Engineering
The Pennsylvania State University

Dr. Mark Costello
School of Aerospace Engineering
Georgia Institute of Technology

Date Approved:

Acknowledgements

This project was funded in part by the U.S. Army Aviation and Missile Research, Development and Engineering Center (AMRDEC) under Technology Investment Agreement W911W6-05-2-0003, entitled Rotorcraft Research and Innovation, with the Center for Rotorcraft Innovation (CRI). I would like to acknowledge that this research and development was accomplished with the support and guidance of the National Rotorcraft Technology Center (NRTC) and the Aviation Applied Technology Directorate (AATD). The views and conclusions contained in this document are those of the authors and should not be interpreted as representing the official policies, either expressed or implied, of the AMRDEC or the U.S. Government.

Finally, I finished. It was not on my own though, I can tell you that. I wish to thank God through whom all of us "live and move and have our being"$_{\text{Acts 17:28}}$. He is my rock and foundation. I could not live without my wife, Jen who I know loves me and has always encouraged me in my research here and believed in me for everything I've ever set my mind to do. Next, my Mom and Dad have always encouraged me to do my best and God's rich blessings through them have given me the resources needed to achieve the things I have.

Academically, I want to thank my advisors Dr. Dimitri Mavris and Dr. Lakshmi Sankar for giving me the opportunities to get this far. Thanks also to Dr. Daniel Schrage for acting as an unstated co-advisor and his assistance on many projects. My other committee members Dr. Mark Costello from Ga. Tech and Dr. Kenneth Brentner from PSU have provided valuable feedback. I would never have been able to figure out WOPWOP if it weren't for the patience and willingness to help of Leonard "Len" Lopes from PSU. He and his fellow graduate students James Erwin and Chris Hennes really helped a lot. I'm thankful that Dr. Brentner for encouraging them to give me some assistance but let me figure it out on my own as well. I certainly learned more from that

process. I also have to thank the other professors and researchers here who have helped me in some way or another: Dr. Bruce Ahn, Dr. Ralph Latham, Dr. Jimmy Tai, Dr. Robert Lowey, Dr. Neal Weston, and Dr. Dewey Hodges.

To my classmates who have made this whole process fun every day: Jeremy Bain, Simon Briceno, Bjorn Cole, Stephane Dufresne, Mandy Goltsch, Dongwook Lim, Alex Moodie, Taewoo Nam, Janel Nixon, Leon Phan, Nischint Rajmohan, Reza Rezvani, Troy Schank, Marcus Smith, Spam, Woong Je Sung, Henry Won, and Jack Zentner to name a few; some of who are now “Doctors” themselves.

In industry I must thank Dr. Stephen Makinen and T. Alan Egolf from Sikorsky as well as Drs. Ram Janakiram and Hormoz Tadghighi from Boeing. And I have to mention Joe Cosgrove and the rest of the Piasecki Family. At NASA, a big thanks to Georgia Tech Skydiving Club Alum David “Doug” Boyd for helping me figure WOPWOP out.

Thanks to all of the above and the many family members, friends, and colleagues not mentioned for your advice, assistance, and friendship.

God Bless and Blue Skies!

Table of Contents

List of Tables

List of Figures

Executive Summary

New helicopter rotor designs are desired that offer increased efficiency, reduced vibration, and reduced noise. This design problem is multidisciplinary, requiring knowledge of structural dynamics, aerodynamics, and aeroacoustics. Rotor optimization requires achieving multiple, often conflicting objectives. This means there is no longer a single optimum but rather an optimal trade off space known as the Pareto Frontier. Rotor Designers in industry need methods that allow them to use the most accurate simulation tools available to search for these optimal designs.

Computer based rotor analysis and optimization have been advanced by the development of industry standard codes known as "comprehensive" rotorcraft analysis tools. These tools typically use table look-up aerodynamics, simplified inflow models and perform aeroelastic analysis using Computational Structural Dynamics (CSD). Due to the simplified aerodynamics, most design studies are performed varying structural related design variables like sectional mass and stiffness. The optimization of shape related variables in forward flight using these tools is complicated and results are viewed with skepticism because rotor blade loads are not accurately predicted. The most accurate methods of rotor simulation utilize Computational Fluid Dynamics (CFD) but have historically been considered too computationally intensive to be used in computer based optimization, where numerous simulations are required.

An approach is needed where high fidelity CFD rotor analysis can be utilized in a shape variable optimization problem with multiple objectives. Any approach should be capable of working in forward flight in addition to hover. An alternative is proposed and founded on the idea that efficient hybrid CFD methods of rotor analysis are ready to be used in preliminary design. In addition, the proposed approach recognizes the usefulness of lower fidelity physics based analysis and surrogate modeling. Together, they are used with high fidelity analysis in an intelligent process of surrogate model building of

parameters in the high fidelity domain. Closing the loop between high and low fidelity analysis is a key aspect of the proposed approach. This is done by using information from higher fidelity analysis to improve predictions made with lower fidelity models.

This thesis documents the development of automated low and high fidelity physics based rotor simulation frameworks. The low fidelity framework uses a comprehensive code with simplified aerodynamics. The high fidelity model uses a parallel processor capable CFD/CSD methodology. Both low and high fidelity frameworks include an aeroacoustic simulation for prediction of noise. A synergistic process is developed that uses both the low and high fidelity frameworks together to build approximate models of important high fidelity metrics as functions of certain design variables.

To test the process, a 4-bladed hingeless rotor model is used as a baseline. The design variables investigated include tip geometry and spanwise twist distribution. Approximation models are built for metrics related to rotor efficiency and vibration using the results from 60+ high fidelity (CFD/CSD) experiments and 400+ low fidelity experiments. Optimization using the approximation models found the Pareto Frontier anchor points, or the design having maximum rotor efficiency and the design having minimum vibration. Various Pareto generation methods are used to find designs on the frontier between these two anchor designs. When tested in the high fidelity framework, the Pareto anchor designs are shown to be very good designs when compared with other designs from the high fidelity database. This provides evidence that the process proposed has merit. Ultimately, this process can be utilized by industry rotor designers with their existing tools to bring high fidelity analysis into the preliminary design stage of rotors.

In conclusion, the methods developed and documented in this thesis have made several novel contributions. First, an automated high fidelity CFD based forward flight simulation framework has been built for use in preliminary design optimization. The framework was built around an integrated, parallel processor capable CFD/CSD/AA

process. Second, a novel method of building approximate models of high fidelity parameters has been developed. The method uses a combination of low and high fidelity results and combines Design of Experiments, statistical effects analysis, and aspects of approximation model management. And third, the determination of rotor blade shape variables through optimization using CFD based analysis in forward flight has been performed. This was done using the high fidelity CFD/CSD/AA framework and method mentioned above. While the low and high fidelity predictions methods used in the work still have inaccuracies that can affect the absolute levels of the results, a framework has been successfully developed and demonstrated that allows for an efficient process to improve rotor blade designs in terms of a selected choice of objective function(s). Using engineering judgment, this methodology could be applied today to investigate opportunities to improve existing designs. With improvements in the low and high fidelity prediction components that will certainly occur, this framework could become a powerful tool for future rotorcraft design work.

Chapter 1

Introduction

1.1 Motivation

Rotary wing vehicles such as helicopters are very complicated machines and operate in a very complex aerodynamic and structural environment as shown in Figure 1-1. The analysis of rotorcraft with conventional rotors responsible for providing lift, propulsion, and control is therefore complex and multidisciplinary in nature. Objectives of the proposed research include the development of new rotary wing design methods and application of these methods to rotor blade preliminary design.

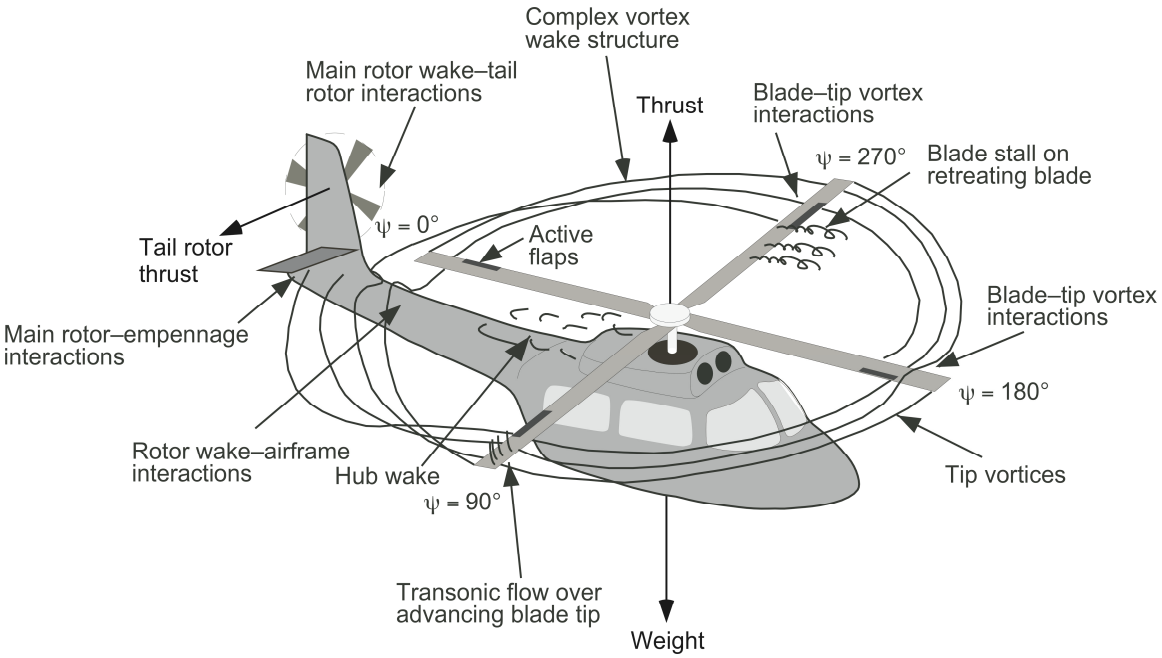

Figure 1-1: Complex Environment of Rotorcraft

(Image Courtesy of J. G. Leishman and Cambridge University Press, reprinted with permission)

The helicopter is an amazing machine that is responsible for saving lives on a daily basis. The capability to land and take off vertically is paramount to its success.

However, the helicopter does have many limitations that researchers are constantly trying to overcome.

Among the limitations, the maximum forward speed is seriously limited. When in forward motion, the blades of the helicopter are moving into the direction of flight on one side and away from the direction of flight on the other. In high forward speed flight, air velocities at the blade tip on what is called the "advancing" side can approach the speed of sound, causing shock waves to form and increased pressure drag. On the "retreating" side of the helicopter, the air velocities are lower since the forward speed is subtracted from the blade's rotational speed, leading to blade stall. These two phenomena limit a helicopter's speed. Another issue is the high power required by the rotor in flight, as compared to a fixed wing aircraft results in a less efficient system, limiting the range of helicopters. Furthermore, another concern is vibration because the helicopter's rotor is a large rotating structure. Finally, the high acoustic levels of the helicopter limit its civil operations. This makes it easily detectable from a long distance and thus is a major concern for the military.

To address these challenges, helicopter manufactures and research institutions are now working to develop new technologies to allow the helicopter to travel faster, farther, be quieter doing it, and vibrate less. These efforts have involved better engines, better main rotor systems, more streamlined fuselages, and more efficient tail rotor systems. Acknowledging that all helicopter subsystems are important, the work presented here focuses on the main rotor system only, considering it the most important subsystem of the helicopter. Varying the rotor blade shape, structural properties, and airfoil shapes enables the designer to expand the limits of previous designs; improving the performance, noise, vibration, weight, cost, etc. of the vehicle. This process is extremely complex as there are many nonlinear constraints that must be satisfied, like stresses in components during flight, aeroelastic stability, autorotation capability, and many others.

In pursuit of main rotor system improvements, researchers have turned to computer based simulation models and advanced numerical optimization techniques. This fact is stressed in two recent surveys of rotorcraft optimization efforts [1, 2]. For example, the rotor blades of an existing helicopter could be enhanced through an optimization process as shown in Figure 1-2. In this approach, designers change some design variables under their control to make improvements to the baseline (or original) with respect to a number of objectives such as noise, efficiency, or vibration.

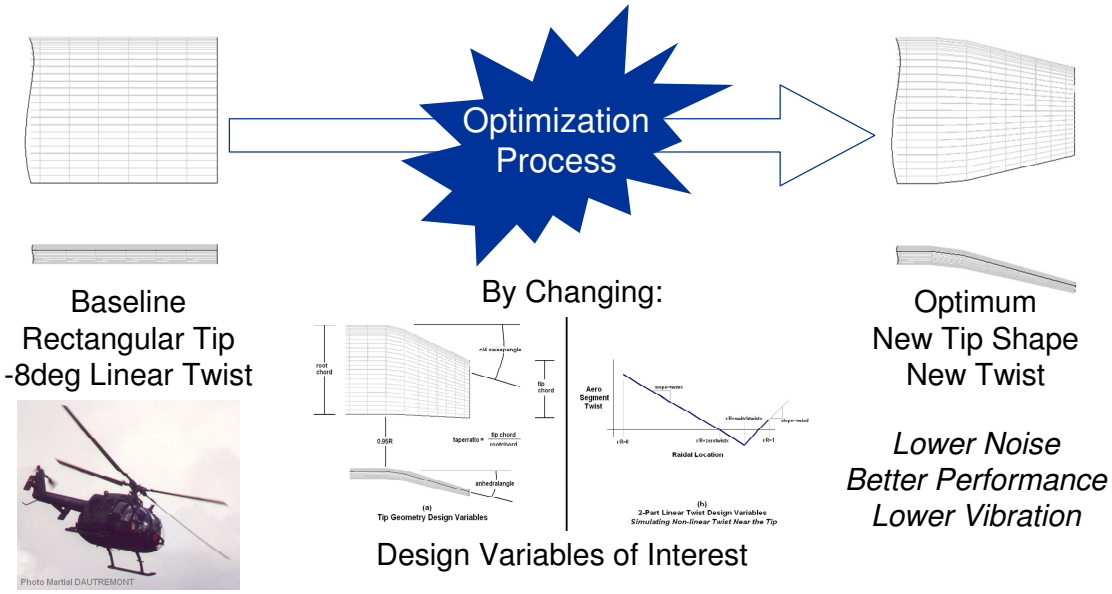

Figure 1-2: Rotor Blade Optimization Process

For practical application, numerical simulation of helicopter rotors in flight always requires the use of some type of simplifying assumptions. In order to fully understand the impact of any newly proposed design concepts, most of the simplifying assumptions must be examined in the preliminary design process stage by replacing them with higher fidelity rotor analysis techniques.

The ultimate goal of most computer based analysis tools is that one day they will find use in the preliminary design of a new or improved rotor system. However, since

preliminary design requires the analysis of numerous design perturbations, any process employed that uses a high fidelity, first principles approach must also be efficient in terms of CPU time to be even considered practical. The techniques proposed here will thus focus on the creation of such a practical rotor preliminary design environment that uses high fidelity analysis for use in advanced design studies and optimization. Therefore, the very essence of the research presented here is to clearly demonstrate the practicality of such techniques that could easily be employed by preliminary designers to arrive at advanced rotor blades that satisfy the required aerodynamic loads, lower noise level, and reduced vibratory airloads.

1.2 Rotary Wing Simulation and Design Optimization Today

The successful design of a helicopter is attributed to its achievement of its mission performance goals and yet has an acceptable vibration level and small noise footprint. In the past, this was done by the various disciplines in a separate fashion. First, the planform of the rotor is designed from an aerodynamic perspective. Second, an aeroelastic analysis is performed on the configuration to check for aeroelastic stability and acceptable vibratory loads. Finally, an aeroacoustic analysis is performed to determine the noise. This process makes it difficult to perform optimization because a large number of tools are used without being integrated into one system.

The fact that integration of the disciplines is key to more accurately representing the physics involved led to the development of "comprehensive" rotorcraft analysis codes [3]. In his paper, Kunz describes first, second, and future third generation rotorcraft comprehensive analysis codes. The current state-of-the-art second generation tools allow the user to build generic models using primitive elements. More specifically, these second generation tools have the capability to perform a computational structural dynamics (CSD) simulation of rotor systems. In addition, most comprehensive rotorcraft analysis tools have some internal means of calculating the aerodynamic loads using 2-D

table look-up coupled with a simple inflow model. Inflow models available range from 1st order uniform to prescribed and free wake types. In addition, empirical corrections can be applied for unsteady aerodynamics, sweep effects, tip loss, or yawed flow. Even still, blade segment airloads versus azimuth location are very difficult to predict. This is evident in Figure 1-3 where various inflow models are used within a comprehensive rotorcraft analysis tool to predict the airloads of a rotor for which experimental data [4] is available.

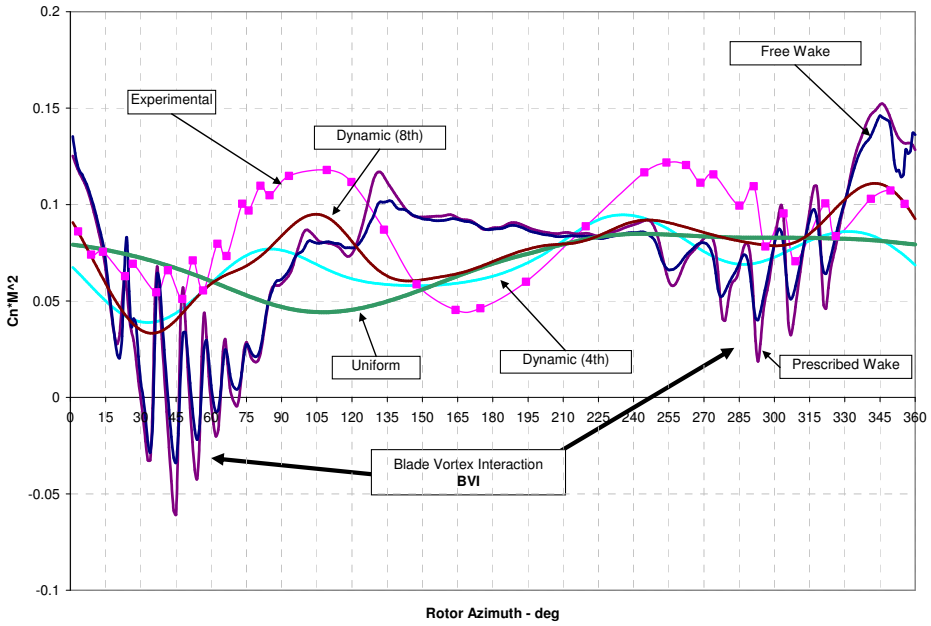

Figure 1-3: Comparison of Blade Airloads using Non-CFD based Wake Models[1]

(HART-I Rotor [4], r/R=0.87, 5.3 deg shaft tilt, descent)

The reason for this difficulty is largely due to the complicated nature of the aerodynamics of the helicopter's wake [5]. To capture the effects of the wake, the

[1] Elastic Blade Simulation was performed by author using the Rotorcraft Comprehensive Analysis System (RCAS) developed by the US Army.

prescribed and free wake model is employed inside the comprehensive code. Both employ Prandtl's lifting line theory in a helical fashion more appropriate to the wake of a rotor blade. Prescribed wake models are based on an empirical knowledge of what the wake structure looks like. Free wake models also usually start from a prescribed wake but are allowed to be distorted. To date, the highest simulation fidelity available within a second generation comprehensive analysis code.is a free wake model coupled with an elastic blade representation of the structure in the CSD model.

To get more accuracy, researchers have worked to couple the results of even higher fidelity aerodynamics such as Computational Fluid Dynamics (CFD) with the aeroelastic analysis performed within the CSD [6-9]. Figure 1-4 highlights the prediction capability of loosely coupled CFD/CSD. The result provides the designer with more accurate values for the quantities of interest to the engineer: thrust, torque, blade motion, and radial and azimuthal distribution of aerodynamic loads.

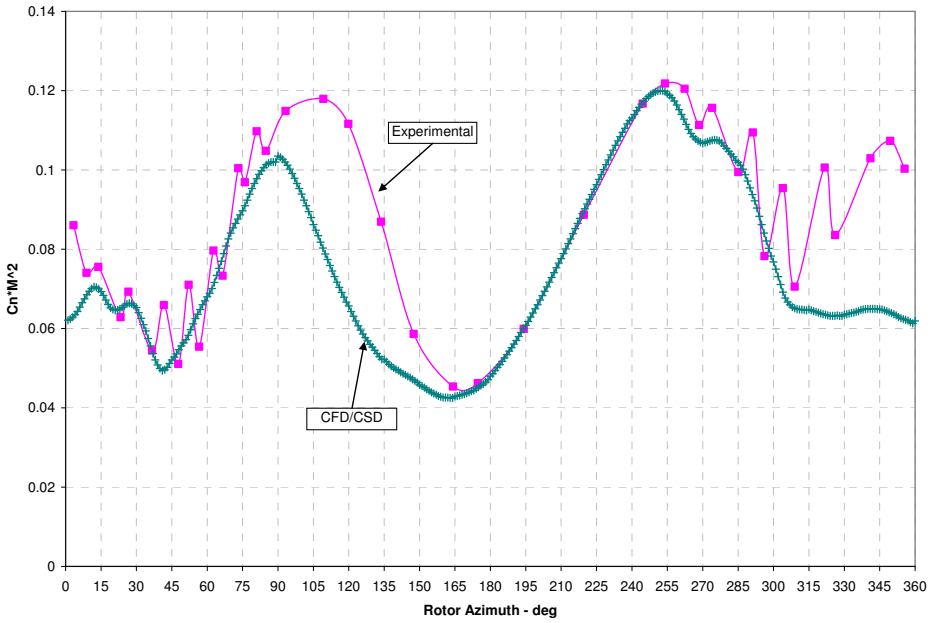

Figure 1-4: Blade Airload Prediction Using Loosely Coupled CFD/CSD[2]

(HART-I Rotor [4], r/R=0.87, 5.3 deg shaft tilt, descent)

Once the rotor airloads are predicted – whether using CFD or non-CFD based aerodynamics – these results along with results for the blade motion can then easily be passed to an aeroacoustics analysis to predict the sound pressure level at any desired observer location or locations. In most cases, the aeroacoustic analysis is capable of taking various forms of input ranging from compact lifting line airloads along the blade to a three dimensional acoustic data surface surrounding the sound source; in this case, the blade. Throughout this thesis, aeroacoustic analysis will be symbolized by the acronym AA which stands for Acoustic Analogy. In section 2.3.6, the differences

[2] Loosely coupled CFD/CSD elastic blade simulation was performed by the author using RCAS coupled to the hybrid Navier-Stokes/free-wake rotorcraft solver GT-Hybrid developed at the Georgia Institute of Technology.

between this and direct computation will be discussed. All aeroacoustic analysis performed in this research has been done using the Acoustic Analogy.

While CFD/CSD is proving to be a viable means of more accurately predicting airloads, its use in design optimization is limited primarily because each computation is very time consuming to run. Also, developing a process to allow design variable changes in an automated fashion requires automatic grid generation for the CFD, which is not trivial. Most rotor optimization studies performed to date have been done with lower fidelity aerodynamics. Even still, these methods have resulted in rotors with improved characteristics [10]. Ad hoc investigations have also been performed using CFD for rotor blade designs with shapes believed to be beneficial [11, 12]. Recently CFD has been utilized in optimization processes [13-15]. The better prediction capability of advanced methods like CFD/CSD is believed to provide the rotor designer with better prediction of future rotor shapes. For this reason, the continued use of advanced aerodynamic tools in optimization is vital to the development of advanced rotors with unique aerodynamic shapes providing lower vibration, increased performance, and lower noise.

1.3 Research Overview

An overview of the research contained in this thesis is given here. The main impetus for this research stems from the basic desire to utilize state-of-the-art high fidelity simulation tools in the design of rotary wing aircraft components such as rotor blades. While the use of high fidelity CFD/CSD/AA analysis is proving to be much better than conventional analysis methods when it comes to more accurately predicting the forces on rotor blades and the noise they make, the use of these tools in design is very limited because they are complicated to use and require long computer run time to get answers. Thus the main focus of this research is on utilizing technologies and developing methods that allow these tools to be more routinely used in the field of design, where numerous candidate designs must be analyzed in a search for a more optimum design.

In addition, it is felt that conventional – let's call them low fidelity – analysis tools can still be useful in design work and should not be completely discarded as we search for ways to bring in higher fidelity analysis. For this reason, this research also uses low and high fidelity analysis tools together, in concert, to find new and improved designs. These two main ideas are captured in the following research questions:

RQ1: What disciplinary analysis elements can be combined to form an efficient high fidelity CFD/CSD/AA simulation for application to rotary wing optimization?

RQ2: In what way can low and high fidelity rotary wing simulations be used together in a process of rotary wing design?

Answering these questions requires an understanding of the state-of-the-art in helicopter rotor simulation combined with an understanding of modern design/optimization tools. In the research presented herein, a combination of low and high fidelity analysis tools are automated within a design framework and shown to be applicable to solving design problems common to the rotorcraft industry.

1.4 Thesis Layout

This thesis is laid out in the following chapters following this introduction. Each chapter begins with a brief overview and ends with a summary. In Chapter 2, a background and review of the literature is given. This begins with a look at the state-of-the-art for rotary wing designs to get a feel for the types of designs that industry is supporting. Chapter 2 also covers various aspects related to concepts of rotary wing simulations as well as concepts in design and optimization. Finally, Chapter 2 shows how optimization techniques have previously been applied to rotary wing design efforts.

In Chapter 3, the objectives of this thesis research are discussed. First, a list of observations related to rotary wing analysis and design is given. This is followed by a

listing of what are felt to be gaps in the current research. These observations and gaps in research focus the reader on the specific research questions this thesis hopes to answer; which of course were discussed briefly in section 1.3. The research questions are followed by a discussion of the overall objectives of this thesis research. Chapter 3 is concluded with a discussion of the enabling technologies and concepts that make the reported research possible and also the challenges related to the application of high fidelity simulation tools to rotary wing design that must be overcome.

In Chapter 4, preliminary methods and results are documented. The preliminary research covers a Design of Experiments and surrogate modeling approach applied to a low fidelity (rigid blade) parametric HART-I rotor simulation environment. Using Monte Carlo Simulation, a compromise optimum is selected and spot checked with higher fidelity tools. The higher fidelity tools used include a CFD hover analysis and an elastic blade CFD/CSD forward flight analysis. In an extension to this preliminary research, more experiments are performed with the low fidelity environment and better surrogated models are built. These improved surrogates are used to pick optimums in every objective of interest (i.e. power required, noise, etc.).

In Chapter 5, a new methodology and results are presented. The low fidelity parametric environment is upgraded with elastic blade modeling. Also, the high fidelity analysis is integrated in a parametric design framework. An initial test of the high fidelity framework is performed on optimums found in Chapter 4. Next, a novel methodology is described for creating surrogate models of high fidelity objectives and constraints using a combination of low and high fidelity results. As a test, this methodology is used to create surrogate models of two important forward flight metrics: rotor efficiency and vibration. These surrogates are then used in three separate processes from the literature to generate designs on the Pareto Frontier. A modification to one of the methods is described and tested as well. Comparisons of how well the four methods perform in finding an even

distribution of designs along the two dimensional “rotor efficiency”/”vibration index” Pareto Frontier are made.

Finally, Chapter 6 gives a conclusion, including key findings. A discussion is given as to how well the research questions and objectives were answered or met, a list of major contributions, and finally, some avenues for future work are mentioned.

1.5 Chapter Summary

The successful design of a helicopter is found in a vehicle which can meet the mission performance goals and yet have an acceptable vibration level and noise footprint. Rotorcraft designers are always looking for ways to improve the design of rotor systems and in particular the blades themselves, but the simple appearance of a rotor blade hides the fact that the design is the result of a complicated process. In the past, this was done by the various disciplines in a separate fashion. First, the planform of the rotor is designed from an aerodynamic perspective. Second, an aeroelastic analysis is performed on the configuration to check for aeroelastic stability and acceptable vibratory loads. Finally, an aeroacoustic analysis is performed to see if the noise is tolerable. This process makes it difficult to create optimized designs because the various tools used are not integrated with one another.

Despite efforts related to rotor optimization, a modern rotorcraft rarely benefits from optimized blades, even though blade replacement is a routine maintenance procedure. This again hints to the complexity behind rotor design. There are many variables under the designer’s control and the end result should provide a calculated compromise between performance, cost, weight, noise, stability and many other objectives and constraints. More and more, rotorcraft designers are looking to computer based simulation to help reduce the time required to design and optimize rotor blades. This fact points to the need for more accurate methods of rotor optimization that can capture the physics necessary to realistically generate a feasible, flyable rotor blade.

To accurately evaluate specific designs based on real life objectives like performance, noise, vibration, or some other measurable metric; an integrated framework of multidisciplinary, high fidelity physics-based analysis tools must be used in the process. The computation time and setup difficulty required by such a high fidelity environment may prohibit its use as the only analysis tool in the optimization process because many designs may need to be evaluated. Thus, lower fidelity tools are still needed to screen the field of potentially optimal designs.

The research presented in the pages to follow will attempt to answer two research questions: "What disciplinary analysis elements can be combined to form an efficient high fidelity CFD/CSD/AA simulation for application to rotary wing optimization?" and "In what way can low and high fidelity rotary wing simulations be used together in a process of rotary wing design?"

These questions have focused the research to create integrated and automated frameworks (both high and low fidelity) for rotary wing simulation with capability to analyze rotors in forward flight as well as hover. These frameworks will ultimately be used in design and optimization studies. Together, these low and high fidelity frameworks can be used in a synergistic process of rotary wing optimization; solving the same problem. Therefore, the very essence of the research presented here is to clearly demonstrate the practicality of such techniques which could easily be employed by preliminary designers to arrive at advanced rotor blades that satisfy the required aerodynamic loads, lower noise level, and reduced vibratory airloads.

Chapter 2

Background and Literature Review

2.1 Overview

A review of the literature related to the multidisciplinary analysis and optimization of helicopter rotors covers many areas. This chapter is sectioned as follows. First, a general look is made into the basics of rotor design to better understand the types of variables a rotor designer has at his or her disposal. This is followed by a section discussing the types of disciplinary analysis methods in current use throughout the rotorcraft industry and academia. Next, a review is made of various concepts related to numerical optimization in general. This leads into a section on optimization efforts related to rotor design.

2.2 Rotary Wing State-of-the-art

The design of rotors has matured greatly from humble beginnings. A brief historical account of rotor blade design is provided by Vaughan Askue of Sikorsky in Reference [16]. Initial wooden blades were susceptible to moisture absorption, changing the blade's characteristics. Metal blades lasted longer and didn't absorb moisture, but a lack of shaping flexibility limited the ability of aerodynamicists to optimize designs. Increasing helicopter speeds in the 1960's led designers to use swept tips as transonic tip speeds produced localized sonic flow [17]. Rotor blade design was significantly changed with the ability to manufacture blades from composites (epoxy, Kevlar®, fiberglass, and graphite). This allowed designers to make subtle changes in twist, chord, and airfoil shape along the span of the blade.

Today the rotor system is defined by many variables. The most basic variables are the number of blades, the blade radius and the blade chord, which may vary with the

radius. The designer also selects airfoils for various sections of the blade span. Usually the airfoils are twisted along the blade, with either linear or nonlinear variation along the blade span. Twisting is done to decrease the rotor's induced drag by making the inflow more uniform. Blade taper and changes in airfoil thickness are also common design variables used to tailor the blade's characteristics by reducing the profile drag. Combinations of sweep, anhedral, and taper are often seen near the tip of rotor blades as shown in Figure 2-1. Sweep reduces transonic drag near the tip by reducing the component of the tip speed air velocity normal to the leading edge. Anhedral enhances performance by placing the tip vortex further down from the rotor disk. All of these variables can be defined as shape variables as they directly affect the aerodynamics.

One of the more unique tip shapes flying today is referred to as the BERP tip [18], for British Experimental Rotor Program. This type of blade tip can be seen in the lower middle image of Figure 2-1. Tip sweep has the potential to reduce the power required at high tip Mach numbers. However, tip sweep can be a problem on the retreating side of the helicopter when stall is an issue. With the BERP tip, however, stable vortex flows created at the tip and the notch delay the onset of stall at high angles of attack giving the BERP tip benefits on both the advancing and retreating side of the rotor disk [19].

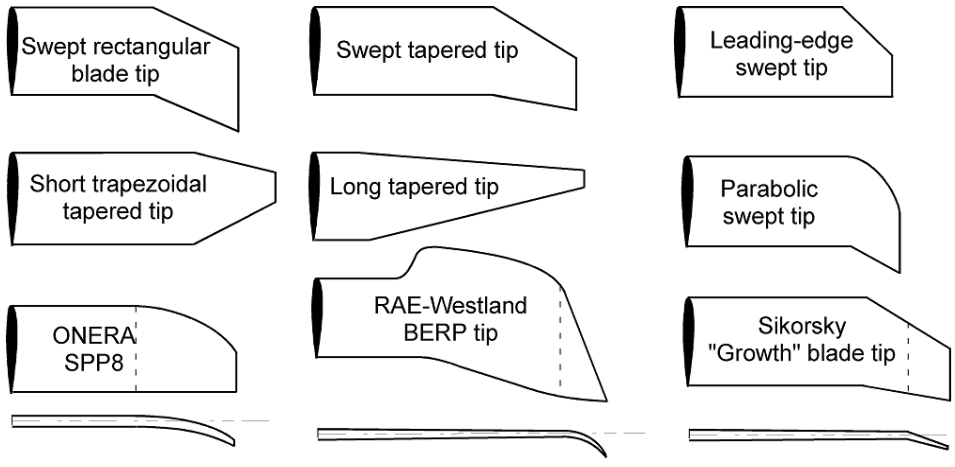

Figure 2-1: Examples of Blade Tip Designs

(Image Courtesy of J. G. Leishman and Cambridge University Press, reprinted with permission)

In addition to these aerodynamically related shape design variables, variables related to structural properties are also considered. By changing structural properties along the blade span, designers can reduce vibration or maintain stability margins. With the advent of composite construction, ply angles and wall thickness become design variables that can create aeroelastically tailored blades.

In short, there are numerous design variables available that the designer can vary and affect the performance of the rotor. With an almost endless number of variable combinations, rotor blade design is a prime candidate for numerical optimization. This requires a computer model capable of simulating a baseline rotor system and derivative designs created by changing some of the aforementioned design variables within the model. A computer model must capture the multidisciplinary aspect of rotor analysis. The following section discusses various concepts related to rotary wing simulation in more detail.

2.3 Rotary Wing Simulation Concepts

2.3.1 **A Multidisciplinary Process**

The analysis of any rotor system is a multidisciplinary process as shown in Figure 2-2. Each dot represents the flow of information. Dots above the diagonal represent information passed from one discipline to the next in a sequential fashion. Dots below the diagonal represent the flow of information back upstream, requiring iteration. At the start of the analysis, the geometry of the rotor blade is defined. All analyses are based on the same geometry. This geometry, combined with information about how the blade is manufactured, can be used to make predictions about the blade's mass and stiffness properties. These properties are subsequently used in the structural dynamics discipline to calculate blade deflections and motion using nonlinear beam theory or finite element

analysis. The blade motion, however, is strongly dependent on the aerodynamic loads. The aerodynamic loads, in turn, are dependent on blade motion. Therefore iteration between the structural dynamics and aerodynamics is needed. When these aeroelastic calculations converge, the rotor's performance and vibration can be determined. To calculate the resultant noise, the aerodynamic characteristics, geometric characteristics, and blade motion are all passed to the aeroacoustics discipline.

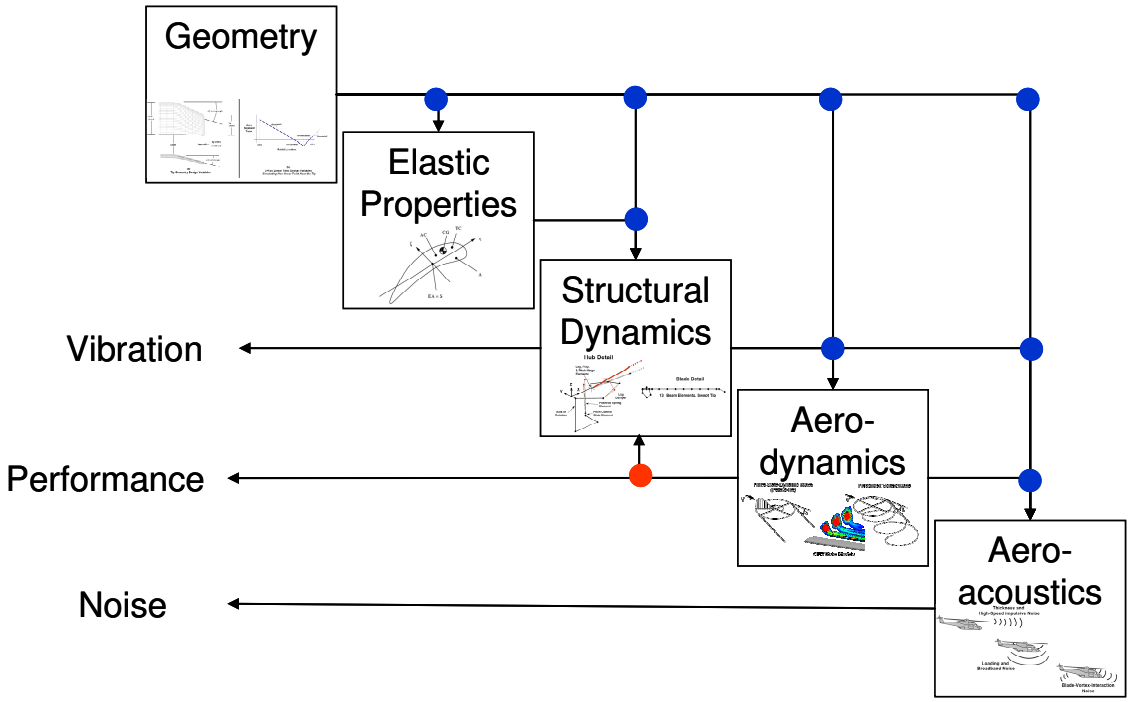

Figure 2-2: The Multidisciplinary Process of Rotor Analysis

2.3.2 **Elastic Blade Modeling**

Initial rotor blade design or high fidelity aerodynamic design may be done assuming the blades to be composed of rigid segments. To accurately capture the vibratory airloads, the elastic deformation of the blades should be included. Modeling the elastic deformation of the rotors also has an impact on how well blade loading noise is captured in the analysis [20, 21].

Because rotor blades have one dimension that is much larger than the other two, a simplification is to treat the blade as a 1-D beam. This simplification allows a three dimensional problem to become two reduced dimensional problems in sequence. First the sectional properties of an equivalent beam are determined and these properties are used in the structural dynamics analysis of the rotor blade. These sectional properties may be determined either from experimental data or using finite element analysis (FEA) tools. One tool that has seen use industry wide is VABS (Variable Asymptotic Beam Section Analysis) described in Reference [22]. Alternatively, researchers have treated the mass and stiffness properties at stations along the blade span as design variables [10], assuming that the blade can be manufactured with desired mass and stiffness properties.

Recent research by Ku [23] divided the problem into two parts, a local and global level optimization. The global level used section stiffness and mass per unit length as design variables with frequency placement and autorotation index as constraints. Once the design variables are found, a local optimization determines the thicknesses and ply angles of the various sections required to generate the stiffness and mass per unit length required at each section.

The science of composite structures and aeroelasticity as applied to rotor blades is a field full of significant research. The intent of this section is to identify the importance of elastic blade modeling in modern rotor design and highlight the basic information required in order to do so.

2.3.3 **Comprehensive Analysis Tools (CSD)**

The coupling between structural dynamics and aerodynamics disciplines in Figure 2-2 represents the classic aeroelastic problem. Over the past several decades, tools have been developed which calculate the structural dynamics and aerodynamics together simultaneously. These tools have become known as “comprehensive” codes. A survey of comprehensive codes is given in Reference [3]. The basic functionality of these tools lies

in the fact that larger systems can be assembled from small primitives. Both rigid bars and nonlinear elastic beams are included. These tools represent the Computational Structural Dynamics (CSD) of the rotorcraft. In addition to performing a multi-body dynamic and aeroelastic simulation, these tools contain the capability to change controls to obtain a state of trim for the rotor. For example, in hover the collective pitch is trimmed to reach a certain thrust. In forward flight, collective and cyclic pitches are trimmed to achieve target thrust and target values for pitch and roll moments. As the complexity of the vehicle or systems grows, so does the complexity of the trim problem. Examples of comprehensive codes can be found in CAMRAD-II [24], Georgia Tech's DYMORE [25], and the Army's Rotorcraft Comprehensive Analysis System (RCAS) [26]. In addition to having the capability of multi-body physics, the tools give the user the ability to use aerodynamic models commonly used in industry (e.g. quasi-steady table look-up, unsteady aerodynamics, stall models) in conjunction with a variety of inflow models such as uniform inflow, dynamic wake [27], prescribed wake [28, 29], and free wake [30].

2.3.4 **Computational Fluid Dynamics (CFD)**

More recently, the table-look up and inflow model approach in the comprehensive analyses is being complemented or replaced by Computational Fluid Dynamics (CFD) analyses. These methods can be used in both two and three dimensions. Their use to analyze fixed wing phenomena dates back to the 1960's. CFD modeling of helicopter rotors is much more recent. The complexity of rotorcraft analysis using CFD is related to the wake below the rotor and the large unsteady variation in flow states that occurs in flight.

Conventional rotorcraft CFD methods mesh, or grid not only the field near the rotor but also the far field. This allows the effects of the wake and trailed vorticies for each blade to be calculated or "captured" as part of the solution. The tool TURNS

(Transonic Unsteady Rotor Navier Stokes) [31] was developed in this manner to analyze rotors in hover. TURNS solves the 3-D compressible Reynolds-Averaged Navier-Stokes equations in integral form using a third order upwind scheme. OVERFLOW [32] can be used for hover and forward flight. It uses a series of overset grids that span the flow field of interest, and is capable of modeling bodies in relative motion to one another. A CFD tool called elsA [33] developed by ONERA in France has been used to model rotorcraft flows.

Other methods use a CFD grid close to the blade and either a prescribed or free wake model to account for the effects of the wake. The benefit of this approach is that it is computationally efficient. The TURNS code was extended to forward flight using this methodology [34]. A hybrid methodology from Georgia Tech called GT-HYBRID [35, 36] also uses this type of strategy. The hybrid method combines Reynolds-Averaged Navier-Stokes and free wake methods as shown in Figure 2-3. A Navier-Stokes solver is used to compute the flow field variables inside a computational grid of the blade surface and a distance away from the blade surface. The trailing vortex from this blade is modeled as a piecewise helix of vortex filaments with freedom to distort. The other blades of the rotor and their trailing vortices are modeled as piecewise vortex filaments as well. The influence of these vortex filaments (free wake) on the blade surface is modeled as a velocity imparted to the grid boundary. The velocity at each boundary location is calculated using the Biot-Savart Law for each vortex filament.

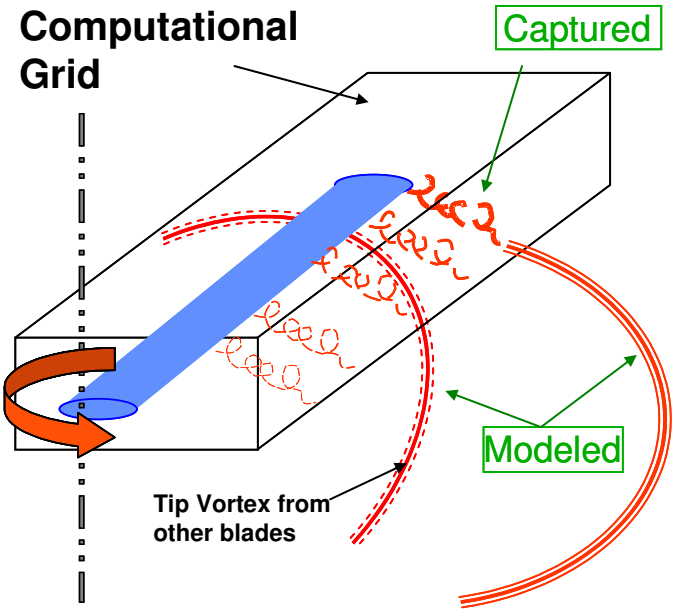

Figure 2-3: Schematic of Hybrid Method (RANS/Free Wake)

This is different from conventional Navier-Stokes methods that use grids to capture both the near and far field. In addition, conventional methods have a computational grid for every blade of the rotor. And compared with conventional methods, GT-HYBRID is an order of magnitude less costly in terms of CPU time. GT-HYBRID's method is similar to most conventional methods in that it uses a blade dynamics module that can handle blade deformation computed by a CSD code. This makes GT-HYBRID capable of being coupled to a CSD code.

2.3.5 **Coupled CFD/CSD**

One goal of the rotorcraft industry in terms of analysis capability is to accurately capture the radial and azimuthal distribution of the blade airloads for any given flight condition. This information is required for accurate predictions of performance, vibratory loads, and noise. In an effort to attain this goal, researchers have been utilizing complex CFD analysis. A recent survey of rotor loads prediction efforts with CFD is given in Reference [37]. Most recently, a topic of industry interest is the combining of CFD

analysis with the multi-body physics capability within comprehensive codes in what is referred to as CFD/CSD coupling. This coupling can be performed at every time step as the case with “tight” coupling. Or coupling can be performed at longer intervals in what is referred to as “loose” coupling. Tight coupling is more computationally intensive and is more commonly used to examine flight conditions that are transient, as with a maneuver. Loose coupling is used for steady state flight conditions and is more common in the literature. To exchange the information between CFD and CSD, a common fluid structure interface (FSI) is used [38]. Algorithms formalizing the loose coupling methodology were originally developed by Tung et al. [39, 40] and applied to airfoil angle attack. Other researchers applied the algorithm directly to airloads [41-43]

In recent years, researchers have utilized the FSI to apply CFD/CSD coupling to various known rotors. Rajmohan et al. at Georgia Tech tightly coupled GT-HYBRID/DYMORE and used an auto pilot algorithm to trim the UH-60A rotor in steady level flight [44]. Potsdam et al. used OVERFLOW-D/CAMRAD-II to model the UH-60 in forward flight [43]. Lim et al. used OVERFLOW-2/CAMRAD-II to model the HART rotor in a descent condition having blade vortex interaction (BVI) [8]. In the Helicopter Quieting Program (HQP) sponsored by the Defense Advanced Research Projects Agency (DARPA), Duque et al. used OVERFLOW-2/DYMORE to model both the UH-60 and HART rotor cases including forward flight and descent respectively including acoustics [9]. Makinen et al. used OVERFLOW-2/RCAS to model the HART rotor during a BVI flight condition [7]. Phanse and Sankar used GT-HYBRID/DYMORE in a loose coupling environment to model the UH-60A rotor in forward flight [45].

2.3.6 **Aeroacoustics**

The aerodynamically generated sound of helicopter rotors is comprised of several distinct noise source mechanisms, which can be separated into the categories of rotational noise sources, impulsive noise sources, and broadband noise sources. Rotational noise

typically refers to the low frequency noise (blade passage frequency and the first several harmonics) due to the blade thickness and the aerodynamic loading. Thickness noise is due to the air moving out of the way of the blade and radiates primarily in the plane of the rotor. Loading noise is due to the acceleration of the local force distribution acting on the rotor blades as they produce the rotor lift. Loading noise radiates primarily below the rotor. Typically two impulsive noise sources can occur in particular flight conditions – blade-vortex-interaction (BVI) noise and high-speed-impulsive (HSI) noise. BVI noise occurs when a blade interacts with a vortex that is shed from the tip of a preceding blade. BVI noise is a particular, impulsive form of loading noise. HSI noise has directivity similar to thickness noise and is generated when the blade travels at transonic speeds. Finally, broadband noise is stochastic form loading noise due to turbulence ingested into the rotor or from several self generated turbulent mechanisms. Figure 2-4 shows the general directivity of these noise sources.

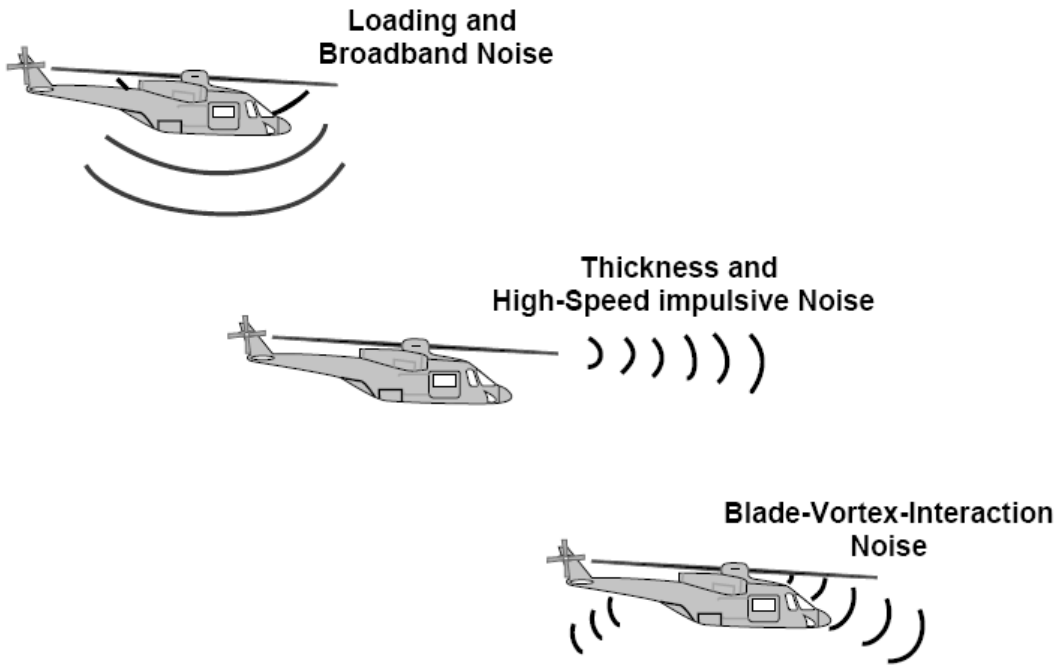

Figure 2-4: Noise Generated by a Helicopter

(Image Courtesy of K. Brentner, reprinted with permission)

The calculation of acoustic pressure at a given observer location can be performed in a number of ways. The compressible Navier-Stokes equations describe both the flow field and the aerodynamically generated acoustic field. Thus, solving the Navier-Stokes equations over a field that includes the rotor and the observer location can, in principle, provide the answer. This method, known as direct computation is very computationally intensive and is difficult because the acoustic pressure is typically many orders of magnitude smaller than the typical aerodynamic pressure. Also, the propagation distance (the rotor and the observer) is usually very large; thus numerical propagation of the small acoustic signal all the way to the observer is impractical – if not impossible. For this reason, the problem is generally broken into two parts. In one part, the flow field defining the source is determined through some type of CFD or lifting line method. Next, the acoustic propagation is calculated using an integral Acoustic Analogy (AA) method. This is the strategy behind the well know rotorcraft acoustics solver developed at The Pennsylvania State University called PSU-WOPWOP [46].

PSU-WOPWOP is an implementation of Farassat's Formulation 1A [47] of the Ffowcs Williams–Hawkings (FW-H) equation [48]. PSU-WOPWOP is able to compute the acoustic pressure at any observer point or on a grid of observers from several different types of sound source definitions, making it ideal for trade studies where multiple systems may be used to compute the blade loading. The blade geometry and either surface pressure or section loading can be used in PSU-WOPWOP. Also, PSU-WOPWOP is able to predict the noise from deformable surfaces or with off body acoustic data surfaces which surround all the physical source mechanisms to capture HSI noise.

Section 2.3 has discussed various concepts related to rotary wing simulation. Using these concepts and computer based tools, optimization methods can be applied to

optimize an existing rotor for better attributes. The following section discusses a few of the many concepts related to optimization in general.

2.4 Design and Optimization Concepts

2.4.1 **Generic Optimization Problem**

In general, the optimization process attempts to achieve a minimum value of an objective function by changing its arguments (certain design variables). Also, the optimum design must adhere to certain constraints defined by the designer before the process starts. Vanderplaats [49] defines optimization using the following equations.

Minimize: $f(\bar{x})$	objective function	**2-1**

Subject to:

$g_j(\bar{x}) \le 0 \quad j = 1, m$	inequality constraints	**2-2**
$h_k(\bar{x}) = 0 \quad k = 1, l$	equality constraints	**2-3**
$x_i^l \le x_i \le x_i^u \quad i = 1, n$	side constraints	**2-4**

by changing:

$$\bar{x} = (x_1, x_2, ..., x_n) \qquad \text{design variables}$$

In equation 2-1, the function $f(\bar{x})$ is some objective. For the rotor design problem, this could be power required, vibration, noise, weight, cost, some other metric, or a weighted combination of metrics. The vector $\bar{x}$ contains at least one but usually more than one design variable. The constraints defined by equations 2-2, 2-3, and 2-4 provide a way that the designer can ensure that particular criteria are met.

There are various types of strategies used to find an optimum; many of which are discussed at length in Reference [49]. Many strategies rely on gradient information to

determine the direction toward the global optimum. Gradient based methods can be problematic when there are local minima. Domain spanning methods, on the other hand, are better at finding the global optimum by examining a more even distribution of the design space. Evolutionary methods like those using a genetic algorithm work by utilizing the survival of the fittest principle. The algorithms work in a way that passes the traits of more optimum designs to offspring. The computer scientist John Koza [50], has used genetic style algorithms and giant computer clusters to create new inventions in various fields by applying these algorithms to certain problems where there exists a computer based analysis that can model numerous design derivatives. The disadvantage of non-gradient based methods is in the large number of function evaluations typically required to find an optimum. However, their ability to find the global optimum regardless of the initial starting design makes them a popular choice in engineering design optimization.

2.4.2 **Multi-objective Optimization and Pareto Optimality**

In multidisciplinary design, especially for rotors, the desired objective function is usually not a single quantity. More often, it is composed of two or more (often conflicting) objectives. For instance, a primary objective of a rotor design may be to reduce vibration. However the designer is also concerned about cost to manufacture, noise, power required, weight, and so on. Thus the optimization problem posted in equation 2-1 may be recast as shown below in equation 2-5.

$$\text{Minimize: } \bar{f}(\bar{x}) = \begin{bmatrix} f_1(\bar{x}) \\ f_2(\bar{x}) \\ \vdots \\ f_n(\bar{x}) \end{bmatrix} \qquad \textbf{2-5}$$

Given that the objective is to minimize several objective functions, there may no longer be a single optimum. Rather, there may be many optima. These optima define what is known as the Pareto Frontier, named after the late Italian economist Vilfredo Pareto [51]. A surface in the design space is called a Pareto Frontier if a design change done at any point on this surface to minimize one objective, does so at the expense of making one or more of the other objectives larger. An example of the Pareto Frontier in two dimensions is shown in Figure 2-5. In this example, f_1 and f_2 represent objectives to be minimized. The space of feasible designs is shown. The line of designs closest to the origin is called the Pareto Frontier.

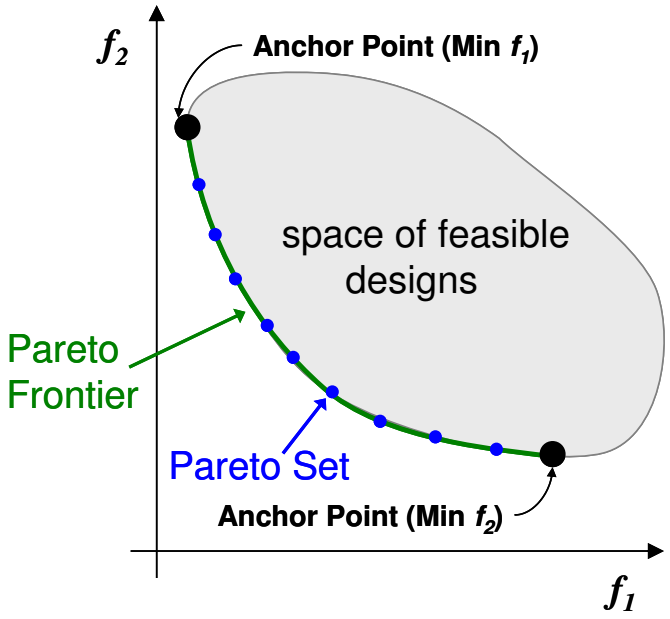

Figure 2-5: Pareto Frontier Example

There are optimization strategies that are specifically reserved for the problem of multi-objective optimization. In many cases, the multi-objective problem is reformulated into a single objective problem by forming some sort of aggregate objective function from the multiple objectives. This may be a sum of weighted objectives as in equation 2-6, developed in Reference [52] and applied to structural optimization in Reference [53].

However, this method requires the designer to know the weights required to achieve a certain level of reduction in a particular objective a priori. After the optimization is complete, the designer may not be happy with the actual value of the individual objectives. In which case he/she must adjust the weights and optimize again. This iteration takes valuable time. An alternate solution is to not use weights, but rather use matters of preference. This is the premise behind physical programming [54]. And there are other methods of creating aggregate objective functions for the purpose of finding a single optimum based on multiple objectives.

$$\text{Minimize: } J = \alpha f_1(\bar{x}) + \beta f_2(\bar{x}) + \cdots + \delta f_2(\bar{x}) \qquad \textbf{2-6}$$

Regardless of the optimum picked, if there are multiple objectives, the designer is forced to make a compromise between objectives. Thus designers would really like to know what the actual landscape of the frontier looks like in terms of design variables and objectives by finding not one, but many designs along the frontier. Methods of tackling this problem are meant to generate an even distribution of designs along the Pareto Frontier. Strategies include the ε-constraint method [55], normal constraint method [56, 57], physical programming [58], and weighted sum of objectives method to name a few. The later method works in that for every unique combination of weights in equation 2-6, a different point on the frontier will be found. Though simple, this method is not without its drawbacks [59], such as finding evenly spaced designs or identifying solutions on non-convex regions of the frontier.

Monte Carlo Simulation [60] is a domain spanning strategy that can be used for multi-objective optimization as well. This method attempts to analyze so many randomly selected designs that the resulting number of designs in the Pareto set is large. This approach assumes that the Pareto Frontier will become "visible" if enough designs are evaluated. Because the method is random, this method may not always generate an

evenly spaced set of designs; however, it should show non-convex regions as it explores the entire design space. Regardless of the specific strategy used to generate the Pareto set, a design can be selected from the set for further analysis.

Because most optimization methods – especially a method like Monte Carlo Simulation – require the analysis of numerous design configurations, the actual analysis is often replaced with an approximation that is computationally much less intensive.

2.4.3 **Surrogate Modeling**

A surrogate model is defined as an approximation of a function that is accurate under certain circumstances. In an optimization problem for instance, for a given set of design variables, the objective function and constraints are the result of some analysis. The analysis could be a physical experiment or a computer based experiment. In either case, the results may take a long time to acquire. A surrogate model would be an approximation to the objective or constraint that is a function of the design variables but is very fast. Surrogate models are created from an existing set of data. To generate this data, experiments must be performed. In statistical terminology, this is usually referred to as a Design of Experiments (DOE) [61]. There are various types of surrogate models used in engineering design. Response Surface Methodology (RSM) [62], Kriging [63], and Neural Networks [64] are just a few of many models available. Each has advantages and disadvantages depending on the application. Comparisons of these and other types of surrogate models are made in References [65, 66].

There are several advantages of using a DOE and surrogate modeling approach. For one, optimization using function calls to a high fidelity simulation is unrealistic since each function call could require days to get a response. Also, because a DOE is a predetermined list of experiments to run, they can be done in parallel. This makes a huge difference in time to completion of high fidelity simulations when parallel processing can be utilized. Another big advantage is that once the surrogate models are built, they can be

used in many different optimization "tasks" such as being used to optimize different objectives. Or they could be used to define the boundary of the Pareto Frontier; which requires numerous sub-optimizations. Using the actual experiments for each optimization "task" would take a very long time.

To be fair, there are drawbacks to using DOE's and surrogate modeling in optimization. A Design of Experiments approach requires that numerous designs be analyzed upfront, before any optimization can be done. Some of these designs may not be good designs, but are analyzed solely for the creation of the surrogate model. Another drawback is that the surrogate model is an approximation to the original experiment and is therefore prone to being less accurate. This is especially true if time only allows for a sparse number of experiments to be performed as is normally the case with high fidelity simulations.

2.4.4 **Optimization using Low and High Fidelity Tools in Concert**

Another optimization strategy stems from the fact that engineers typically have various fidelity level analysis tools at their disposal and attempts to make use of both low and high fidelity analysis to find an optimum that is in the high fidelity domain. Low fidelity could mean a simplified physics-based model, a finite element model evaluated over a coarse mesh, or a variety of the reduced order models available [67]. This specific type of research is ongoing in aerospace as evidenced by the research of Alexandrov [68] and Robinson [69]. In general, their methods use simplified (low fidelity) physics-based analysis tools to perform the optimization, but incorporate some type of correction factor to make the simplified analysis yield a more accurate analysis. This is done by making periodic checks with a more accurate (high fidelity) analysis as the optimization progresses. A common theme is in the use of the concept of a "trust region" [70]. Even these methods, however, require that the high fidelity analysis be completed within a reasonable timeframe.

2.5 Rotor Design and Optimization Efforts

2.5.1 **Comments on Simulation Accuracy**

The application of optimization methods to the design of rotors is growing in popularity. A survey of optimization efforts in rotorcraft design can be found in Reference [1] and more recently in Reference [2]. For the most part, optimization in rotorcraft has been performed using analysis tools and methods that lack predictive capability. This has the potential of reducing the authority of the results as stated by Celi in Reference [1]:

> If the analysis models are not sufficiently accurate, it is inevitable that the results of an optimization based on them be looked upon critically if not with skepticism.

However, this skepticism may be unfounded depending on the problem at hand. Ganguli [2] sums this up saying:

> …, although aeroelastic analyses may not accurately predict the absolute values of vibration and other helicopter system properties, they capture the essential physics of the problem and, therefore, the relative changes in the design between the baseline and the optimum design may be more reliable than the absolute values themselves.

Both of the above statements are true to some degree. Inaccurate results will always be viewed with some skepticism. However, optimization using the tools available can be beneficial and lead to improved designs. The question is when more accurate tools are needed. Ganguli also addresses this in Reference [2] with the following:

> Whereas sweep and other advanced geometry design variables cause important dynamic couplings between the blade modes, their effect [on] the aerodynamic flow is also very important, and three

> dimensional effects can become important at the blade tip. In addition, noise reduction is a key objective in advanced geometry rotor design, and the use of sophisticated aerodynamic models such as those based on CFD may be needed for better acoustic noise predictions.

The above statement sheds light on when more accurate aerodynamic tools should be brought into the analysis. This really depends on the design variables under investigation. Some design variables have a direct impact on the aerodynamics while others have an indirect impact. Variables related to the internal structure of the blade itself that affect the sectional mass and elastic properties have an indirect impact on aerodynamics by affecting deflection and subsequently aerodynamics through an aeroelastic response. Variables such as airfoil shape, taper, twist, and tip geometry – basically any shape related variable – have a direct impact on aerodynamics. In a similar manner, structural design variables have a direct affect on blade deflections whereas shape related variables have an indirect affect on deflections, again through an aeroelastic response.

Optimization that involves shape related variables which have a strong impact on the aerodynamics benefit from using higher fidelity aerodynamics such as CFD. For simplicity, those variables being studied that have an indirect impact on aerodynamics are often studied with the use of simplified aerodynamic calculations.

The remainder of this section is divided into a review of the literature involving optimization with structure related variables, structure and shape related variables, and those involving only shape related variables.

2.5.2 **Optimization of Structure Related Variables**

Structure related variables affect the mass and stiffness properties of the blade. In general, the blade is modeled as a series of finite elastic beam segments. Each segment is defined by specific properties. These properties include but aren't limited to mass per unit

length (including nonstructural mass), chordwise bending stiffness, flapwise bending stiffness, flap-chordwise bending stiffness, torsional stiffness, radial stiffness, radius of gyration in both y and z, cross radius of gyration, chordwise center of gravity (CG) offset, vertical CG offset, chordwise tension center offset, vertical torque center offset, Young's modulus, and shear modulus. Some of these properties at each segment may be selected as design variables.

For the most part, rotor optimization methods using structure related variables only are aimed at reducing vibration levels. Constraints commonly used are those of natural frequency placement, autorotational inertia, and aeroelastic stability. Vibration reduction optimization problems have the objective of reducing the peak-to-peak value of hub shear and moments in the B/rev frequency, where B is the number of blades. One type of objective function is given in equation 2-7 where K_{Fx}, K_{Fy}, K_{Fz}, K_{Mx}, K_{My}, and K_{Mz} are weighting factors. The weighting factors are normally given the value of either 0 or 1. A common set of weighting factors would be all zero except K_{Fz}=1 to minimize only the vertical vibratory hub shear. An example objective function derived from Lim and Chopra [71] is given in equation 2-8. This objective consists of all three B/rev vibratory hub forces and three B/rev vibratory hub moments and K_F and K_M are weighting factors.

$$J(\bar{x}) = K_{Fx}F_{xH}^{BP} + K_{Fy}F_{yH}^{BP} + K_{Fz}F_{zH}^{BP} + K_{Mx}M_{xH}^{BP} + K_{My}M_{yH}^{BP} + K_{Mz}M_{zH}^{BP} \qquad \textbf{2-7}$$

$$J(\bar{x}) = K_F\sqrt{\left(F_{xH}^{BP}\right)^2 + \left(F_{yH}^{BP}\right)^2 + \left(F_{zH}^{BP}\right)^2} + K_m\sqrt{\left(M_{xH}^{BP}\right)^2 + \left(M_{yH}^{BP}\right)^2 + \left(M_{zH}^{BP}\right)^2} \qquad \textbf{2-8}$$

Lim and Chopra [71] used a blade model with five finite elements. The properties of each element were used as design variables. These were the flap, lag, and torsional stiffness along with the nonstructural mass and its offset from the elastic axis. The

authors used the gradient based optimizer CONMIN [72] to perform optimization by reducing the objective given in equation 2-8. Results obtained at an advance ratio of 0.3 showed a reduction in the objective function of 20-50%.

Tarzanin and Young from Boeing optimized a rotor for low vibration and validated the design with a Mach-scale wind tunnel test [73]. They published a separate paper [10] further describing the procedures used over a twelve year period. The optimization was performed by minimizing an objective function consisting of a weighted sum of the three components of vibratory hub shear forces and the x and y vibratory rolling moments (equation 2-7 with K_{Mz}=0 and all other factors set to one) . The design variables were the spanwise mass and stiffness distribution and constraints were placed on the static and dynamic behavior of the blades. The authors noticed that the gradient based optimization used tended to get stuck in local minima. Nonetheless, the test validation proved that a lower vibration rotor could be developed using the optimization methods presented.

There are numerous other references related to the optimization of rotors using structure related design variables. This includes work on the optimization of composite structures. Using the ply angles as design variables can provide couplings that enhance stability or reduce vibration [74]. Two level optimizations can be performed where one optimization finds the desired stiffness properties and a second optimization finds the ply angles that will yield those properties [23, 75, 76].

This very brief summary of studies that focused on optimization using structure related design variables show the tremendous potential for rotor vibration reduction using optimization methods. This potential is also realized without the use of high fidelity aerodynamics.

2.5.3 **Optimization of Both Structure and Shape Related Variables**

This section will point out some notable studies involving the use of both shape and structure design variables. Chattopadhyay, Walsh, and Riley [77] optimized a rotor using three separate objective functions. The first objective was for minimum blade weight. The second was for minimum 4/rev vibratory vertical hub shear (equation 2-7 with K_{Fz}=1 and all other factors set to zero). The third was to minimize both the blade weight and 4/rev vibratory vertical hub shear simultaneously. The design variables were the blade taper ratio, root chord, root radius of gyration, root flap bending stiffness, root lag bending stiffness, root torsional stiffness and the non-structural weight at each of six blade segments. Constraints were placed on the natural frequencies, autorotational inertia, and maximum centrifugal stress. The reference blade was optimized at an advance ratio of 0.3. The analysis was performed in CAMRAD with uniform inflow. All optimizations produced blades having both lower weight and lower vibration. The lowest weight blade resulted from the objective of minimizing both blade weight and vibration. This was explained by the fact that minimizing the blade vibration has an impact on blade weight reduction by reducing the stiffness in flap and lag.

Yuan and Friedman [78, 79] used an aeroelastic simulation with numerical optimization to reduce vibration in forward flight. The design variables used were composite ply orientations along with tip sweep and anhedral. Results indicated that tip sweep was a dominate factor affecting the vibratory response.

Ganguli and Chopra [80] optimized a rotor for vibration reduction minimizing the objective given in equation 2-8 for a four bladed rotor. The authors modeled each blade with an arbitrary number of elastic beam segments. To create advanced geometry, each segment could have its own sweep, anhedral, and taper. Structural design variables included the nonstructural mass, nonstructural mass offset, flap bending stiffness, chordwise bending stiffness, and torsional stiffness of each segment. Constraints were placed on aeroelastic stability, frequency placement, and autorotational inertia. The

optimization was performed for an advance ratio of 0.3 using quasi-steady aerodynamics and a linear inflow model. The authors were able to reduce the objective function 45 percent using both shape and structure variables together. With just shape variables, a 25 percent reduction was realized and with structure variables alone, the reduction was 30 percent. The authors analyzed the optimum designs further at other advance ratios and also using a free wake model and verified similar percentage reductions in the objective.

2.5.4 **Optimization of Shape Related Variables**

The optimization of shape related variables has benefited from advanced aerodynamic simulations like CFD. However, there have been contributions in this arena using lower fidelity aerodynamics as well. Jones and Crossley [81] used a genetic algorithm to create optimized rotor blade airfoil shapes for lower noise using Xfoil for 2-D aerodynamics and WOPWOP for aeroacoustics. The optimization of shape variables using lower fidelity aerodynamics has been particularly useful in predicting benefits of actively controlled flaps [82-84]. In these studies, the motion of the flaps is determined as a design variable to reduce vibration.

Using CFD in the process, Pape and Beaumier [13] used a Navier-Stokes flow solver and a gradient based optimizer to design rotors for maximum figure of merit. Baeder [11] investigated various planform shapes using TURNS to determine the effect certain parameters had on high-speed impulsive noise. The study was not so much an optimization exercise as it was a parametric study to understand the non-linear effects of sweep, taper, thinning, and tip speed. The authors started with an untwisted UH-1H rotor as the baseline and performed the investigations for hover as a preliminary approach. The results indicated that forward sweep was better at noise reduction that rearward sweep. Combinations of forward sweep, taper and thinning were seen to reduce noise by 10 dB when compared to the baseline. The investigation did not include any constraints and assumed rigid blades. Similarly, Zhao and Xu [12] investigated advanced tip shape rotors

for aerodynamic and acoustic characteristics using a hybrid flow solver and wind tunnel testing. More recently, Yang et al. [15] combined CFD and optimization to find arbitrary planform tip shapes to reduce high speed impulsive (HSI) noise in a hover flight condition. While these studies highlight the considerable interest in bringing the predictive power of CFD into preliminary design, they have focused on hover only and have not attempted to tackle the problem of forward flight optimization using CFD/CSD.

Rotorcraft related optimization efforts are now and will continue to be a topic of interest to both academia and industry. Continued research is needed to bridge the gap between state-of-the-art high fidelity rotor blade simulation and the preliminary design stage to allow the optimization of rotor blades to be done for arbitrary shape variables in forward flight as well as hover.

2.6 Chapter Summary

Modern helicopters are built using composite blades designed with subtle changes in shape, airfoil section, twist, and even ply angle to achieve desired levels of performance. The preliminary design of rotor blades involves the convergence of concepts in both rotary wing simulation and optimization.

Those concepts related to rotary wing simulation highlight the fact that it is a multidisciplinary process. The long and slender blades of helicopters operate in a very complex aerodynamic environment. Simulating this accurately requires a complex aeroelastic analysis which requires an elastic model of the blades. Over the past several decades, tools have been developed which calculate the structural dynamics and aerodynamics together simultaneously. These tools have become known as "comprehensive" codes and perform Computational Structural Dynamics (CSD) and trim of the rotorcraft under the influence of various types of aerodynamic models. The aerodynamic analysis built within these comprehensive codes is typically done using a 2-

D table look-up of airfoil aerodynamic coefficients combined with some type of inflow model. More recently, the table look-up and inflow model approach in the comprehensive analyses is being complemented or replaced by Computational Fluid Dynamics (CFD) analyses. State-of-the-art rotor simulation involves coupling Computational Fluid Dynamics and Computational Structural Dynamics together in what is coined CFD/CSD analysis. Information from the converged aeroelastic rotor analysis such as blade motion and aerodynamic loading can be used in an aeroacoustic analysis to evaluate the noise created by the rotor while in flight.

A discussion of concepts related to optimization begins by defining the general form of the problem: to minimize some quantity by changing certain design variables while remaining within some constrained boundaries to be feasible. This problem can be recast to include the fact that most real world problems – including rotor blade optimization – have more than one quantity that needs optimizing. For example, while increased efficiency may be important, so are vibration and noise. There is no single optimum for this multi-objective problem, but rather many optimal designs that make up what is called the Pareto Frontier. A surface in the design space is called a Pareto Frontier if a design change done at any point on this surface to minimize one objective, does so at the expense of making one or more of the other objectives larger.

Another concept related to optimization is modeling parameters of interest as functions of the design variables in what is called surrogate modeling. By planning and executing one or more set of experiments in a DOE, approximate (surrogate) models of quantities can be built from the acquired data. Because these approximate models are very fast to execute, they can be used in a variety of optimization methods where number of function calls is no longer an issue.

Designers typically have access to a variety of analysis tools capable of simulating the problem. Some of these tools make more simplifying assumptions than other tools. This makes some very fast yet less accurate (low fidelity) and others more

accurate yet very computationally intensive (high fidelity). Making use of both types of tools in a synergistic process is a great way to get benefits from both and has been explored by some researchers with the goal being able to arrive at optimums in the high fidelity domain.

Using optimization techniques, researchers have made progress in the field of rotor blade optimization. In general, these efforts have generated rotors with better characteristics despite the fact that the prediction accuracy of most comprehensive analysis tools used in the process is limited. This deficiency in prediction accuracy is most likely due to the simplified aerodynamic models used. These simplified aerodynamic models have led most researchers to more commonly investigate structure related variables having an indirect impact on aerodynamics. Using comprehensive codes with simplified aerodynamics to optimize shape related variables is much less common. Optimization of shape related variables using high fidelity CFD analysis is receiving more attention from researchers as computer processor speeds increase. Still, the examples in the literature focus on hover using CFD and rigid blades. Optimization in forward flight using an aeroelastic CFD/CSD process is a task deserving research.

Chapter 3

Research Objectives

3.1 Overview

The objectives of this research are rooted in the idea that high fidelity simulation models are badly needed for use in rotary wing design. The design of rotary wings requires the cooperation of many disciplines to solve a highly coupled problem. High fidelity models are needed to provide accurate predictions of airloads for arbitrary shaped rotor blades in arbitrary flight conditions. These high fidelity tools have yet to make a strong presence in the routine solution of engineering design problems in some form of computer based optimization. This is mainly attributed to the complex nature of high fidelity aerodynamics and the large computer resources that are normally required.

Advanced methods are now becoming available to solve actual real world rotary wing design problems using high fidelity simulation such as CFD/CSD/AA. Given the success that lower fidelity tools have had in rotorcraft related optimization, it makes sense to utilize them in the optimization process to reduce the number of high fidelity simulations that are required. Thus the work performed can be listed: 1) Application of high fidelity CFD/CSD/AA simulation tools to a rotary wing design problem and 2) A synergistic approach to using intelligently selected experiments with both high and low fidelity simulations to arrive at an optimized rotor design.

The following approach is employed in the remainder of this chapter. First, several observations related to rotary wing design optimization using state-of-the-art simulation are presented with hope that these observations lead the reader to appreciate that there exists a list of gaps in the current research. The results presented in this thesis will add to the knowledge base pertaining to these gaps. The chapter is concluded with research questions and clear objectives to define and guide the work.

3.2 Observations

Investigation of the state-of-the-art concerning rotor design and optimization utilizing physics-based analysis tools paves the path to several observations. These observations confirm the strong need for research to further advance the use of high fidelity simulation tools in rotary wing preliminary design.

3.2.1 **Rotary Wing Simulation is Multidisciplinary and Complex**

As shown in Figure 1-1 and Figure 2-2, it is clear that the art of rotary wing simulation is complex and multidisciplinary in nature. This makes the design of rotary wing systems also very complex and multidisciplinary. Among all aerospace vehicles, the one that would seem to qualify most for regular upgrades of its aerodynamic surfaces is the helicopter. In fact, rotor blades are regularly replaced from time to time as part of its routine maintenance. However, behind their somewhat benign look, rotor blades are actually very complex and many factors must be considered in their design. Consider the redesign of a rotor blade for instance. The rotor hub is designed for specific centrifugal load limits, so the weight of the redesigned blade must be equal to or less than the old blade if the rotational speed is to remain the same. Steady state and oscillatory pitch link loads must be kept below max design values. The natural bending and torsion frequencies of the redesigned blade should be similar to the baseline as well. In short, the design or redesign of a rotor blade is not a trivial a process to say the least. Many different disciplines are involved: Aerodynamics, Structures, Acoustics, and others. A recent example of the effort required to redesign an existing rotor blade can be seen in the BERP IV project [85].

The design of rotary wing systems is further complicated by the fact that designers seek to not just find a rotor which is clearly the best in a single objective, like reduced vibration for instance; they also try to create designs which have better lift to drag ratio, better hover efficiency, lower weight, and lower noise. In short, rotor design

and optimization is clearly a multi-objective problem. Thus any optimum selected is in reality just a compromise between various objectives. There are actually many optimums, and these optimums make up the space known as the Pareto Frontier. Picking an optimum from this design depends uniquely on the mission.

3.2.2 **Integrated, High fidelity Tools for Rotorcraft are Needed**

Given the complicated nature of rotary wing design, it is not surprising that there is a need for integrated high fidelity disciplinary simulation tools. More importantly, it is important that these high fidelity tools be suitable for engineering design applications. High fidelity aerodynamic analysis methods are by nature time consuming, but still there is tremendous interest in the industry for high fidelity based methods that can be useful in design and optimization. In the 2006 Research Opportunities in Aeronautics [86], the desire for the development of high fidelity, multidisciplinary design tools for rotorcraft is easily demonstrated in the following statement:

> The challenge of the Subsonic Rotary Wing project of the NASA Fundamental Aeronautics program is to develop validated physics-based multidisciplinary design and analysis tools for rotorcraft, integrated with technology development, enabling rotorcraft with advanced capabilities to fly as designed for any mission. Meeting this challenge will require innovative technologies and methods, with an emphasis on integrated, multidisciplinary, first-principle computational tools specifically applicable to the unique problems of rotary wing aircraft.

3.2.3 **Automated Computer Optimization is Key to Rotor Design**

The nature of optimization is that certain design variables are changed in a search for their optimum values. A large degree of automation is required for the process of

finding the optimum to be efficient and effective. Tarzanin and Young from Boeing, in reflecting on twelve years of rotor optimization studies [10] reiterate this by saying:

> Only computer-automated optimization could efficiently juggle all the variables and find its way through the conflicting requirements.

This observation is true regardless of the degree of fidelity of the analysis being considered. Assuming a computer based simulation of a rotor analysis is available, the automation of simulations for given design derivatives is a key component in being able to utilize the simulation in any given optimization process.

3.2.4 **Accurate Airloads Prediction is Difficult**

Today's comprehensive rotorcraft codes combine a finite element based flexible body dynamic analysis with some type of aerodynamic analysis. Although this type of analysis is complicated, the ability of the analysis to accurately predict blade airloads is still very poor. This fact is conveyed by Ganguli by saying in Reference [2]:

> However, the predictive capacity of even the most sophisticated helicopter aeroelastic analysis code remains quite poor, as evidenced in a recent study…where hub load predictions from several codes are compared with flight-test data.

3.2.5 **Comprehensive Codes Useful in Optimization**

Normally, comprehensive codes have been automated when using non-CFD based aerodynamics. And despite the general deficiencies mentioned above, Ganguli also states in Reference [2] that

> …, although aeroelastic analyses may not accurately predict the absolute values of vibration and other helicopter system properties, they capture the essential physics of the problem and, therefore, the

> relative changes in the design between the baseline and the optimum design may be more reliable than the absolute values themselves.

This can also be seen in literature related to rotor optimization, especially those involving the reduction of vibration by changing blade structural properties. It also highlights how important automation is to optimization.

3.2.6 **Simplified Aerodynamics is a Limitation in Rotorcraft Optimization**

The lack of literature related to the optimization of blade shape such as the addition of advanced tip shapes, non-linear blade twist, or enhanced airfoils is perhaps due to the lack of accurate and efficient aerodynamic analysis. When commenting in his survey of rotorcraft optimization studies [2] about those that involved advanced rotor planform and tip geometry, Ganguli states:

> An important limitation of the preceding [Advanced Geometry Rotor Optimization] studies is in the use of relatively simple aerodynamic models for the aeroelastic analysis.

3.2.7 **Coupled CFD/CSD Aeroelastic Analysis is Promising but Costly**

It is important to mention that the state-of-the-art in computational rotor analysis involves coupling the airload computation from high fidelity CFD with the blade motion calculated from a CSD model. Although these methods are proving to provide fairly accurate blade load predictions, they are still time consuming in general. A statement by Truong in Reference [87] summarizes this fact:

> In some research centers, the coupling of aerodynamic CFD solver and structural dynamic codes has been undertaken. However, this methodology which is certainly interesting for understanding 3-D unsteady aerodynamics, demands large CPU time and therefore cannot be used routinely as an engineering tool.

3.3 Gaps in Research

There are many gaps in the research today where valuable contributions can be assessed. These gaps do not exist because of a lack of good work done so far by other researchers in the various aeromechanics and design disciplines involved. They are merely indicative of the many places where work can be done to merge the latest technologies in physics-based simulation with state-of-the-art, innovative design methodologies. Subsequently, this work would lead to the creation of an integrated, high fidelity framework for rotary wing design and optimization.

The thesis work here is aimed at adding to the knowledge base in such a way that could reduce the magnitude of the gaps in research that are discussed below.

3.3.1 **Lack of Shape Variable Optimization**

There are numerous design variables related to the shape of a rotor blade. Aerodynamic twist, taper, sweep, anhedral, and airfoil shapes are just a few of these design variables. There are few optimization studies conducted today which focus on changes in these types of design variables. The reason for the lack of a sufficient database is that in order to have confidence in the results of an optimization using shape related design variables, high fidelity aerodynamics like CFD must be used. A common understanding is that this could increase the run time of each experiment significantly. Because of this, tackling a shape related design variable optimization is considered a formidable challenge as of today because it requires the use of high fidelity aerodynamic simulations to achieve accurate and thus believable results. The gap mentioned here is very related to a second gap, which is the limited use of high fidelity simulation tools in design or optimization exercises in rotary wing design.

3.3.2 **Limited Use of High Fidelity Simulation Tools in Rotary Wing Design**

So far, the tools that have been used in rotary wing design for the most part have been those that use simplified aerodyamics. The lower runtime, decreased setup complexity, and ease of automation have enabled the use of these tools in automated optimization problems.

Due to a number of reasons from steep learning curves, tedious grid generation, and very long run times, the use of high fidelity rotor analysis tools in the design and optimization process is limited. This is an area of needed research and one that will grow as the computational power of computers increases in the future. Keys to closing this gap will include efficient high fidelity simulations and automation.

3.3.3 **Multi-Fidelity Optimization Not Exploited in Rotary Wing Design**

As of today, high fidelity tools have found limited use in optimization studies. Yet these tools are a must in shape variable optimization. On the other hand, low fidelity tools have found much use in optimization processes. These tools are usually used in sequence. First the low fidelity tools are used to narrow the field of potential candidates. Then the high fidelity tools to examine a chosen few. The question remains, why not find a way to exploit the benefits of both from the beginning of preliminary design. Novel methods of using both low and high fidelity analysis together in the search for optimal designs in the high fidelity domain have not been exploited in rotor design.

The time required to use even the most efficient coupled CFD/CSD analysis dictate that using these tools alone to search for more optimum designs is not practical. Thus utilizing both low and high fidelity rotor analysis tools together as an integrated design tool is an area in need of further research. Even as computational power increases, the need to use different levels of analysis complexity in design optimization will most likely remain.

3.4 Research Questions

From the design optimization gaps mentioned above, two main research questions emerge related to this topic area. Both stem from the idea that a framework for optimization is needed that integrates the required disciplines of structures, aerodynamics, and aeroacoustics in a way that allows both low and high fidelity analysis tools to be synergistically utilized and applied to a rotary wing optimization problem.

RQ1:
What disciplinary analysis elements can be combined to form an efficient high fidelity CFD/CSD/AA simulation for application to rotary wing optimization?

Coupled CFD/CSD analyses have been shown to produce good estimates of blade loads and vibration even in conditions that produce localized events like blade vortex interaction (BVI). These analyses, however, can take many days to provide an answer. In addition, the CFD grids required may be difficult to create. Preliminary design optimization would require generating a new grid(s) for CFD/CSD analysis of each unique candidate design. The computational time and setup challenges have been a large reason why these types of methods have been avoided in the past. In contrast, they have mainly been used to model known rotors for which experimental data is available, such as the UH-60 Airloads Program. In this approach, the developers of the analysis methods can validate their process by comparing predictions with corresponding experimental results. Finding CFD/CSD methods that are efficient enough to be employed to investigate multiple designs configurations in a design study is obviously a natural next step that has been conducted for the research topic presented in this thesis.

RQ2:
In what way can low and high fidelity rotary wing simulations be used together in a process of rotary wing design?

Which designs – if analyzed by high fidelity analysis – will give us the best chance of correcting our low fidelity estimates near optimum regions in the design space? Can a combination of low and high fidelity experiments pinpoint true optimums faster than high fidelity alone, yet more realistic than low fidelity alone?

For each answer from the low fidelity analysis, there is a correction factor that could be applied to make the answer equal to that obtained using high fidelity analysis. Can this factor or scaling function be modeled and used effectively to solve an optimization problem?

Though simply stated, these research questions are complicated to answer due to the fact that rotary wing simulation is not a simple process. Yet attempting to answer these questions in this research has successfully led to the advancement of rotary wing design by achieving the following objectives.

3.5 Research Objectives

The core objective of this research is to create an integrated and automated high fidelity framework for rotary wing simulation for use in design and optimization studies. This framework should be capable of analyzing rotors in forward flight as well as hover flight conditions. A second objective is to also develop an integrated and automated low fidelity framework for rotary wing simulation for use in design and optimization studies. The third objective is to combine both frameworks together in a process of rotary wing optimization to solve the same problem. A final objective is to test these various frameworks and processes and document the findings in this thesis.

3.6 Enabling Technologies and Concepts

The research and methodology presented is made possible by a variety of enabling technologies and concepts. Below are a few of the reasons that the research has the required technologies in place to succeed.

3.6.1 **Design Frameworks**

The design framework ModelCenter® by Phoenix Integration [88] simplifies and automates the process of combining analysis together to form a larger simulation. Its main capability is the ability to instantiate each analysis tool as a component within a framework of other components, linking parameters common between them. In addition, ModelCenter® is equipped with various built in design tools like Design of Experiments, Surrogate Modeling, Optimization, and more.

3.6.2 **Hybrid RANS Solver for Rotary Wing Simulation**

An efficient rotorcraft CFD methodology and tool GT-HYBRID has been shown to be less computationally intensive when compared to OVERFLOW and other full 3-D Navier-Stokes CFD tools for rotorcraft. The efficiency is gained by using a hybrid of Reynolds-Averaged Navier-Stokes and full potential methods together. In its current version, GT-HYBRID is somewhat limited in its ability to capture local events such as Blade Vortex Interaction (BVI). However, the potential it offers as a relatively fast, high fidelity analysis tool capable of predicting airloads in forward flight accurately should be exploited in design.

The capability of GT-HYBRID to utilize multiple processors using Message Passing Interface (MPI) provides additional time savings. Time savings have been seen using up to 12 processors.

3.6.3 **Parallel Computing**

The research reported in this thesis is possible by having access to a cluster (or perhaps computational grid) of 128 processors. This computing capability gives this research the technology required to bring high fidelity analysis within the designer's reach. From an optimization standpoint, a cluster of computers can be very beneficial in examining a large number of separate designs in parallel, even if the individual codes themselves are not parallel. In the future, access to large parallel computing facilities to solve complex engineering problems will be more widespread. Thus any framework and design process developed to incorporate high fidelity simulation must be capable of utilizing this valuable asset.

3.6.4 **Multi-Fidelity Optimization**

Other fields of aerospace are seeing the benefit of using two or more levels of analysis fidelity during an optimization process. The basic idea is to use the low fidelity (faster) analysis to make steps towards the high fidelity optimum. Periodically, a check is made with the actual high-fidelity analysis. A correction factor is updated to make the low fidelity answer equal to high fidelity. Studies have shown [68] significant reductions in the overall time required to arrive at the high fidelity optimized answer by using both low and high fidelity tools together in a approximation model management framework.

The research required to develop the frameworks will be greatly aided by the enabling technologies and concepts just mentioned. Nonetheless, there are challenges seen at this time that will affect the direction of research or the way that it is performed.

3.7 Challenges

Meeting the research objectives requires overcoming numerous obstacles to produce the low and high fidelity frameworks and develop the methods required to use

them together in a process of rotor optimization. A few notable challenges to this research are given below:

3.7.1 **Analysis Tool Integration is not Trivial**

There exists many disciplinary analysis tools in academia and industry. However, integration of these various contributing analysis (CA) tools into a common simulation framework is not a trivial undertaking. Most CA's require a special input data structure. For instance, the aeroacoustics code PSU-WOPWOP requires pre-processing computer programs to be written to convert information from comprehensive codes and CFD codes to the format required by PSU-WOPWOP in order to make predictions of noise. This makes the process of integrating the various CA's into an automated framework tedious work.

The design frameworks mentioned as an enabling technology make this type of integration easier. However, they do not totally remove the burden of getting the correct information from one contributing analysis to another. Doing this requires a lot of setup time and debugging.

3.7.2 **High Fidelity Simulation is Time Consuming**

High fidelity 3-D Navier-Stokes CFD is a time consuming process even for the most efficient tool when compared to a low fidelity model that can be completed in less than and hour. This large time difference along with the desire of finding more than one optimum may require modifications to current ways of managing variable fidelity tools during optimization.

3.7.3 **Automated Grid Generation Required**

The use of CFD requires grid generation. Automating this process may be difficult as many times the grid must be manually adjusted by hand before it is trusted to deliver reasonable results.

3.7.4 **Parallel Optimization Strategies Required**

Although making use of the efficient GT-HYBRID rotorcraft CFD code on multiple processors provides considerable time savings when compared to other full 3-D Navier-Stokes CFD tools, the time is still on the order of days for a nearly converged CFD/CSD solution. This means that in order to make the best use of the processors available, multiple design cases should be executed simultaneously. This makes serial optimization strategies like gradient based search methods unattractive if the high fidelity framework is being used as a "black box" function. Instead, using the high fidelity framework in a Design of Experiments, grid search, genetic algorithm, or some other domain spanning method is better suited. This may provide a challenge in devising a methodology that truly uses high fidelity results in an optimization process.

While integration of analysis tools in general is challenging, most of these challenges deal specifically with the integration of high fidelity analyses into a simulation framework. The progression of the research follows an undeniable path of low fidelity integration first and high fidelity integration second. Though unforeseen at the time, this progression allowed various elements of the problem to be understood in a logical sequence, by learning with more simplified methods before progressing to higher fidelity simulations.

3.8 Chapter Summary

This chapter has set forth the stage for the research needed to advance the high fidelity simulation tools for rotary wing design. Several observations have been presented related to the state-of-the-art concerning rotor design and optimization utilizing physics-based analysis tools. Namely, rotary wing simulation is multidisciplinary and complex. Also, automating the process of candidate design simulation with high fidelity tools is a key to their use in optimization.

Another observation that is very significant to this research is the fact that regardless of the simulation fidelity used, accurate airloads prediction is difficult. However, higher fidelity aerodynamics – when applied as in a CFD/CSD process – have been shown to provide better predicted airloads when compared to using the simplified aerodynamic models available in most second generation comprehensive codes. Nonetheless, the literature is full of examples in the past where these second generation comprehensive codes have been useful in optimization.

For the most part, use of comprehensive codes in optimization has been limited to mostly structure related design variables. Though there have been cases of these codes being used in shape variable optimization. Simplification of the aerodynamic analysis does not provide the physics to capture all the effects that shape variable changes have on the design's performance.

Higher fidelity analysis using CFD for aerodynamics in a coupled CFD/CSD methodology has shown much promise but it is costly in terms of computational run time. This aspect clearly appears to be a reason that there is a lack of shape variable optimization. However, as the cost of processing run time goes down, more researchers are now beginning to use higher fidelity tools in their optimization processes. Still, most if not all of this emerging field of research is being focused on rotors in hover where CFD/CSD is known to be less effective and important than forward flight.

In other fields of aerodynamics, researchers are seeing benefit from using both low and high fidelity tools in concert to solve optimization problems. However, this has not been exploited in the rotary wing design sector yet.

These gaps and corresponding observations point to two research questions. One, "What disciplinary analysis elements can be combined to form an efficient high fidelity CFD/CSD/AA simulation for application to rotary wing optimization?" And two, "In what way can low and high fidelity rotary wing simulations be used together in a process of rotary wing design?"

These questions however lead to research aimed at creating integrated and automated frameworks (both high and low fidelity) for rotary wing simulation with capability to analyze rotors in forward flight as well as hover. These frameworks will ultimately be used in design and optimization studies. Together, these low and high fidelity frameworks can be used in a synergistic process of rotary wing optimization; solving the same problem.

Chapter 4

Preliminary Methodology and Results

4.1 Overview

The analysis of a rotor in flight is a very complicated problem and very dependent on the aerodynamic flow field. Tremendous research has been put towards accurately capturing this flow field through simulation with CFD in hopes of accurately predicting the loads experienced by the blades. This, in turn drives the accurate prediction of other characteristics such as vibration, performance, and noise. To date, however, this is a challenging field of research and simulations take a lot of time to set up and even more to complete. This facet has kept this level of analysis from seeing extensive use during optimization, where several or more simulations are required to examine even a small portion of design space.

Numerical rotor optimization is gaining popularity. Lower fidelity, non-CFD tools have seen much use in rotor optimization. And while not always providing accurate predictions of blade airloads, optimization efforts using these tools have led to better designs. A majority of these efforts however, involve only structure related design variables as the lack of high fidelity aerodynamic analysis makes the selection of specific shape related variables difficult.

In Figure 1-2 of Chapter 1, a notional sequence was shown where the rotor of the BO-105 is optimized through some process to improve its characteristics. For a computer based redesign process to realistically arrive at a truly feasible design with desired improvements, it must accurately consider all of the important constraints and allow an improved rotor blade to be designed in their presence. The research questions in the previous chapter reflect the need for a design methodology and framework that has the capability to capture the physics needed to lead the design process towards an optimized,

flyable design in the shortest time possible using either structure or shape related design variables.

In Section 4.2, a preliminary methodology is followed that uses a simplified physics based simulation in a process to redesign a rotor blade's tip shape and twist. The baseline rotor considered is the HART-I rotor [4]. A design framework is used to integrate and automate the comprehensive rotorcraft analysis code RCAS with the aeroacoustics code PSU-WOPWOP into a low fidelity, rigid blade framework. A design of computer experiments is performed. 2nd order Response Surface Equations of objectives are built and subsequently used to examine four million stochastically generated design variable combinations in a Monte Carlo Simulation. High fidelity tools are used to evaluate an optimum from this group. The evaluation reveals the optimum to exhibit better performance characteristics and reduced noise. An a posteriori examination of vibratory characteristics reveals the optimum produces more vibration in forward flight than the baseline. This highlights the need to consider vibration during the first phase using low fidelity tools.

An extension to the methodology of Section 4.2 is made in Section 4.3. In an effort to better select designs for future high fidelity analysis, additional low fidelity experiments are performed to improve the surrogate models. New surrogate models using 4th order Response Surface Equations are used to find optimums in each objective. These new optimum designs are checked in the low fidelity model and found to provide improved designs, but questions on global optimality still remain.

4.2 Preliminary Methodology

Research began under the assumption that integrating the low fidelity tools together first and performing optimization using this framework would be an appropriate start. The development of the high fidelity simulation could be done to check optimums picked ultimately from experiments performed with the low fidelity framework. This idea

was followed in the research performed in this chapter which has also been documented in References [89, 90].

This preliminary research follows the methodology of Figure 4-1. A parametric, low fidelity physics-based rotor design environment is automated to perform hundreds of computer experiments in a Design of Experiments (DOE). The data from the experiments is used to build 2nd order Response Surface Equations (RSE's) of the objectives. These surrogates are used in a Monte Carlo Simulation where millions of design points are evaluated. Pareto optimal points are identified. An optimum is selected from this Pareto set and investigated using high fidelity tools. Finally, the loop is closed as feedback from this process is used to update the lower fidelity model as required or as computational power allows the inclusion of fewer simplifying assumptions.

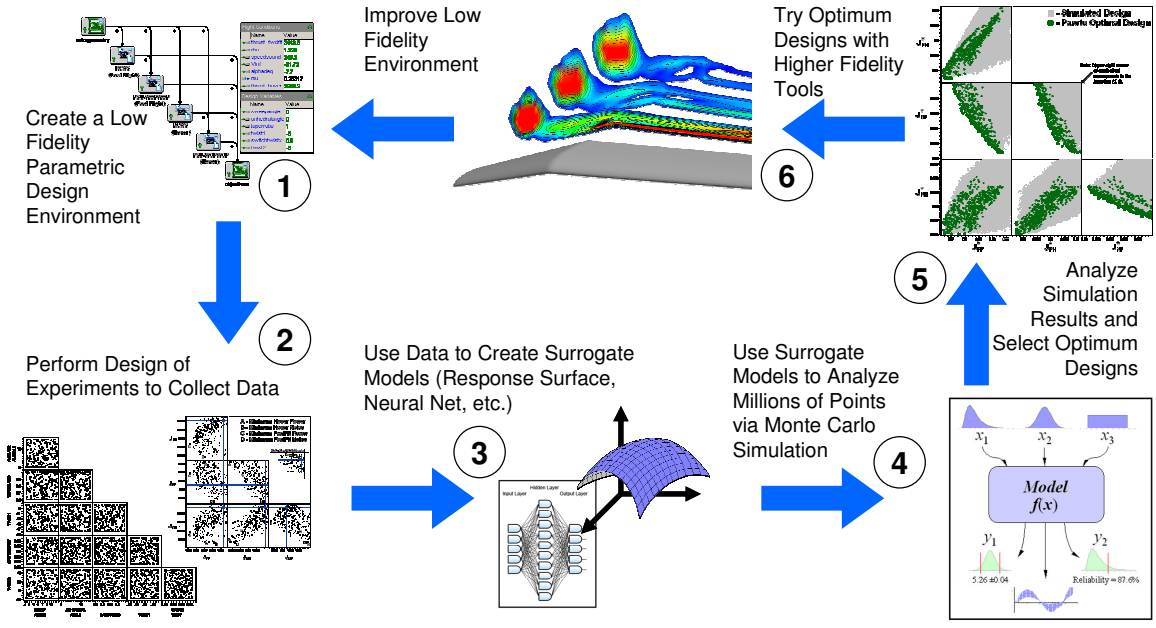

Figure 4-1: Preliminary Design Methodology

4.2.1 **Simplified Parametric Simulation**

To analyze designs in a reasonable amount of time, a parametric rotor simulation model is needed within an automated design environment. To avoid long computational times, a simplification is made to the process as shown in Figure 4-2. The simplified rotor is modeled assuming rigid blades for structures, quasi-steady table look-up for aerodynamics, and a prescribed wake inflow model. The rigid blade segments are given mass inertias and connected using hinges, springs, and dampers where appropriate to model the first flap, lag, and torsion natural frequency modes. The inflow model used for forward flight is the classical undistorted prescribed wake model. In hover, the Langrebe prescribed wake model is used.

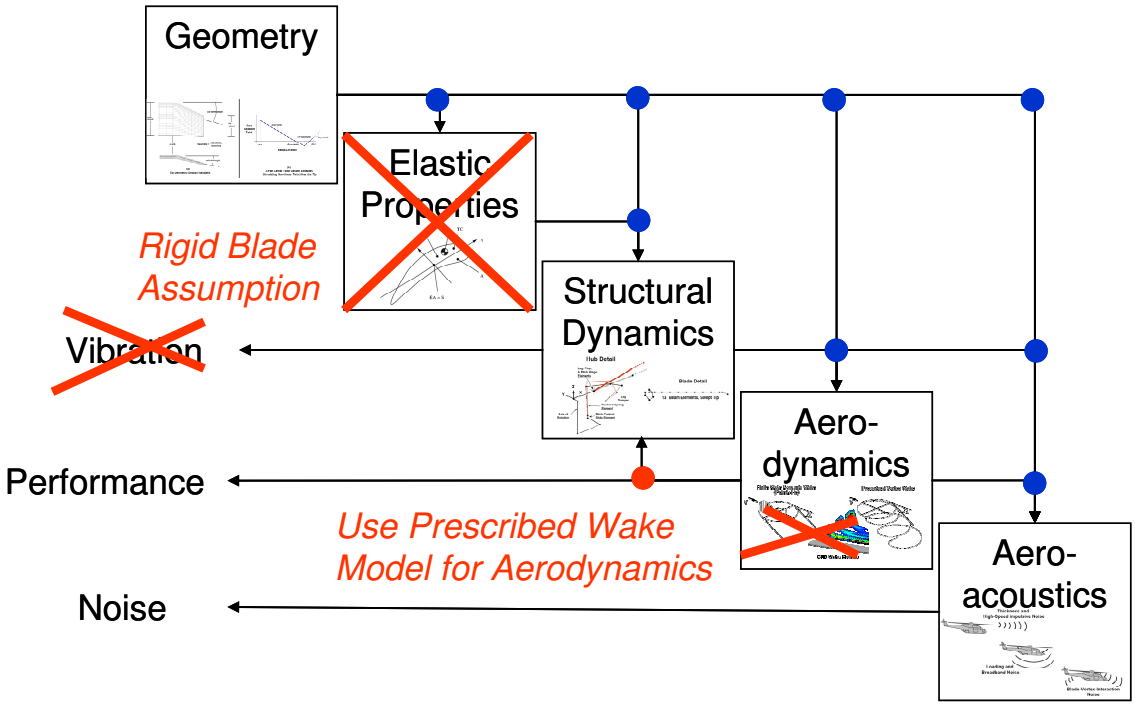

Figure 4-2: Simplified Multidisciplinary Process of Rotor Analysis

The analysis was performed using the integration of several tools. The geometry is calculated in an Excel® spreadsheet. This geometry spreadsheet is responsible for

calculating any parameters needed by other analyses as design variables or flight conditions are changed. The structural dynamics and aerodynamics are performed by the comprehensive code RCAS. Blade lifting line loads and motion from RCAS is connected with the aeroacoustics code PSU-WOPWOP. This tightly integrated system of analyses is shown in Figure 4-3.

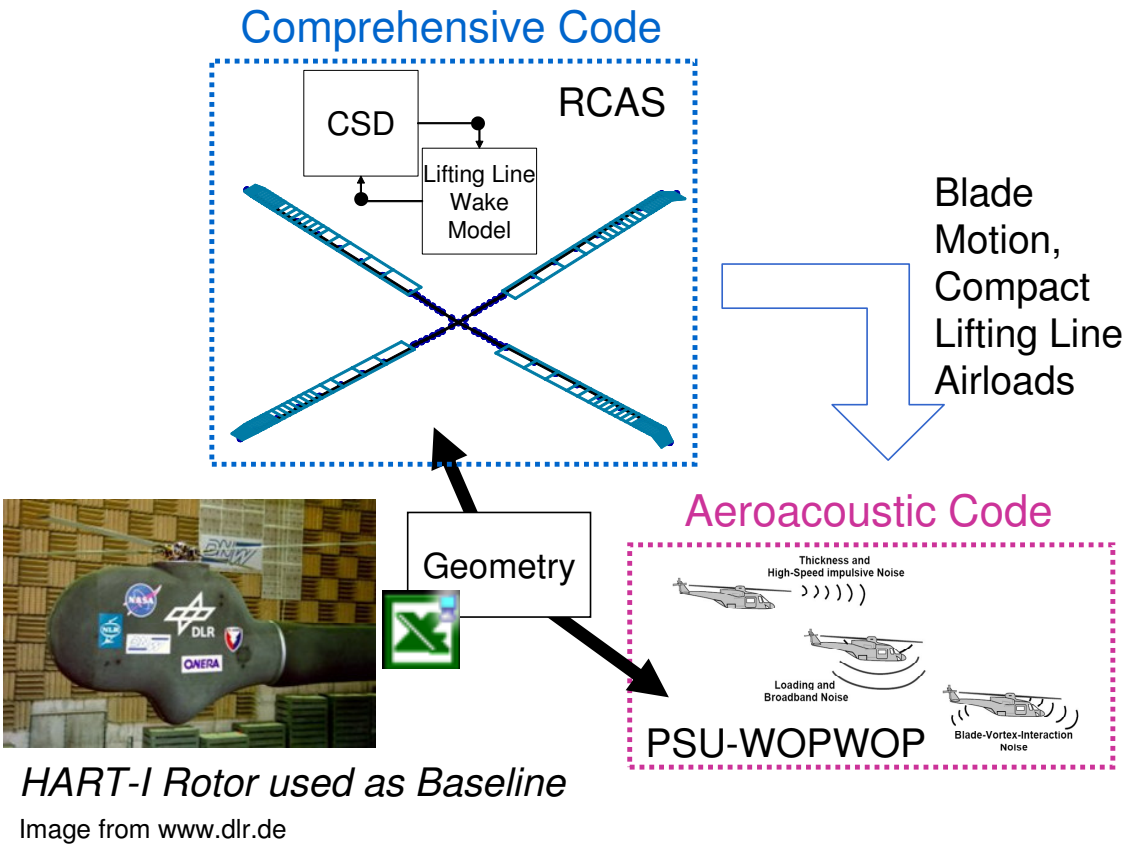

Figure 4-3: Low Fidelity Tool Integration

The RCAS model is made parametric and integrated with other analyses such as PSU-WOPWOP using ModelCenter® as shown in Figure 4-4. A scaled version of the BO-105 rotor is modeled as the baseline using structural data from the HART-I rotor tests [4]. For more information on this rigid blade RCAS model see Appendix A. The flight conditions of hover and forward flight are investigated for this model rotor with a rotor

speed of 110 rad/sec (Vtip = 220 m/sec [722 ft/sec]). Hover is performed at sea level and C_T/σ =0.08, while forward flight is performed at sea level with C_T/σ =0.06, a shaft tilt of 7.7 deg forward, and an advance ratio, μ=0.28. Parametric design variables include tip sweep, anhedral, and taper occurring in the last 5% of the blade span as shown in Figure 4-5 (a). Other design variables include those defining a two-part linear twist as shown in Figure 4-5 (b). Any number of shape variables and structural design variables could be used. There are an infinite number of ways in which the blade geometry alone could be parameterized. The purpose of choosing these six tip shape and twist design variables was to keep the number of design variables manageable and at the same time, to have a parameterization that could create design features of interest to the helicopter industry.

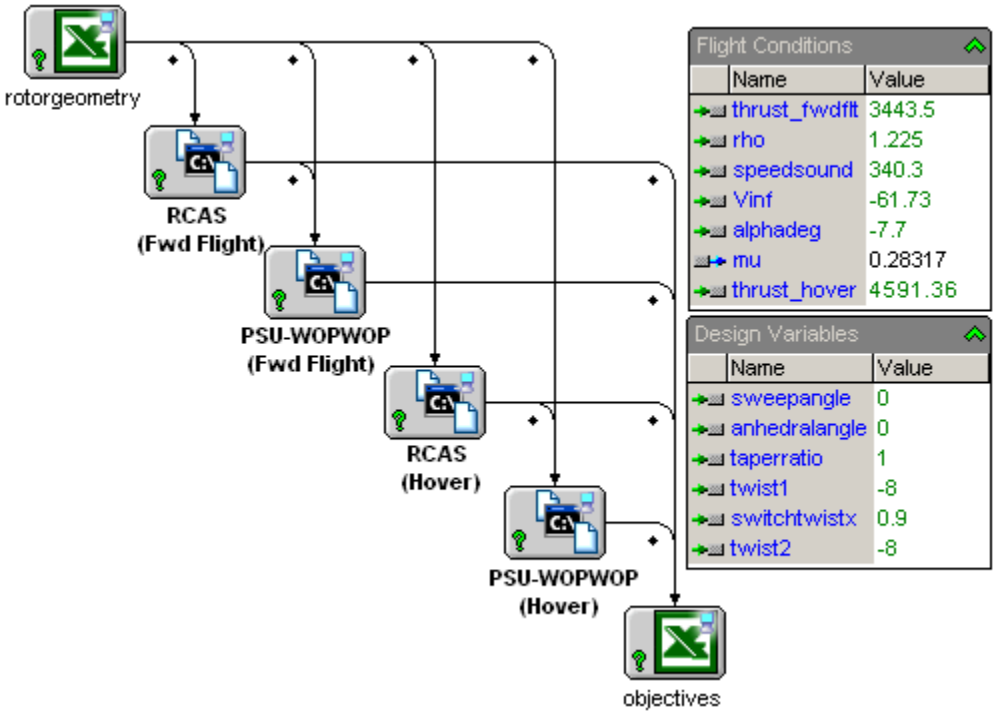

Figure 4-4: ModelCenter® Design Environment

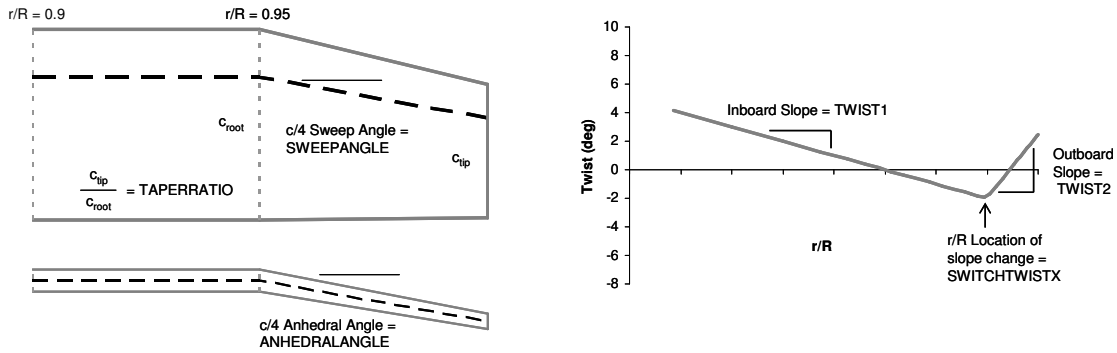

(a) (b)

Figure 4-5: Design Variables (a) Blade Tip Geometry and (b) Spanwise Twist

Compact, lifting line blade loads from RCAS are passed directly to PSU-WOPWOP within the design framework for noise predictions. An Excel® spreadsheet is used to calculate various parameters needed to update input files for RCAS and PSU-WOPWOP as design variable changes are made. As the tip geometry is changed, the thrust weighted solidity is kept constant by changing the root chord as necessary. This is done to keep the blade loading similar for maneuver and stall characteristics. The definition of thrust weighted solidity can be found in Leishman [19] and Prouty [91]. A variation of the equation by McVeigh and McHugh [92] to account for tip sweep is also described in Leishman. This definition of thrust weighted solidity is defined in equation 4-1 where $x = r/R$.

$$\sigma_e = 3\int_0^1 \sigma(x) x^2 \cos^2 \Lambda(x) dx \qquad \textbf{4-1}$$

Using this environment, various experiments can be performed to investigate how performance and noise compare to baseline values as changes are made to the various

design variables. Vibration is not tracked in this lower fidelity environment, and thus is not considered in the selection of an optimum. It will be shown with examination using higher fidelity analysis however, that tracking vibration and using it as an objective to reduce will make a more robust process since vibration is a major concern for both manufactures and users. In Chapter 5, this low fidelity environment is upgraded to include elastic blades.

The lower fidelity model was validated as much as possible by comparisons against the NASA full scale BO-105 rotor tests [93] and data from the HART-I model rotor tests [4]. A comparison of the rigid blade's first natural frequency modes compared with HART-I values is shown in Table 4-1. For forward flight, the general performance of the RCAS model using the classical prescribed wake with no distortion is compared with experimental results in Figure 4-6. The hover RCAS model using the Langrebe prescribed wake is compared with experimental in Figure 4-7. Reasonable agreement is found between the computations and measurements, taking into account the limitations of the low fidelity model.

Table 4-1: RCAS Rigid Blade Model Frequencies Compared with HART-I

HART-I Experimental Data Reported in Reference [4]

	RCAS*		HART-I	
	non-rotating	rotating	non-rotating	rotating
Flap	3.014	19.42	2.50	20.00
Lag	10.62	13.426	9.00	11.50
Torsion	55.454	58.087	65.5	67.5

* Rigid Blade Model

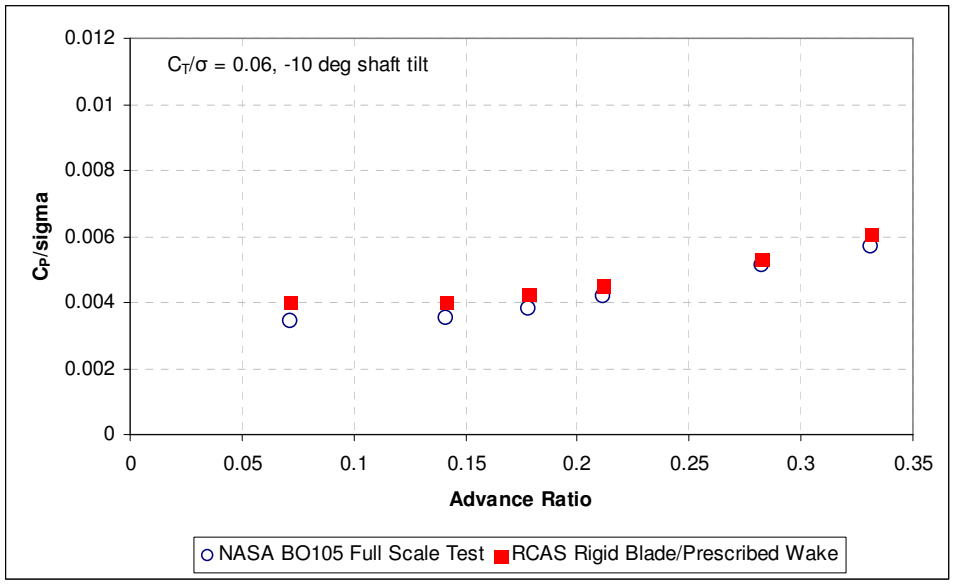

Figure 4-6: RCAS Rigid Blade Model Compared with Full Scale Test (Fwd Flt)

Experimental Data from NASA Full Scale BO-105 Rotor Test [93]

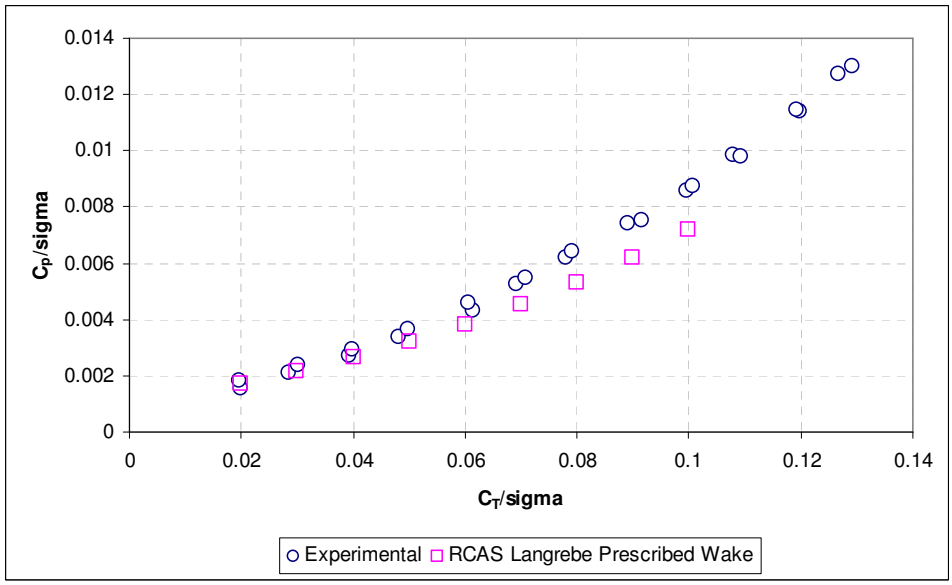

Figure 4-7: RCAS Rigid Blade Model Compared with Full Scale Test (Hover)

Experimental Data from NASA Full Scale BO-105 Rotor Test [93]

Objectives are chosen that compare the performance and noise of a particular design with respect to the baseline in both hover and a forward flight cruise condition.

Because the metrics define multiple objectives – noise and power – the general optimization problem can be defined as given in equation 4-2.

$$\text{Minimize: } \bar{J}(\bar{x}) = \begin{bmatrix} J_{PH}(\bar{x}) \\ J_{PF}(\bar{x}) \\ J_{NH}(\bar{x}) \\ J_{NF}(\bar{x}) \end{bmatrix} \qquad \textbf{4-2}$$

In equation 4-2, J_{PH} and J_{PF} are metrics for power required in hover and forward flight respectively. These metrics are defined by the value of C_P/σ in equations 4-3 and 4-4.

$$J_{PH} = \left\{ \frac{C_P}{\sigma} \right\}_{\text{Hover}} \qquad \textbf{4-3}$$

$$J_{PF} = \left\{ \frac{C_P}{\sigma} \right\}_{\substack{\text{Forward} \\ \text{Flight}}} \qquad \textbf{4-4}$$

J_{NH} and J_{NF} are metrics for noise in hover and forward flight respectively. Defining a single metric to measure noise in each flight condition is not as trivial. The strategy used was to average the overall sound pressure level (OASPL) over all locations of an observer grid. Trade studies were performed to identify the size and location of the observer grids for each flight condition.

In hover, a 4 point observer grid is used as shown in Figure 4-8. The observer grid for forward flight consisted of 16 points spread across a portion of a sphere three rotor radii ahead of the rotor center as shown in Figure 4-9. The points span from in plane to 60 deg below the rotor and 60 deg to the right and left of the forward flight direction

vector (Other positions could be used as well for the noise metric - with possibility the result may be slightly different.). The noise metrics J_{NH} and J_{NF} are thus defined as in equations 4-5and 4-6. This choice of noise metrics does not guarantee the noise will definitely go down at all locations, but rather the average noise must decrease.

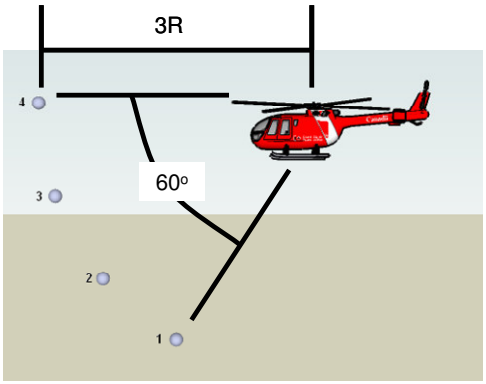

Figure 4-8: Hover Noise Observer Locations

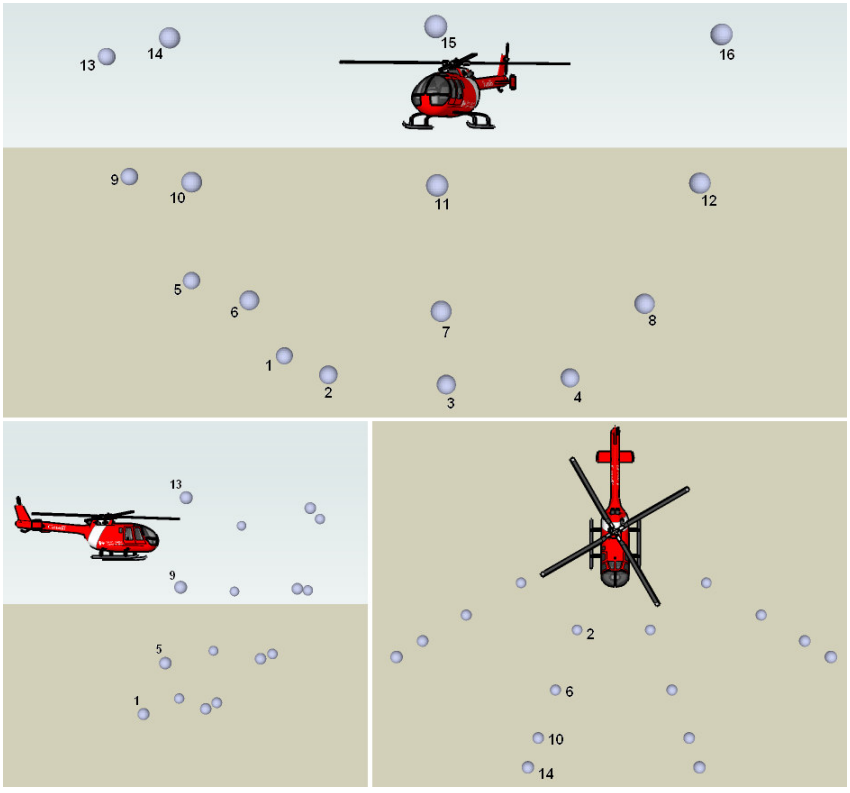

Figure 4-9: Forward Flight Observer Locations

$$J_{NH} = \sum_{i=1}^{4} OASPL(i)_{Hover}^{Total} \Big/ 4 \qquad \textbf{4-5}$$

$$J_{NF} = \sum_{i=1}^{16} OASPL(i)_{FwdFlt}^{Total} \Big/ 16 \qquad \textbf{4-6}$$

4.2.2 **Design of Experiments**

A Design of Experiments approach is used to examine a sample of the design space in an intelligent fashion so as to provide the data necessary to build the surrogate models. These models can then be used to investigate the sensitivities that each of the design variables has on the variability of both performance and noise in hover and forward flight. Table 4-2 lists the design variables and the ranges through which each is varied. There are various different methods used to sample the design space. In Step 3, the Design of Experiments given in Table 4-3 are used to build 2nd order Response Surface Equations (RSE's).

Table 4-2: DOE Design Variables and Ranges

Design Variables	min	max	baseline
c/4 Sweep Angle	0 deg	15 deg	0
Anhedral Angle	0 deg	15 deg	0
Taper Ratio	0.6	1	1
Twist1	-18 deg.	-8 deg.	-8
SwitchTwistx	0.85	0.95	0.9
Twist2	-18 deg.	45 deg.	-8

Table 4-3: DOE's Performed in Step 2

Test Description	# Runs	*Modeling*
Single Variable Trades	22	*Use to Build 2nd Order RSE's*
Minimum Entropy	200	
Sphere Packing	200	

Initial analysis of the data from Step 2 is made in Figure 4-10 where the data points can be compared to the baseline in each of the metrics given in equations 4-3 – 4-5. Points displayed in Figure 4-10 corresponding to minimum power and noise have design variable values listed in Table 4-4.

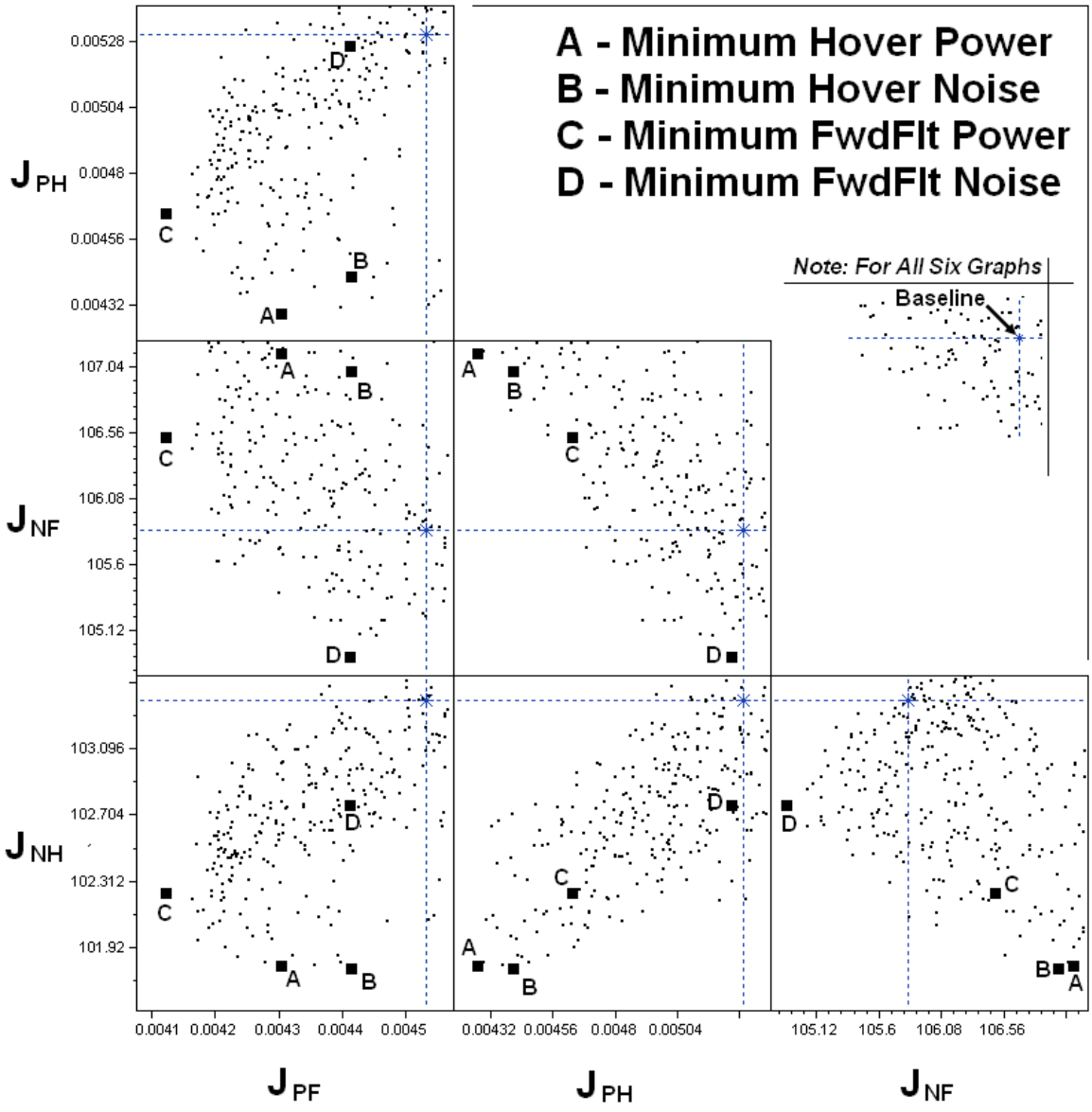

Figure 4-10: Data from Design of Experiments

Table 4-4: Design Points from DOE in Figure 4-10

Design Variables	A	B	C	D
c/4 Sweep Angle	0	7.71	15	0
Anhedral Angle	15	0	3.71	0
Taper Ratio	0.6	0.6	0.6	0.6
Twist1	-18.00	-18	-16.74	-8
SwitchTwistx	0.95	0.85	0.95	0.9
Twist2	11.53	-18	45	-8
	min hover power	*min hover noise*	*min fwdflt power*	*min fwdflt noise*

4.2.3 **Surrogate Modeling (2nd Order RSE's)**

Using data obtained from the 422 experiments performed using the environment of Figure 4-4, 2nd Order response surface models are constructed for the normalized metrics: J^*_{PH}, J^*_{PF}, J^*_{NH}, and J^*_{NF} with the statistical analysis software package JMP® [94]. The normalized metrics: J^*_{PH}, J^*_{PF}, J^*_{NH}, and J^*_{NF} are derived by dividing each metric given in equations 4-3 – 4-6 by the value of the metric when all design variables are set to the baseline value. The actual versus predicted plots for the 2nd Order RSE's are shown in Figure 4-11and Figure 4-12.

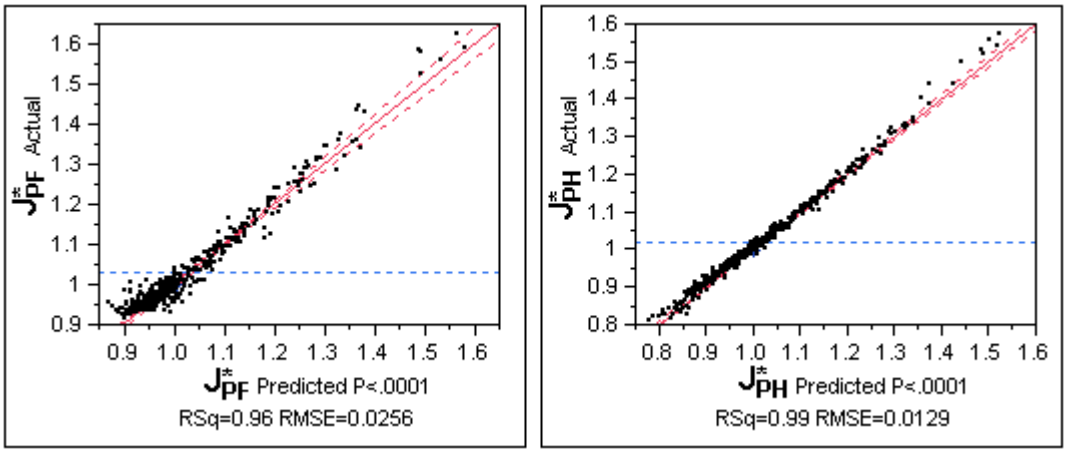

Figure 4-11: Actual versus Predicted Plots for 2nd Order Power RSE's

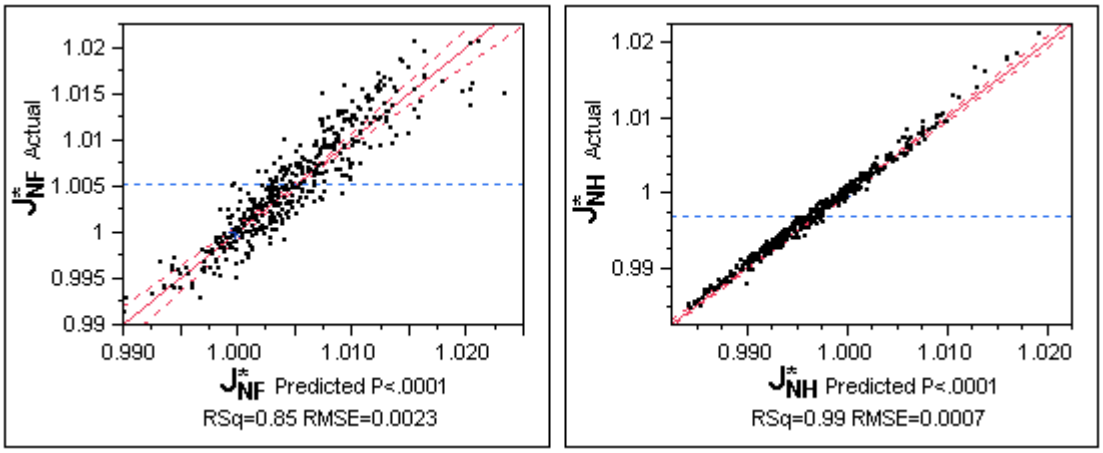

Figure 4-12: Actual versus Predicted Plots for 2nd Order Noise RSE's

Using these Response Surface Equations, sensitivities of the metrics to the design variables can be displayed in JMP® as shown in Figure 4-13, which shows the sensitivities from the baseline design.

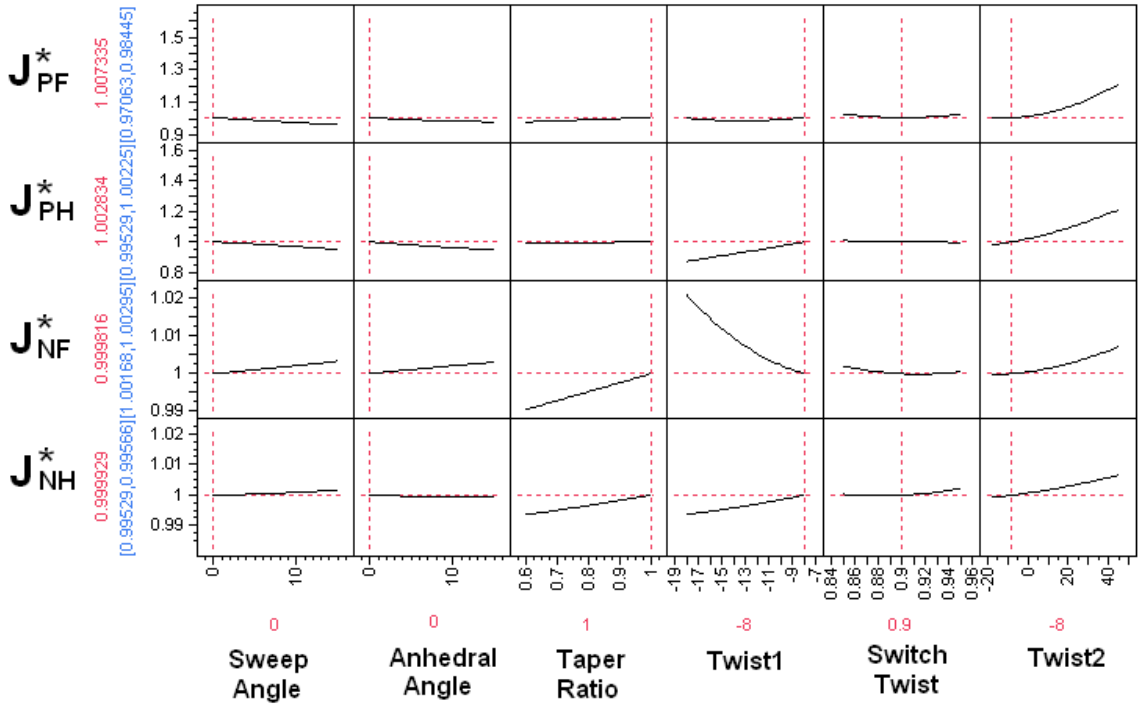

Figure 4-13: Response Surface Metric Sensitivities from Baseline using JMP®

4.2.4 **Monte Carlo Simulation**

In Step 4, a Monte Carlo Simulation is performed where four million randomly generated design cases are evaluated using the surrogate models. Because surrogate models are used, the process of calculating millions of randomly generated design points takes a few seconds on a single processor.

The Pareto Frontier of this problem is a hyper surface in four dimensions; power and noise in both hover and forward flight. As a continuous hyper-surface, this Pareto Frontier can contain an infinite number of points. Picking a single optimum on this surface is the goal of the designer. In order to do this, the designer will ultimately have to choose the relative importance of each dimension. Is reducing noise more important than reducing power? What about forward flight performance? The designer would like to have as much freedom in the design process as possible. The ability to make these types of trade-offs later in the design process gives the designer freedom. It also gives him the knowledge of how the design variable values change across the landscape of the Pareto Frontier.

In this work, the data from the Monte Carlo Simulation is filtered based on membership in the Pareto set[3]. If a design is a member of this set, then no other design has an objective that is better without making one or more of the other objectives worse. In Figure 4-14, the results of the Monte Carlo Simulation are shown. 588 designs were found to be Pareto Optimal and are shown in the figure as well. Because all Pareto optimal designs are shown in this figure, it is more difficult to picture a two dimensional frontier in each graph similar to that of Figure 2-5. This is because the Pareto Frontier is in more than two dimensions. These 588 points represent the optimal trade-off set for this

[3] MATLAB® functions used were front=paretofront(objMat) created by Yi Cao (y.cao@cranfield.ac.uk) and membership=isParetoSetMember(objectiveMatrix) created by Gianluca Dorini (g.dorini@ex.ac.uk)

simulation. Which objective is chosen for higher fidelity analysis would be up to the designer's discretion and obviously more than one design could be carried further.

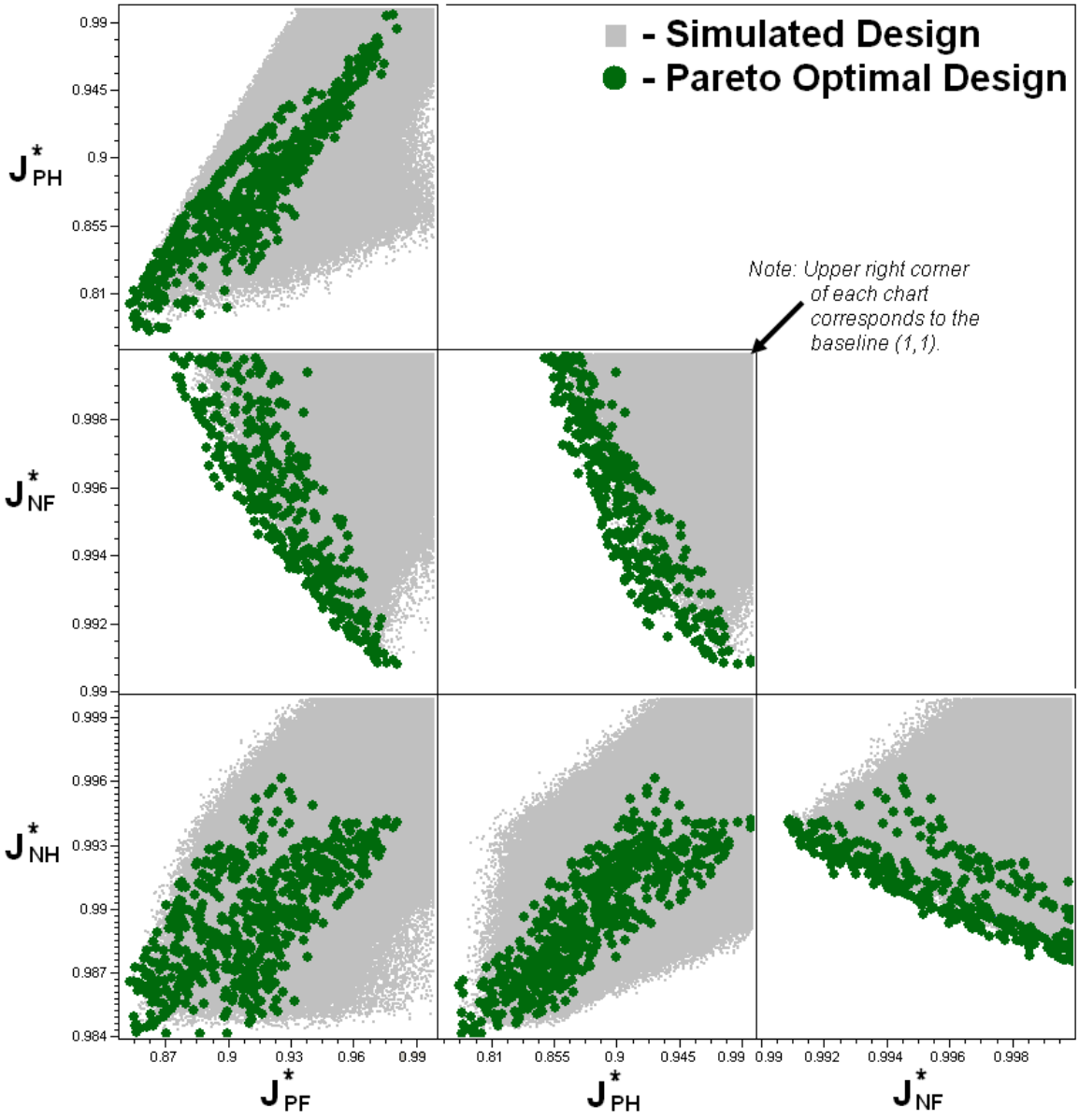

Figure 4-14: Monte Carlo Simulation Results

(With Pareto Set Identified)

4.2.5 **Selection of an Optimum Designs from Monte Carlo Results**

To bring the high fidelity analysis into play, a single design is picked from the set of Pareto optimal designs by finding which design has the minimum value for a weighted sum of normalized objectives as given in equation 4-7. A formal methodology of picking the weights used to select the next optimum design slated for examination with higher fidelity tools is a subject for future work. For now, the weights are picked arbitrarily to achieve a compromise of improvement in all objectives.

$$J^* = \alpha\left(J^*_{PH}\right) + \beta\left(J^*_{PF}\right) + \gamma\left(J^*_{NH}\right) + \delta\left(J^*_{NF}\right) \qquad \textbf{4-7}$$

Selecting an optimum in this manner is unconstrained. However, the optimization of a rotor is most definitely a constrained problem. Any real rotor redesign option would have to adhere to certain constraints. The author recognizes this and plans to address this in future work.

The optimum was selected using weights of $\alpha = 0.04$, $\beta = 0.04$, $\gamma = 0.22$, and $\delta = 0.70$. The optimum selected is thus entirely dependent on the values given to the weights. Without the heavier weights given to noise – forward flight noise in particular – designs having a minimum value of the objective were not better than the baseline in the category of noise. Various weights were tried until an optimum design was found which gave a good compromise of improvement in all four objectives.

The selected design is labeled optimum in the Monte Carlo results of Figure 4-15 along with the four designs having minimum values in each objective.

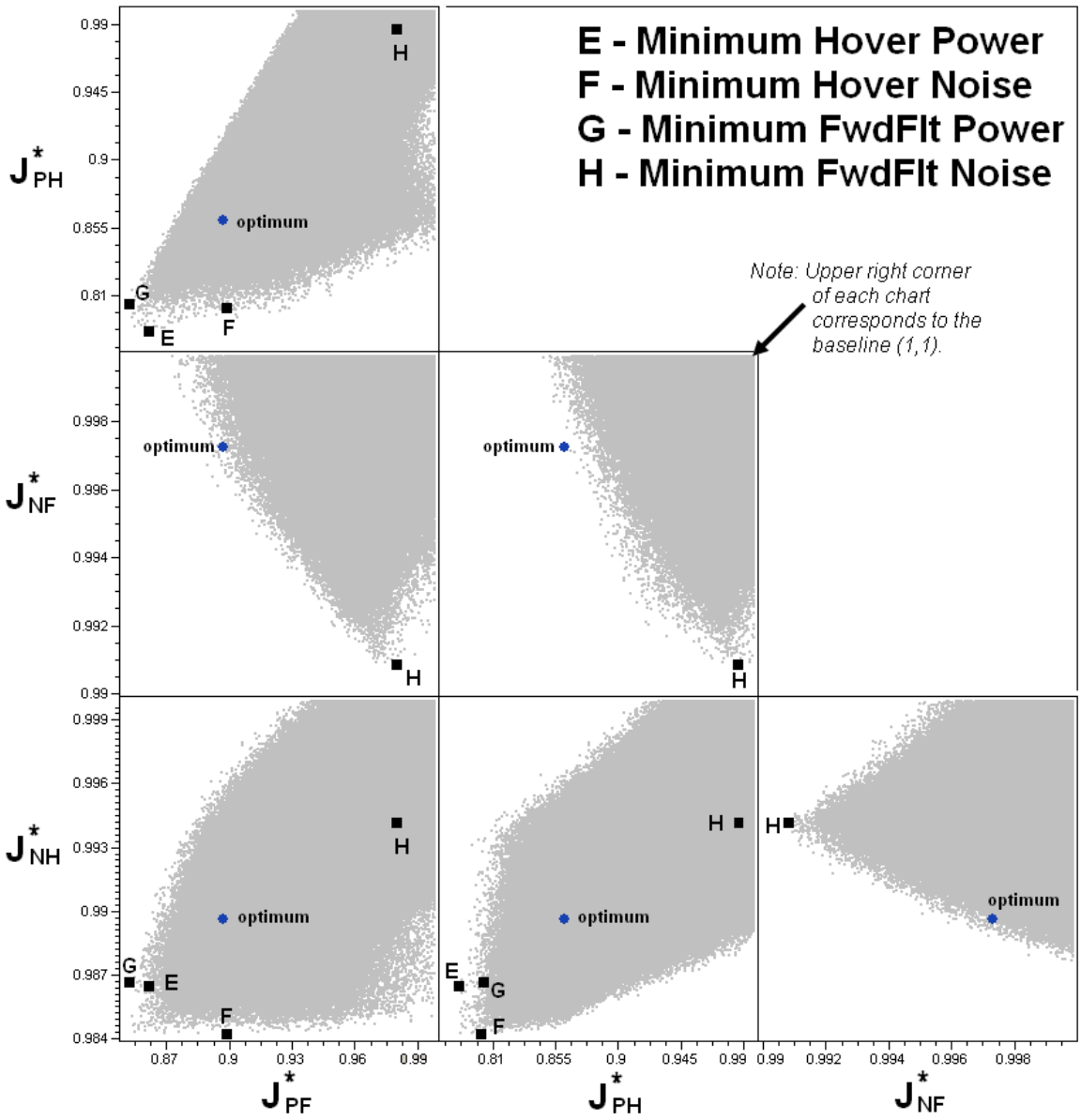

Figure 4-15: Monte Carlo Simulation Results

(with Pareto Anchors and Optimum)

These four designs (designs E-H) are referred to as Pareto anchor points since they mark the ends for each dimension of the Pareto Frontier. The design variable values of the designs in Figure 4-15 are given in Table 4-5. The tip shape of the design labeled optimum is displayed in Figure 4-16. Table 4-6 compares the low fidelity metric values

for both the baseline and the optimum. In the next phase, this optimum is compared to the baseline using higher fidelity tools.

Table 4-5: Pareto Anchors-Monte Carlo Simulation in Figure 4-15

Design Variables	E	F	G	H	optimum
c/4 Sweep Angle	0.31	0.15	14.44	0.96	0.19
Anhedral Angle	14.59	13.84	0.63	1.19	14.56
Taper Ratio	0.71	0.60	0.62	0.61	0.60
Twist1	-17.77	-17.90	-17.65	-8.05	-12.44
SwitchTwistx	0.95	0.93	0.95	0.93	0.95
Twist2	17.42	1.55	27.17	-5.36	14.99
	min hover power	*min hover noise*	*min fwdflt power*	*min fwdflt noise*	*good compromise*

Table 4-6: Low Fidelity Design Study Metric Values

Metrics	Baseline	Optimum	
J_{PH}	0.00531	0.00469	
J_{PF}	0.00454	0.00421	
J_{NH}	103.382	102.32	dB
J_{NF}	105.851	105.739	dB

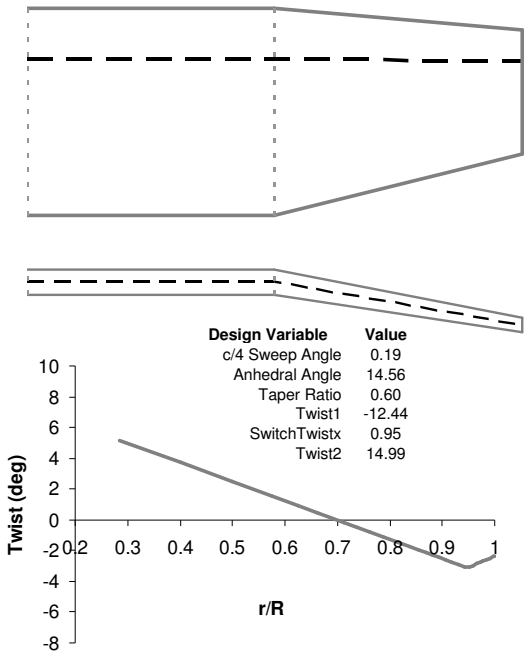

Figure 4-16: Optimum Design for Evaluation with Higher Fidelity Analysis

4.2.6 **High Fidelity Simulation of Point Design**

During the second phase of the design, an optimum selected using a form of equation 4-7 is examined with high fidelity CFD analyses. The examinations are performed at similar but slightly different flight conditions from the low fidelity DOE to make use of previously performed analysis runs. The rotor speed is set to 109 rad/sec (V_{tip} = 218 m/sec [715 ft/sec]). Hover is performed at sea level and C_T/σ =0.07, while forward flight is performed at sea level with C_T/σ =0.06, a shaft tilt of 7.7 deg forward, and an advance ratio, μ=0.28.

High fidelity hover analyses is done using TURNS assuming rigid blades. The results from TURNS are used by PSU-WOPWOP to calculate the noise at the same observer locations shown in Figure 4-8. The TURNS model was validated against the NASA full scale BO-105 rotor tests [93] and found to agree reasonably well as shown in Figure 4-17.

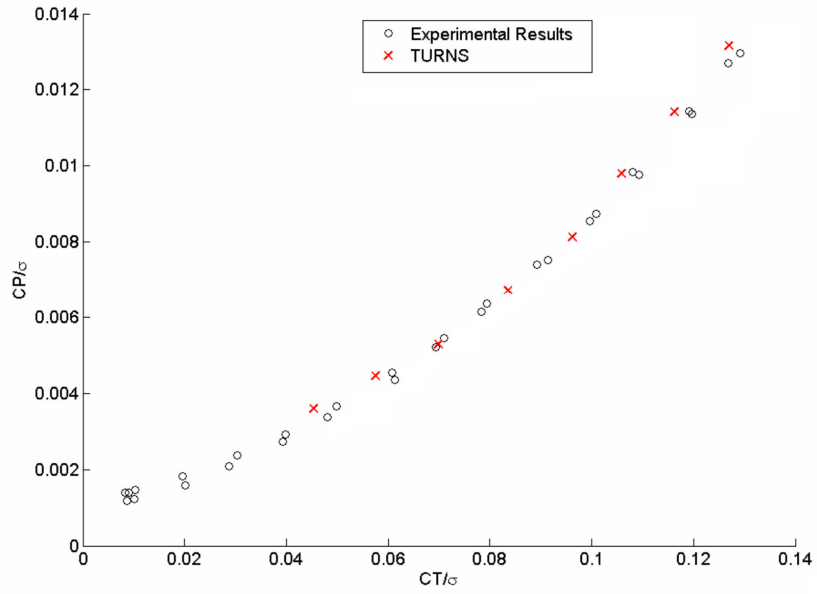

Figure 4-17: TURNS Validation with Experimental Results

Experimental Data from NASA Full Scale BO-105 Rotor Test [93]

To check the forward flight characteristics at a higher level of fidelity, a coupled CFD/CSD approach was used. The rotorcraft CFD code, GT-HYBRID is loosely coupled with the comprehensive code RCAS using an elastic blade RCAS model of the HART rotor from previous research [7] as depicted in Figure 4-18. Specifics about the RCAS elastic blade model of the HART-I rotor can be found in Appendix B and specifics about GT-HYBRID can be found in Appendix C. Blade surface pressures from GT-HYBRID are used as input to PSU-WOPWOP to predict the noise at the forward flight observer locations shown in Figure 4-9.

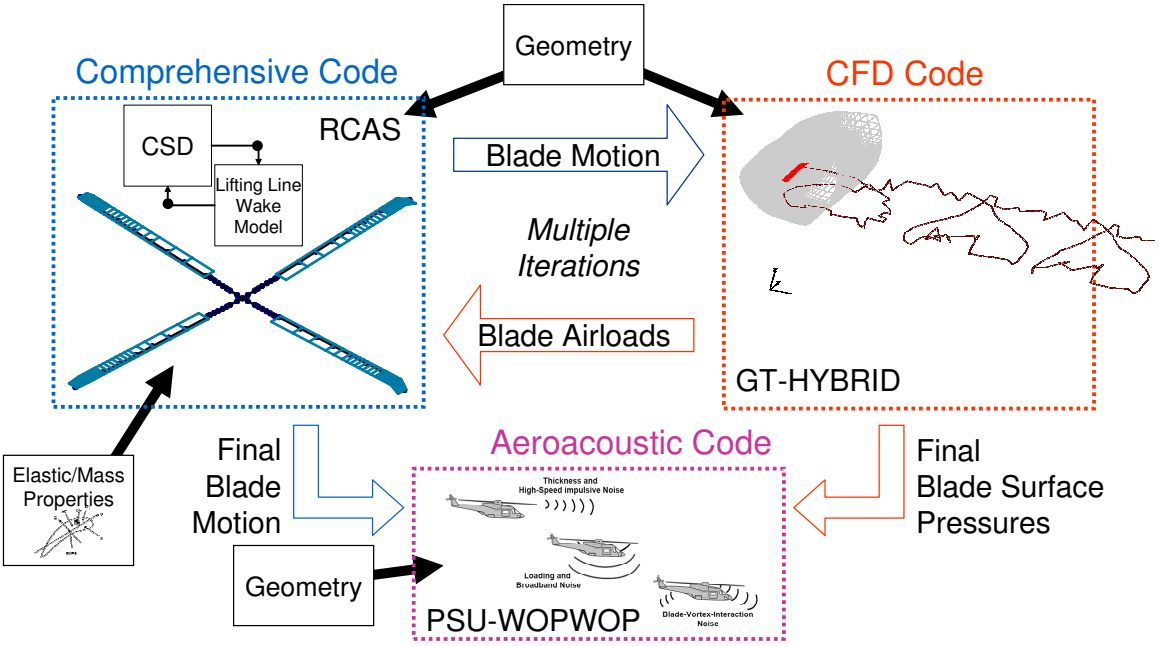

Figure 4-18: High Fidelity Forward Flight Tool Integration

GT-HYBRID was chosen due to its efficiency. A two revolution analysis with GT-HYBRID can be completed in about five hours when parallel processing is employed. Performing seven loosely coupled iterations (iterations 0 thru 6) with RCAS/GT-HYBRID takes about 40 hours to complete. This coupled approach using the hybrid methodology is more efficient computationally than coupled approaches that use

OVERFLOW and has a much simpler grid setup since only one grid surrounding the blade is required. This factor may lend this type of high fidelity analysis to be more useful in design studies since more design points can be analyzed in a given time frame, at least until computer processors are an order of magnitude faster than today's processors. A drawback to using GT-HYBRID is the current method it uses to compute the velocities imparted by the free wake vorticity makes it difficult to accurately capture local events like BVI in an efficient manner.

The loose coupling procedure used is shown in Figure 4-19 and is applicable to virtually all CFD and CSD capable comprehensive tools. The process follows a basic algorithm and begins with a comprehensive analysis tool performing a trim analysis of the elastic rotor with CSD and predicting the blade motion using simplified aerodynamics such as 2-D table look-up and uniform inflow. This motion is then input into the CFD which produces values for the trim targets as well as more accurate representations of the airloads (forces and moments) along the blade span. These airloads are compared with the airloads predicted by the CSD tool using lower fidelity aerodynamics. A "delta" airload is calculated and added to the CSD prediction and new blade motions are generated. CFD is then performed again with these new motions and the delta airloads calculated. This process is repeated until the CFD and CSD are converged to the same values for the trim targets. Once converged, the final blade motions and airloads can be input into an aeroacoustic tool to make predictions of noise. The AA in Figure 4-19 refers to noise prediction using an acoustic analogy (AA), like that used in PSU-WOPWOP.

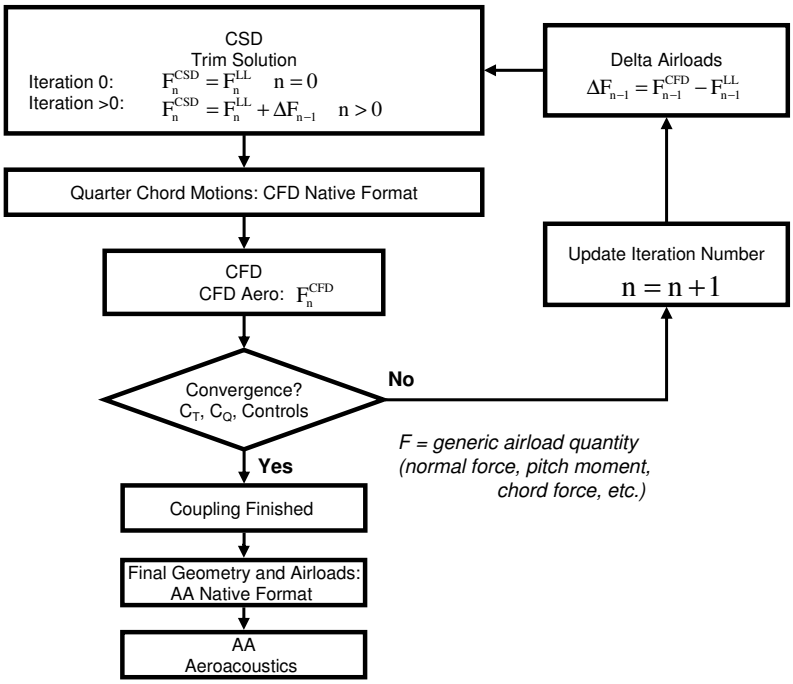

Figure 4-19: CFD/CSD Coupling Methodology with Aeroacoustic Analysis

Validation of the loosely coupled GT-HYBRID/RCAS for the baseline HART-I rotor was performed using two different experiments for comparison. First, the model was used to perform the descent condition of the HART-I dp140 rotor test [4], for which blade airloads are available for comparison. This validation can be seen in Figure 4-20. While the higher harmonics of BVI in the first and fourth quadrants are not captured well, the lower harmonics and airload magnitude are adequately predicted. Not capturing the BVI of a descent condition is not a major concern for this work, however, since only steady level forward flight is considered.

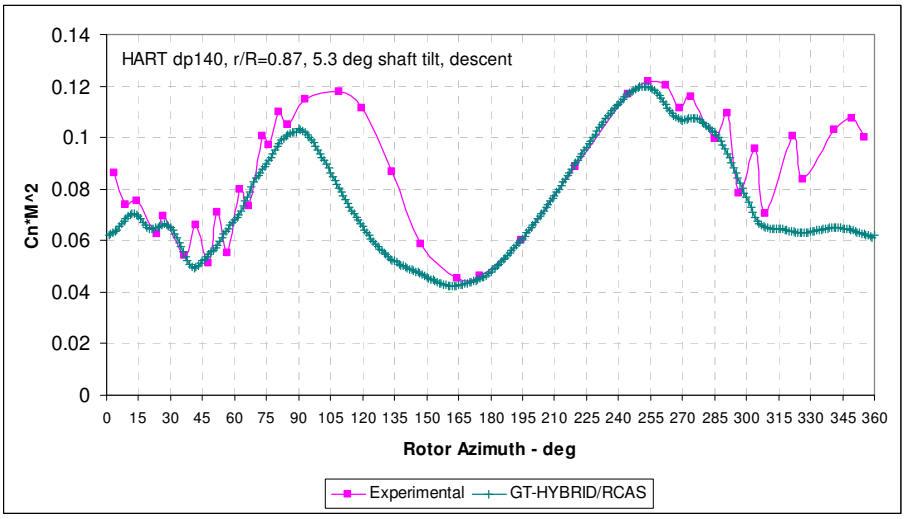

Figure 4-20: GTHYBRID/RCAS Model HART dp140 Experiment

Experimental Data from HART-I Rotor Test [4]

A more appropriate flight condition for this model is that of forward flight. For this validation, again the results from the NASA full scale BO-105 rotor tests [93] are employed. However, blade airloads are not available, so comparisons can only be made for performance only. This comparison can be seen in Figure 4-21 where very good correlation between model and experiment is made.

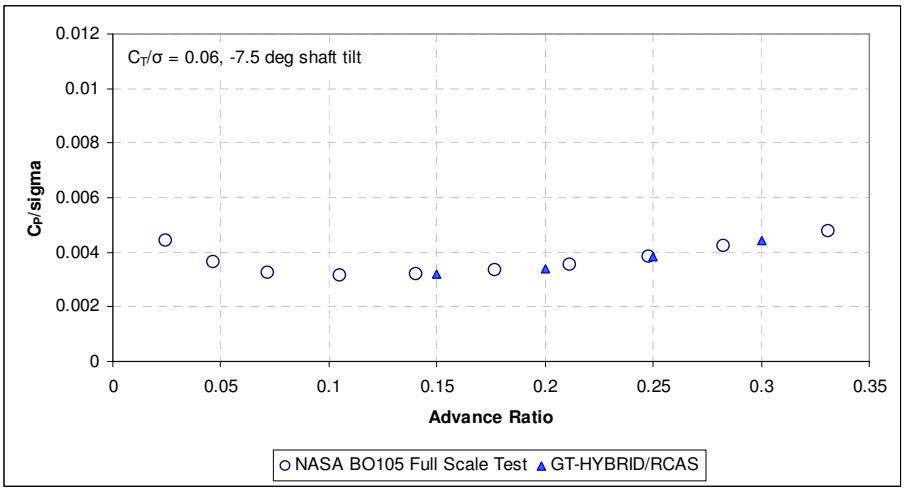

Figure 4-21: GTHYBRID/RCAS Model Compared with Full Scale Test (Fwd Flt)

Experimental Data from NASA Full Scale BO-105 Rotor Test [93]

The sectional properties of the baseline and optimum are required to model the elastic beam segments. This requires properties that vary along the span such as mass density, stiffness about each axis, radius of gyration, CG offset, and others. These values for the baseline HART-I rotor are known. With a detailed description of blade cross sectional dimensions, material, etc., a tool such as VABS could be used to predict the sectional properties of the optimum. For now, the sectional properties of the optimum blade are estimated from the baseline using the following assumptions.

The main difference between the optimum and the baseline rotors is in tip geometry and built-in twist at each aerodynamic section. The nominal chord length for the optimal varies slightly since thrust weighted solidity is held constant. The definition of the optimum's structural twist is altered for the aerodynamic sections of the span to represent the different built in twist. The sectional stiffness about each axis is assumed to be the same for the optimum as the baseline at all radial stations. While this assumption may be less accurate in the tip region, stiffness is not as important near the tip. Mass variation along the span is assumed to be more important near the tip. Since the design is changing at the tip, a method is needed to estimate the mass per unit length for each new design. The mass per unit length (MPL) is assumed to vary from the baseline value based on the square of the ratio of the local chord length to the baseline chord length as given in equation 4-8.

$$\mathrm{MPL}(r) = \mathrm{MPL}_{\mathrm{baseline}} \left(\frac{c(r)}{c_{\mathrm{baseline}}} \right)^2 \qquad \textbf{4-8}$$

For both the baseline and optimum configurations, seven loosely coupled iterations are performed. After the last iteration, various results can be investigated using both RCAS and GT-HYBRID. The high fidelity RCAS power required differed from the

GT-HYBRID power required. This occurred even though both produced similar values for the trim targets for thrust, pitch moment, and roll moment. Until we understand and resolve the discrepancies, high fidelity results for power in the following section correspond to values from GT-HYBRID because they were closer in value to results seen using the low fidelity RCAS model as well as results from full scale tests [93] for a similar flight condition.

As previously stated, the examination using higher fidelity tools is performed at similar but slightly different flight conditions to make use of previously performed analysis runs. In the tables where high fidelity results are presented, comparisons are made with the low fidelity model. To make this comparison, the low fidelity RCAS model in ModelCenter® is run at the same flight condition as the high fidelity analysis described above.

For the hover analysis, an interesting result is that the sound pressure levels predicted with high fidelity data were approximately 10 dB lower when compared to noise results from low fidelity data. The reason for this is unknown at this time, but the results are being looked at more closely in hopes of determining the reason.

The high fidelity analysis in hover was performed using TURNS. The optimized rotor consumed less power than the baseline rotor for the same thrust. Figure 4-22 shows the radial distribution of drag for the baseline and optimized rotor. The optimized rotor has more drag inboard due to the higher negative twist rate but produces significantly less drag outboard especially once the taper begins. The profile drag is also reduced because the rotor requires less collective to achieve the same thrust. Table 4-7 contains the performance metrics calculated using TURNS. The optimized rotor reduced the power required by approximately 5%. In a full scale BO-105, this results in reduced power by more than 20 horsepower. This improvement is slightly less than the 10% power reduction predicted with the low fidelity model. This power reduction allows for beneficial increases in payload or improved high/hot hover capability.

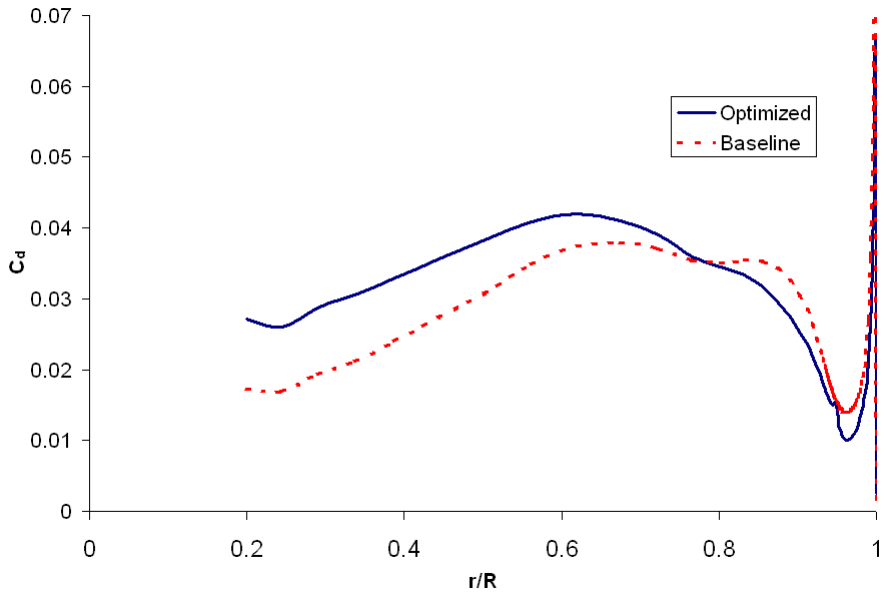

Figure 4-22: Sectional Drag of Baseline and Optimized Rotor in Hover from TURNS

Table 4-7: High Fidelity Hover Perf' Metric

(with Low Fidelity Comparison)

Hover		
Ct/sigma	0.07	
Cp/sigma (J_{PH})	**Baseline**	**Optimum**
High Fidelity	0.0053	0.0050
Low Fidelity	0.0045	0.0040

The total noise produced at the four hover observer locations is calculated by PSU-WOPWOP using the higher fidelity flow field information from TURNS. Table 4-8 lists the sound pressure level at the observer points for hover and the average value. While the low fidelity model predicted a 1.1 dB reduction in the average total OASPL from the baseline for the optimum, the high fidelity results predict only a 0.2 dB reduction.

Table 4-8: High Fidelity Hover Noise Metric

(with Low Fidelity Comparison)

Hover	High Fidelity Baseline	High Fidelity Optimum	Low Fidelity Baseline	Low Fidelity Optimum	
J_{NH}	114.30	114.10	102.07	100.99	dB
Pt 1	*111.688*	*111.539*	*97.866*	*97.672*	*dB*
Pt 2	*115.625*	*115.362*	*101.228*	*100.785*	*dB*
Pt 3	*116.547*	*116.183*	*98.684*	*97.022*	*dB*
Pt 4	*113.329*	*113.330*	*110.520*	*108.470*	*dB*

Optimum Louder at Observer Location

Optimum Quieter at Observer Location

Table 4-9 compares the performance metrics in forward flight. The high fidelity results indicate the optimum has a 2% reduction in power required relative to the baseline. This is close to the 5% predicted by the lower fidelity model.

Table 4-9: High Fidelity Fwd Flt Perf' Metrics

(with Low Fidelity Comparison)

Forward Flight		
Ct/sigma	0.06	
Cp/sigma (J_{PF})	Baseline	Optimum
High Fidelity	0.00424	0.00417
Low Fidelity	0.00464	0.00443

The forward flight high fidelity noise metrics are compared in Table 4-10. In this case, the high fidelity results predict the optimum has noise reduced by 1.89 dB compared to only 0.27 dB reduction predicted by the low fidelity model.

Table 4-10: High Fidelity Fwd Flt Noise Metrics

(with Low Fidelity Comparison)

Forward Flight	High Fidelity Baseline	High Fidelity Optimum	Low Fidelity Baseline	Low Fidelity Optimum	
J_{NF}	106.02	104.13	105.17	104.90	dB
Pt 1	106.483269	104.484825	105.52	105.65	dB
Pt 2	106.910126	105.033356	106.08	106.18	dB
Pt 3	105.476181	103.891991	103.21	102.04	dB
Pt 4	104.032486	101.414795	107.21	105.14	dB
Pt 5	109.248611	107.085838	107.30	107.97	dB
Pt 6	109.118896	108.346756	109.11	109.43	dB
Pt 7	103.93647	103.418594	109.17	108.56	dB
Pt 8	103.721436	99.430786	108.88	105.97	dB
Pt 9	109.96405	107.796013	105.30	106.90	dB
Pt 10	111.4776	110.549431	106.82	107.67	dB
Pt 11	103.997208	103.336647	106.98	106.83	dB
Pt 12	96.944046	92.073944	103.38	100.50	dB
Pt 13	108.061478	107.532417	101.47	104.23	dB
Pt 14	109.367249	107.737465	101.93	102.88	dB
Pt 15	108.118507	106.523445	99.54	97.81	dB
Pt 16	99.512573	97.502373	100.83	100.68	dB

Optimum Louder at Observer Location

Optimum Quieter at Observer Location

The results in Table 4-9 and Table 4-10 are different from those presented in References [89] and [90] due to an error that was found in the GT-HYBRID grid file used for the results published in those papers. In addition to the changes in the grid file, the high fidelity work presented in these tables (both baseline and optimum) uses the HART-II rotor as a baseline as opposed to the HART-I rotor which was used in the aforementioned papers. Though very similar, the HART-I and HART-II rotor blades differ in where the zero twist location is on the span. The low fidelity results presented in Table 4-9 and Table 4-10 are based on a HART-I model. The HART-II rotor was used in the new methods and results presented in Chapter 5 as this is the HART rotor currently being analyzed in industry, so it was felt that this was the rotor that should be used as the baseline. Because it was decided to rerun the optimum case from preliminary research

due to the error in the original grid file, this was done using the latest framework which had the HART-II rotor as a baseline.

Although the performance and noise predictions using high fidelity analysis show improvement with the optimum, a look at vibration reveals a drawback. Figure 4-23 shows the vibratory vertical hub loads for both the baseline and optimum. It is clear from this chart that the optimum vibrates more than the baseline at this flight condition. It is believed that this is a result of the larger negative inboard twist rate of the optimum, causing blade stall.

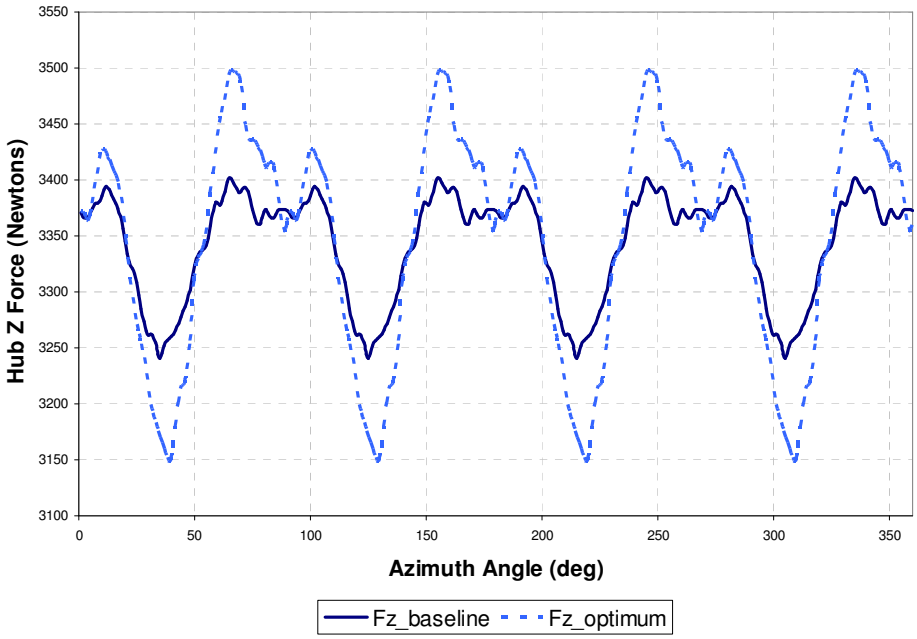

Figure 4-23: Baseline and Optimum Hub Z-Force History in Forward Flight

The methodology presented previously in Figure 4-1 provides a way in which many designs can be evaluated in a short amount of time. Picking candidate optimums found with lower fidelity tools and surrogate models is an efficient way to bring the higher fidelity tools into action. However, aside from the problems with using rigid

blades as mentioned above, there are some questions related to the surrogate modeling of the low fidelity framework that must be asked.

The Monte Carlo Simulation method used provides a quick and easy way to randomly investigate a large portion of the design space. Because of this, it can be used to visually inspect the Pareto Frontier, assuming that points on the frontier or near the frontier are found through this random process. However, the random process does not guarantee that global optimums will be found. To illustrate this, the 2nd Order surrogate models were used in a genetic algorithm to find the minimums in each objective. These optimums found were then added back to the Monte Carlo Simulation data set to see if the designs were indeed better. Figure 4-24 shows the results. It is easy to see that the genetic algorithm does a much better job of finding the optimums of the surrogate than Monte Carlo Simulation. This could be due to a number of factors. Perhaps the type of distribution for each variable in the Monte Carlo Simulation could be selected differently to better seek out optimum designs. Also, the Monte Carlo Simulation uses somewhat of a shotgun approach. This is evident by noticing that there is a much higher density of points away from the Pareto Frontier. This means that there is less likelihood that the random nature of the Monte Carlo Simulation will find a true optimum on the frontier.

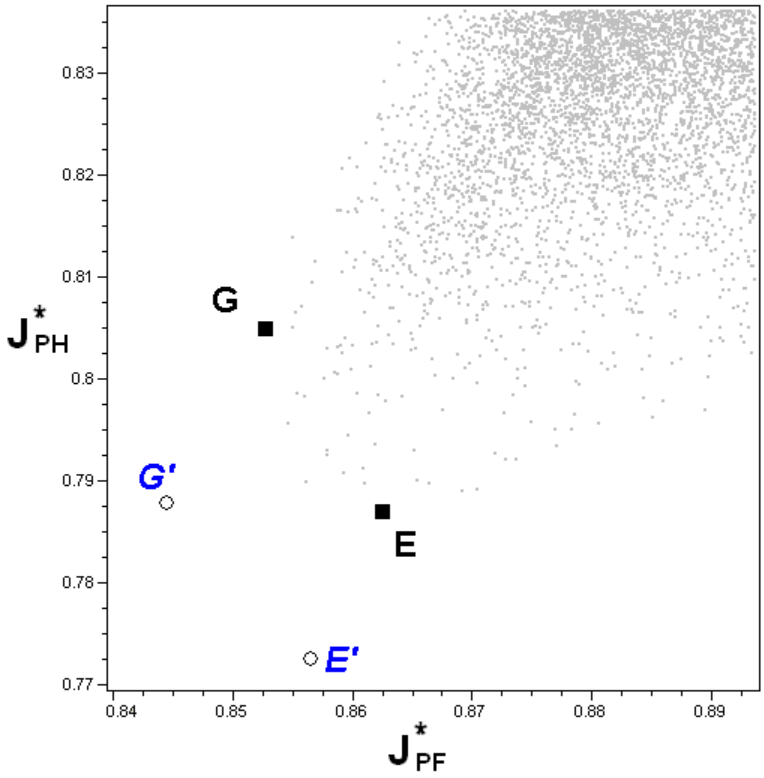

Figure 4-24: Genetic Algorithm versus Monte Carlo Simulation Optimums

The points in Figure 4-24 labeled G and E are the Pareto Anchor designs shown previously in Figure 4-15 and listed in Table 4-5. The optimums found using the Genetic Algorithm corresponding to these same anchor designs are shown as G' and E'. The design variables for these more optimum designs are given in Table 4-11. Still however, these designs only reflect the optimums of the 2nd Order surrogates which may not be as accurate as a higher order model.

Table 4-11: Optimums Found using 2nd Order Surrogates and Genetic Algorithm

Design Variables	E'	G'
c/4 Sweep Angle	0	15
Anhedral Angle	15	0
Taper Ratio	0.6	0.6
Twist1	-18	-18
SwitchTwistx	0.95	0.95
Twist2	17	29
	min hover power	*min fwdflt power*

Due to these findings, an extension to the preliminary methodology of Figure 4-1 is performed in Section 4.3. This extension moves away from Monte Carlo Simulation and focuses more on various other optimization techniques such as gradient based search, evolutionary (genetic) algorithm, and structured grid search. In addition, more low fidelity experiments are performed to build 4th order surrogate models which more accurately represent the objective values of the low fidelity framework.

4.3 Extension to Preliminary Methodology

The preliminary methodology presented in Section 4.2 was successful in screening designs with low fidelity tools, selecting an optimum, and evaluating this optimum with high fidelity tools. The research presented in Section 4.2 and here (Section 4.3) were combined in Reference [90].

In this extended work described here, additional low fidelity experiments were done to enrich the original database. More accurate surrogates could be built using the larger low fidelity data set. Then making comparisons between the "optimal" results of more accurate RSE's and the actual low fidelity model would provide some interesting insight that might help understand the larger problem of relating low and high fidelity results as this work proceeded toward a high-fidelity helicopter rotor redesign framework.

The extension to the methodology of Figure 4-1 is shown in Figure 4-25. In this process, the Pareto Optimal points found using surrogates were filtered to create a "First

Pareto Guess" set by including only those better than the baseline. This "First Pareto Guess" group of designs became the next set of experiments to be performed by the original low fidelity physics-based rotor design environment. In addition, the environment also was used to perform a Central Composite Design of Experiments. Using this now larger data set of low fidelity runs, more accurate, 4th order surrogate models were built. These new surrogates were then used in several different optimization schemes to find newer optimum designs. These optimums were checked using the low fidelity analysis to see how the new surrogates were performing and if they were indeed finding optimal points. Some interesting points are discussed in the results section.

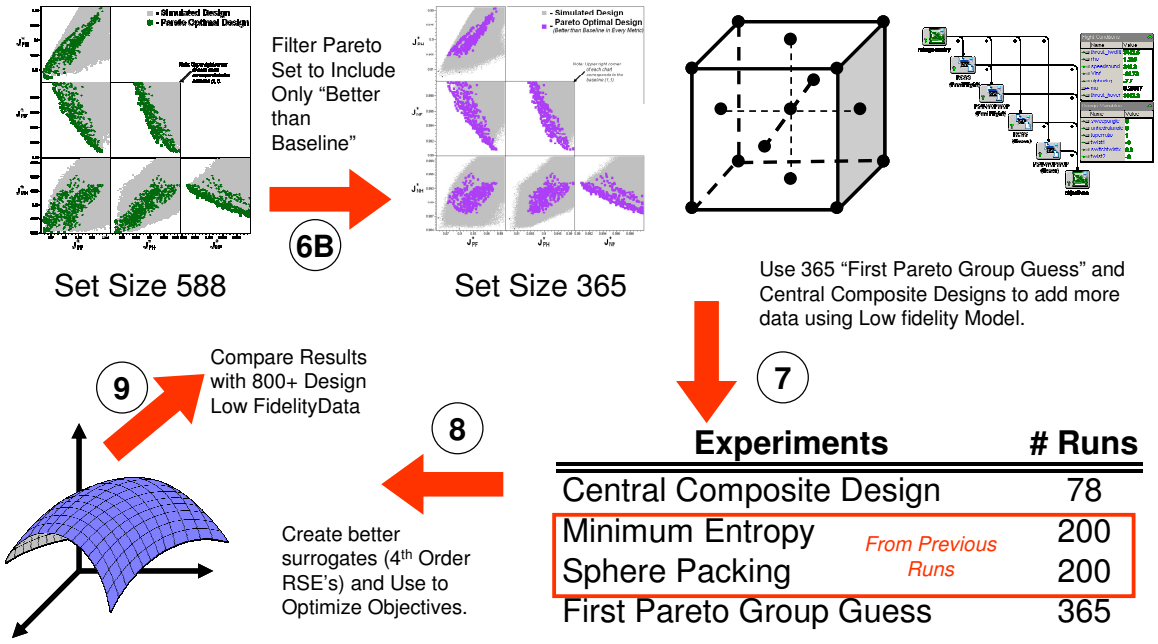

Figure 4-25: Extension of Design Methodology

4.3.1 **Low Fidelity Database Enrichment**

To begin to understand how information from various fidelity levels can be compared and used to enhance the lowest fidelity models, recent work focused on selecting designs to be checked with the original low fidelity model. In the process, the

database of rigid blade/prescribed wake low fidelity model was enriched with 400+ additional designs. 365 of these were determined using the data from the Monte Carlo Simulation of Step 5. In addition to being filtered for Pareto optimality, a second filter (Step 6B) is added to keep only designs better than baseline in all metrics as shown in Figure 4-26.

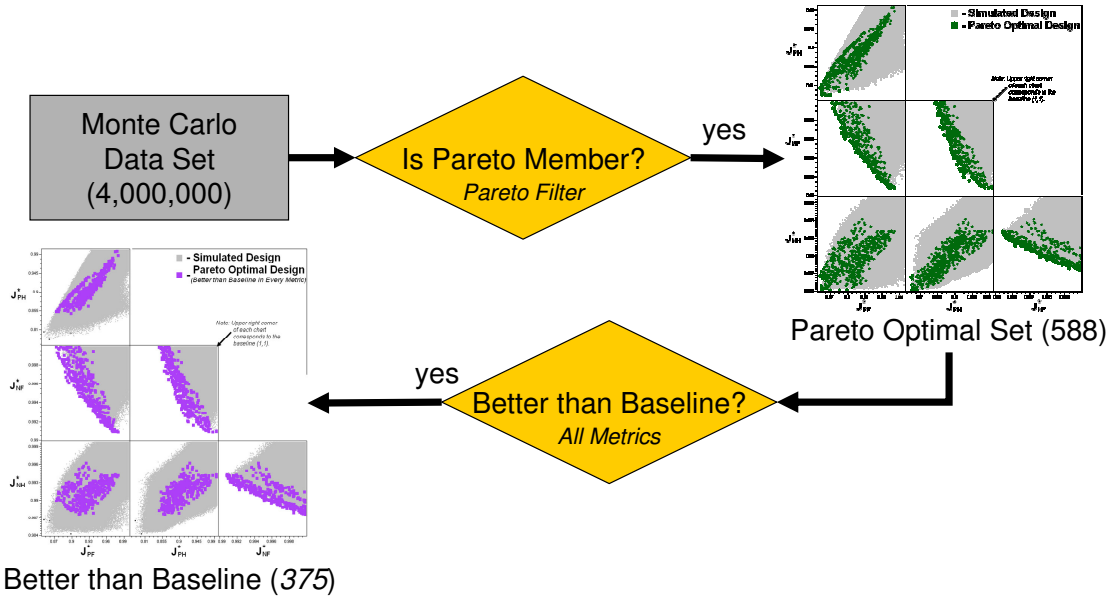

Figure 4-26: Filtered Selection of Pareto Group Guess

An additional 78 designs were evaluated using a Central Composite Design of Experiments. Table 4-12 lists the data used in creating more accurate 4th Order RSE's.

Table 4-12: New Composition of the Low Fidelity DOE's

Test Description	# Runs	*Modeling*
Central Composite Design	78	*Use to Build 4th Order RSE's*
Minimum Entropy	150	
Sphere Packing	150	
First Pareto Group Guess	319	
Minimum Entropy	50	*Use to Check Model Representation Error*
Sphere Packing	50	
First Pareto Group Guess	50	

4.3.2 **Surrogate Modeling (4th Order RSE's)**

Using the data collected in the DOE's listed in Table 4-12, 4th order polynomial based Response Surface Equations were created and shown to have improved accuracy over previous 2nd order models. The statistical analysis of the data using stepwise regression was performed using an automated RSE generator that works with MATLAB® [95] called STARS [96]. The value from the surrogate models are compared to the values calculated in the low fidelity framework. Plots of the values and residuals are shown in Figure 4-27 through Figure 4-30.

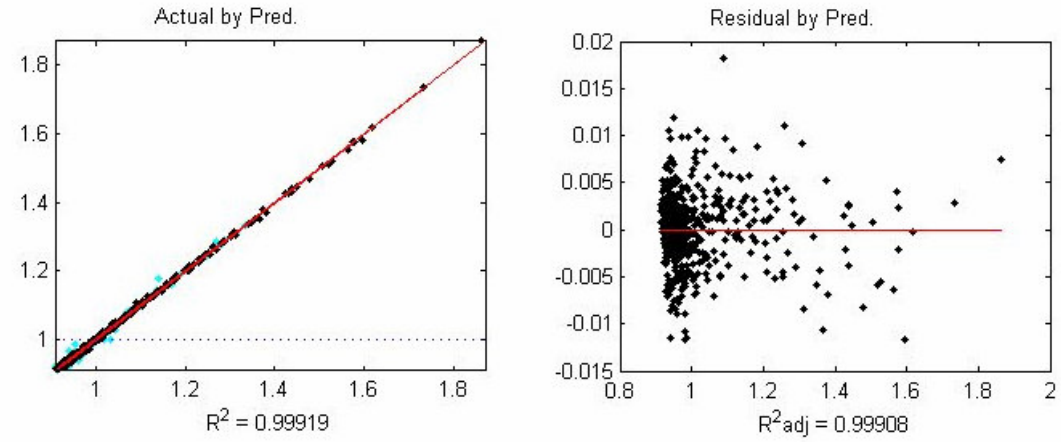

Figure 4-27: 4th Order RSE Model fits for Fwd Flight Power (J_{PF})

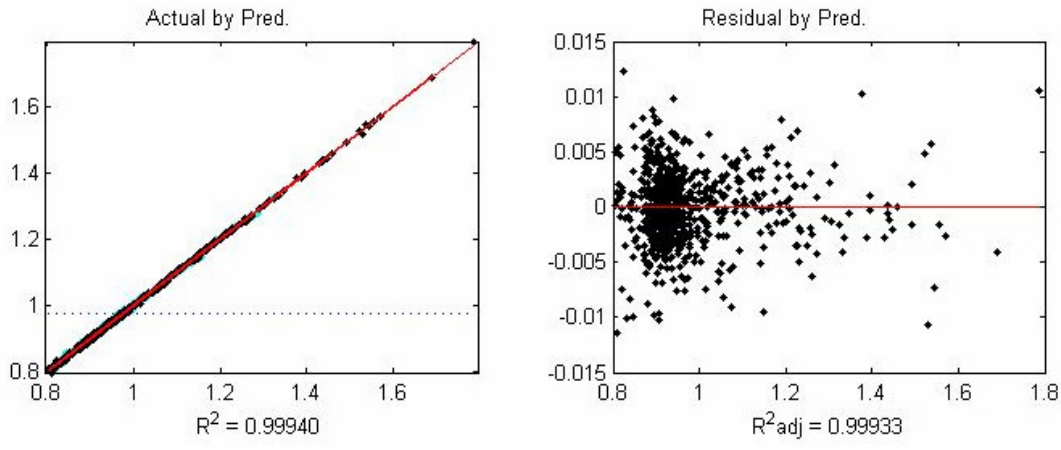

Figure 4-28: 4th Order RSE Model fits for Hover Power (J_{PH})

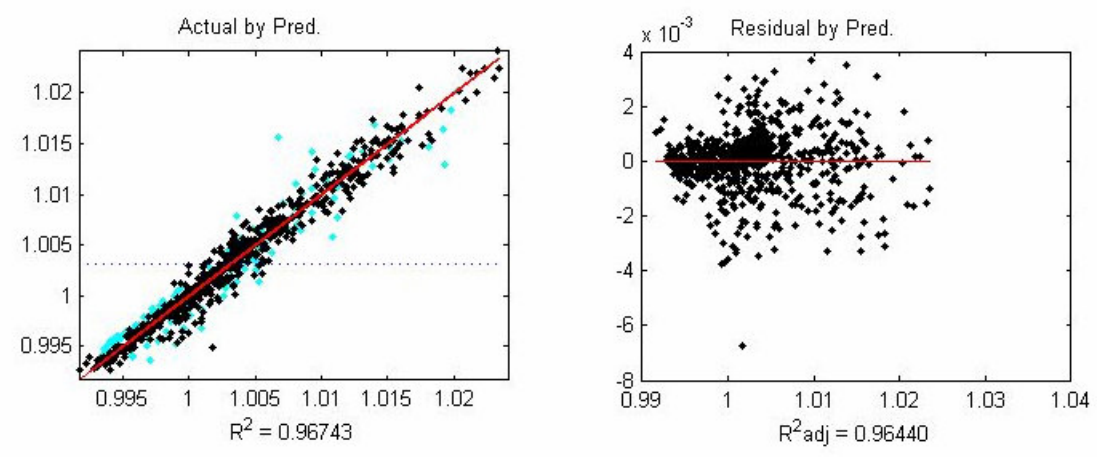

Figure 4-29: 4th Order RSE Model fits for Fwd Flight Noise (J_{NF})

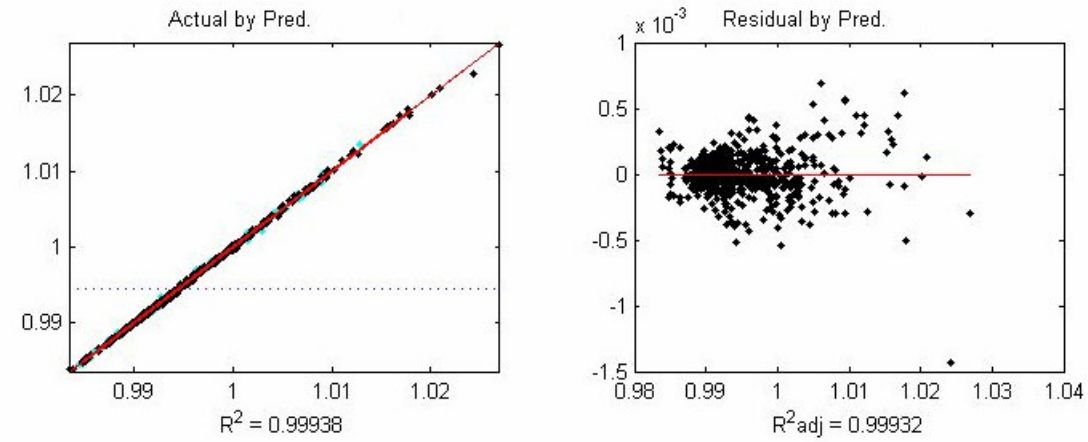

Figure 4-30: 4th Order Surrogate Model fits for Hover Noise(J_{NH})

A R^2>0.999 was achieved for all values except forward flight noise. This indicates that forward flight noise is difficult to model. This may be due to the fact that an average of 16 noise locations is modeled. Perhaps using a surrogate model for each observer location would work better to account for changes to the design variables having different effects in plane and out of plane as well as on the advancing and retreating side of the rotor. Also, using more observer locations in the grid may make the average value easier to predict.

4.3.3 **Optimization using Surrogate Models**

These 4th order surrogates were used in 3 separate methods of optimization. All three methods are designed to work with a multi-modal problem and look for global optimums. The first method used was the Genetic Algorithm toolbox in MATLAB®. The second method was the Multi-Starting Point Gradient Based Optimization. This method used the gradient based search `fmincon` in MATLAB® from every corner of the design space as shown in Figure 4-31. Finally, the last method used was a full factorial DOE for 16 sweepangle settings between 0 and 15 degrees, 16 anhedralangle settings between 0 and 15 degrees, 5 taperratio settings between 0.6 and 1, 11 twist1 (inner twist rate) settings between -18 and -8, 3 switchtiwstx (twist change location) settings between 0.85 and 0.95, and 64 twist2 (outboard twist rate) settings between -18 and 45 degrees. This DOE contains a total of of 2,703,360 cases.

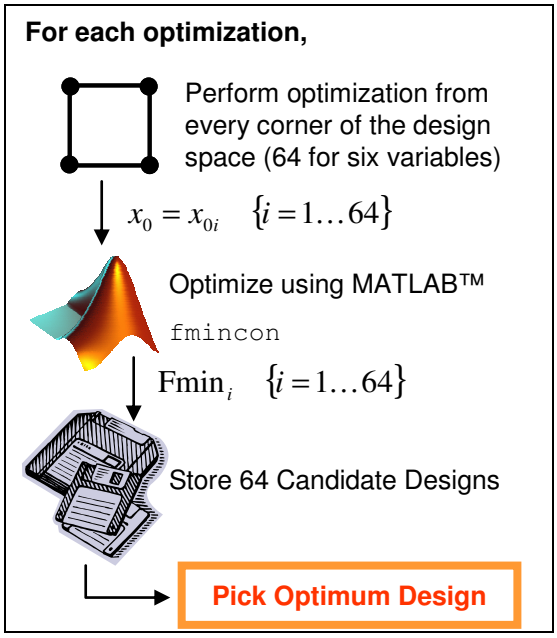

Figure 4-31: Multi-Starting Point Gradient Based optimization

All three methods of optimization found very similar optimum designs. However, the method that was most efficient was the Multi-starting Point Gradient Based Optimization. The design variable settings using the Multi-starting Point Gradient Based Optimization of Figure 4-31 are given in the upper part of Table 4-13 (a). Results are given in Table 4-13 (b). All optimums were tested in the low fidelity model and those designs added to the database of low fidelity designs. Optimums of the database are also selected. These design variable settings are given in the lower part of Table 4-13 (a) with results shown in Table 4-13 (b).

Table 4-13: 4th Order RSE Optimization Results

	c/4 Sweep Angle	Anhedral Angle	Taper Ratio	Twist1	SwitchTwistx	Twist2
Pareto Anchors Found Using 4th Order RSE						
Minimum J_PF	15	1	0.76	-17	0.95	36
Minumum J_PH	0	15	0.6	-18	0.95	6
Minumum J_NF	0	11	0.6	-8	0.9	-18
Minimum J_NH	0	15	0.6	-18	0.85	-18
Pareto Anchors of Low Fidelity DATA						
Minimum J_PF	15	3.7	0.8	-17	0.95	45
Minumum J_PH	15	0	0.6	-18	0.95	45
Minumum J_NF	0	0	0.6	-8	0.9	-8
Minimum J_NH	0	15	0.6	-18	0.85	-18

(a) Design Variable Settings

	Low Fidelity	Surrogate Model	% Model Error	Baseline Low Fidelity	% Low Fidelity Change
Pareto Anchors Found Using 4th Order RSE					
Minimum J_PF	0.00417	0.00411	1.55%	0.00454	-8.05%
Minumum J_PH	0.00429	0.00423	1.33%	0.00531	-19.15%
Minumum J_NF	105.18	104.85	0.32%	105.95	-0.72%
Minimum J_NH	101.71	101.68	0.03%	103.38	-1.61%
Pareto Anchors of Low Fidelity DATA					
Minimum J_PF	0.00413	0.00414	-0.45%	0.00454	-9.10%
Minumum J_PH	0.00423	0.00429	-1.44%	0.00531	-20.27%
Minumum J_NF	104.91	105.14	-0.22%	105.85	-0.89%
Minimum J_NH	101.71	101.68	0.03%	103.38	-1.61%

(b) Low Fidelity and 4th Order Surrogate Results

Interesting to note is that the surrogates chose an optimum with respect to hover power that had 15 degrees anhedral while the actual optimum of the database had a 15 degree sweepangle with no anhedral. Also, the surrogates picked a design with 11 degress of anhedral for minimum forward flight noise while the minimum of the actual data set had no anhedral. A careful look at the results in Table 4-13 (b) will show how this happens even with surrogates predicting power to within 2%. Good designs from the actual data set are different by a margin smaller than the surrogate prediction error. This means that knowing the deviations of data in the set around the values of interest can help determine the accuracy required by the surrogate model in this area.

To help visualize the shape of these tips, the four tip shape optimums found using the 4th order RSE's are shown in Figure 4-32 and Figure 4-33.

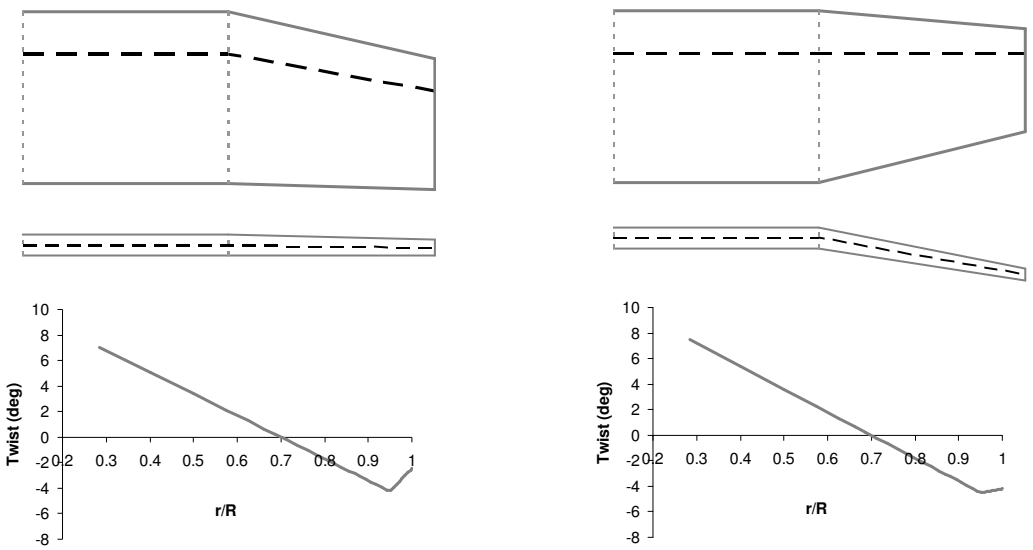

(a) (b)

Figure 4-32: 4th Order RSE Minimum Power Designs

(a) Forward Flight Power (J_{PF}), (b) Hover Power (J_{PH})

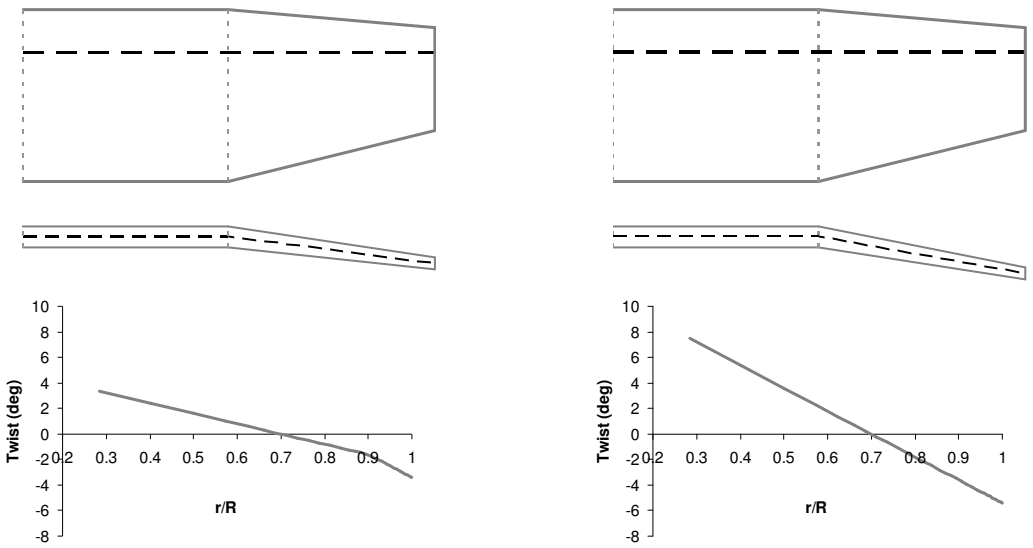

(a) (b)

Figure 4-33: 4th Order RSE Minimum Noise Designs

(a) Forward Flight Noise (J_{NF}), (b) Hover Noise (J_{NF})

The design for minimum hover power from all low fidelity runs is shown in Figure 4-34 (a). The design for minimum forward flight noise from all low fidelity runs is shown in Figure 4-34 (b). The other minimums from the low fidelity data are not shown as they are very similar to those in Figure 4-32 and Figure 4-33.

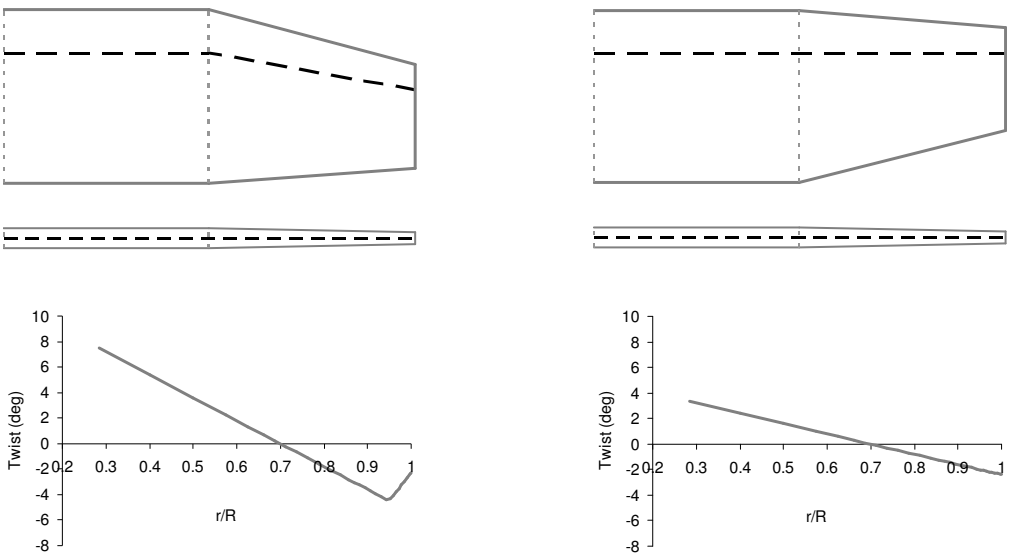

(a) (b)

Figure 4-34: Minimums of Low Fidelity Data

(a) Minimum Hover Power (J_{PH}), (b) Forward Flight Noise (J_{NF})

4.4 Chapter Summary

A preliminary methodology and results have been presented in this chapter. In general, this research involved using a low fidelity rotor analysis to select an optimum configuration. Then this optimum configuration was spot checked using higher fidelity tools. In The rotor under investigation as a test case is the HART-I rotor. The HART-I rotor is a 40% scale model of the BO-105 that was tested in Europe in 1995. Optimizations are performed by changing six design variables: three variables define the tip shape while three define the spanwise twist distribution.

This preliminary research covers the development of the automated low fidelity framework. This low fidelity framework included RCAS coupled to PSU-WOPWOP. RCAS is capable of modeling elastic blades. However, for simplification the low fidelity RCAS model assumed rigid blades. Also, a prescribed wake inflow model with 2-D table look-up blade section aerodynamics was employed. The framework was used to perform

hundreds of computer experiments in a Design of Experiments (DOE). The data from the experiments is used to build 2nd order Response Surface Equations (RSE's) of the objectives. These surrogates are used in a Monte Carlo Simulation where millions of design points are evaluated. Pareto optimal points are identified. An optimum is selected from this Pareto set and investigated using and integrated high fidelity simulation. High fidelity hover analysis was performed using TURNS. Forward flight analysis loosely coupled the CSD capability of RCAS with the CFD code GT-HYBRID. Blade surface pressures from TURNS and GT-HYBRID were passed to PSU-WOPWOP to make higher fidelity predictions of noise. Overall, high fidelity analysis results predicted the optimum to be better than the baseline in all four metrics. The optimum did not reduce vibration. In fact, vibration of the optimum is worse compared to the baseline.

In an extension to the preliminary research, an additional 400+ designs were run in the low fidelity model, enriching the low fidelity database. Using the enriched database, 4^{th} order RSE's were built and put to the task of finding the Pareto Anchor designs using a variety of optimization strategies. These new guesses for the Pareto Anchors were tested in the low fidelity environment and the results added to the database. Finally, comparisons are made between the minimums found with the 4^{th} order RSE's and the minimums of the database. The different designs seen for both minimum hover power and minimum forward flight noise adds an understanding of how model representation error relates to response deviation within the actual data set and how this can put uncertainty in the optimization process.

The methods described in this chapter have been successful in meeting elements of the research objectives. For one, an integrated and automated low fidelity simulation has been used to analyze over 800 candidate designs in various experimental designs. Unfortunately, this low fidelity simulation did not model elastic blades. This makes it difficult to accurately predict aeroelastic effects and vibration. Second, an integrated high fidelity simulation framework was built and tested to evaluate a single point design. The

high fidelity simulation framework used was not automated enough to be called upon to analyze numerous designs in a Design of Experiments.

A new method is needed to combine these elements with new elements to fully meet the research objectives. One of these elements is to enhance the low fidelity model to include elastic blades and thus include vibration as a metric in addition to performance and noise. Another element required is the automation of the high fidelity simulation process – including GT-HYBRID/RCAS coupling and GT-HYBRID grid generation - as much as possible to allow faster evaluation of new designs at the higher level of fidelity. With the elements in place and tested, a method is needed to use both low and high fidelity simulation frameworks to optimize a rotor blade. In the section that follows, these elements are described along with a method of using them in an optimization process.

Chapter 5

New Methodology and Results

5.1 Overview

Techniques documented in this chapter make final strides toward the research objectives stated in Chapter 3. The low fidelity, rigid blade RCAS/PSU-WOPWOP model of Chapter 4 is updated with elastic blades to better capture important aeroelastic effects. The high fidelity CFD/CSD/AA process using GT-HYBRID/RCAS/PSU-WOPWOP is automated in a multi-processor environment to allow a small DOE to be performed in a reasonable amount of time. With automated low and high fidelity simulations available, a method is proposed that uses both to perform a selected set of DOE's in order to ultimately build approximation models of both high and low fidelity objectives and constraints.

The method is tested by building RSE approximations of two high fidelity forward flight metrics: lift to drag ratio and a vibration index. The approximations are used to develop the two dimensional Pareto Frontier for these two metrics. Testing points on the frontier in the high fidelity framework reveals that the methodology was successful in leading to designs optimum in the high fidelity domain.

5.2 Low and High Fidelity Framework Updates

The general multidisciplinary process of the updated low and high fidelity analysis are shown in Figure 5-1. Each box shown is a Contributing Analysis (CA) in some respect. For instance, GEO represents some analysis that defines the geometry of the rotor shape. Table 5-1 describes the various CA's shown in Figure 5-1 (a) and (b). In addition to an update of elastic blades, a different but similar rotor was chosen as the baseline. For research performed in this chapter, the HART-II [97, 98] rotor was used as

the baseline as opposed to the HART-I baseline of Chapter 4. The models differed in two aspects. The spanwise location for zero twist is located at the 70% radius for the HART-I and at the 75% radius for the HART-II. In addition, the mass and elastic properties are slightly different. More information regarding the HART-I and HART-II elastic blade RCAS models can be found in Appendix B.

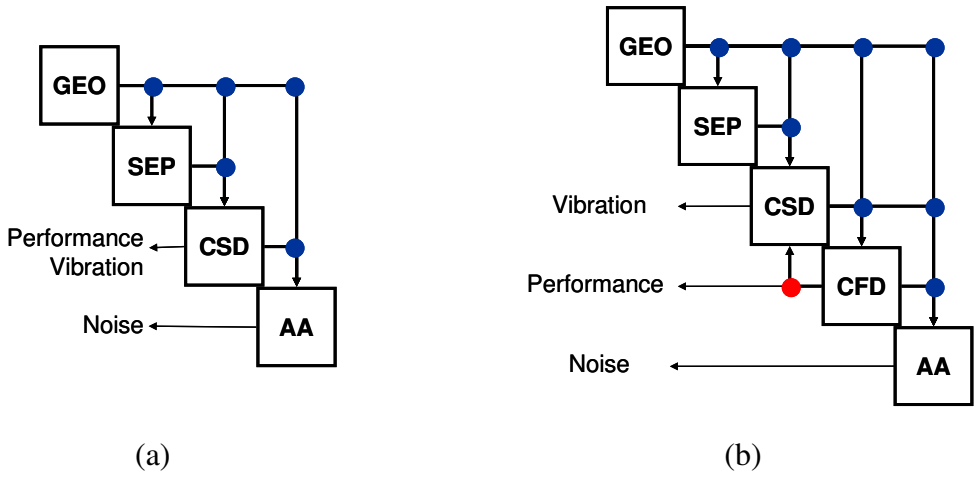

Figure 5-1: Low Fidelity (a) and High Fidelity (b) Rotor Analysis Processes

Table 5-1: Descriptions for Low and High Fidelity Rotor Analysis Processes

CA	Contributing Analysis Description
GEO	Geometry of rotor configuration. Each analysis requires its own unique geometry definition.
SEP	Sectional Elastic and Mass Properties. These properties define the nonlinear elastic beam segments used in CSD.
CSD	Computational Structural Dynamics. This analysis calculates the blade control trim and final motion including elastic deformation under aerodynamic loads. In the low fidelity model, these airloads are computed with internal table lookup aerodynamics and dynamic inflow model. In the high fidelity model, the airloads are computed via a separate CFD analysis.
CFD	Computational Fluid Dynamics. This analysis uses first principles based analysis to numerically calculate the flow field surrounding the blade. It is not used in the low fidelity analysis.
AA	Aeroacoustic Analogy. This analysis uses information regarding blade motion and flow field to predict the noise generated at specified observer locations.

The low fidelity analysis pictured in Figure 5-1 (a) uses non-CFD aerodynamics. Instead, blade element analysis is used with aerodynamic loads calculated using a 2-D table look-up of airfoil characteristics with inflow velocity calculated using dynamic inflow. Dynamic inflow was chosen due to its robustness when analyzing a variety of different designs. It is felt that a prescribed or free wake models would produce a more accurate representation of the physics occurring near the blade tip where geometry is being changed. However, issues with non-convergence and other problems using these vortex wake models made dynamic inflow more appealing for use in the design studies being performed. The blade motion and quarter chord lift and drag information will be passed to the aeroacoustics analysis capable of using this lower fidelity information to predict the sound pressure level at specific observer locations. A unique approach was used to turn the elastic deformation from RCAS into deformed geometry that could be used by PSU-WOPWOP. This process is shown in Figure 5-2.

A rotor geometry spreadsheet contains information that gets updated based on changes to design variables and/or flight condition parameters. The information includes but is certainly not limited to node locations, spanwise twist and chord distributions; as well as changes to the spanwise mass distribution approximated using equation 4-8. This information is passed to RCAS for an elastic blade (see Appendix B) analysis using dynamic inflow. It is also used by GT-GRIDGEN to create a blade grid file normally used by GT-HYBRID. This grid file along with a motion file created using output from the RCAS analysis is used by GT-HYBRID to create the deformed geometry of the blade at a specified number of azimuthal locations for a complete revolution. This means the data is both time dependent and periodic. Finally, the deformed geometry from GT-HYBRID and the blade airloads from RCAS are given to PSU-WOPWOP for aeroacoustic analysis. No CFD calculations are made by GT-HYBRID during this low fidelity process. It is only used to calculate the deformed geometry. Many rotor CFD

codes have this capability and could be used in a similar manner when deformed rotor blade geometry is required by another application.

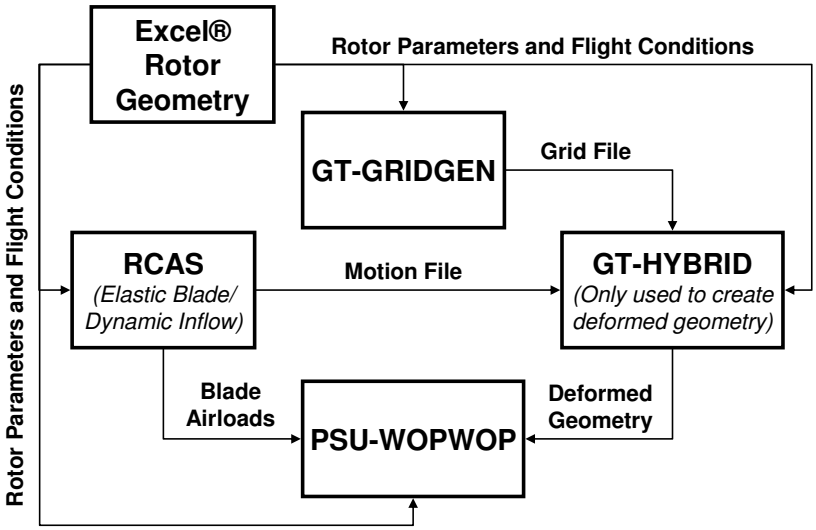

Figure 5-2: RCAS Elastic Blade to PSU-WOPWOP Process

The HART-II rotor represents a 40% scale model of the BO-105 hingeless rotor. For this reason, the elastic blade HART-II model in RCAS can be validated against NASA's full scale BO-105 rotor test [93]. A comparison is made in Figure 5-3 for forward flight performance. It is seen that the power required (i.e. C_P/σ) is over predicted with the RCAS model. This over prediction is similar to that seen with the rigid blade/prescribed wake model in Figure 4-6. However, in both cases RCAS seems to do a good job of predicting the trend of power with forward speed.

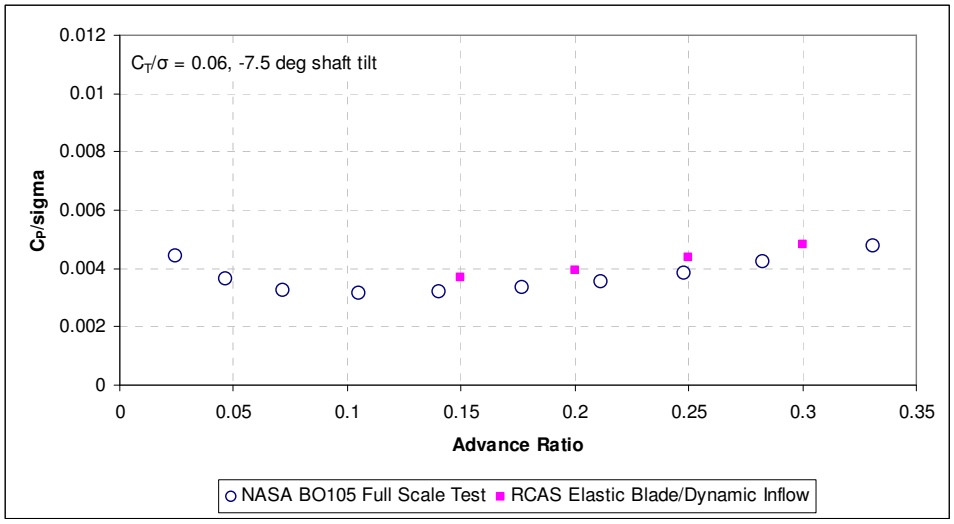

Figure 5-3: RCAS Elastic Blade Model Compared with Full Scale Test (Fwd Flt)

Experimental Data from NASA Full Scale BO-105 Rotor Test [93]

In Figure 5-4, a comparison is made between the NASA full scale tests and the RCAS elastic blade / dynamic inflow model in hover. The RCAS model is seen to better predict the hover performance than the previous low fidelity model (refer to Figure 4-7).

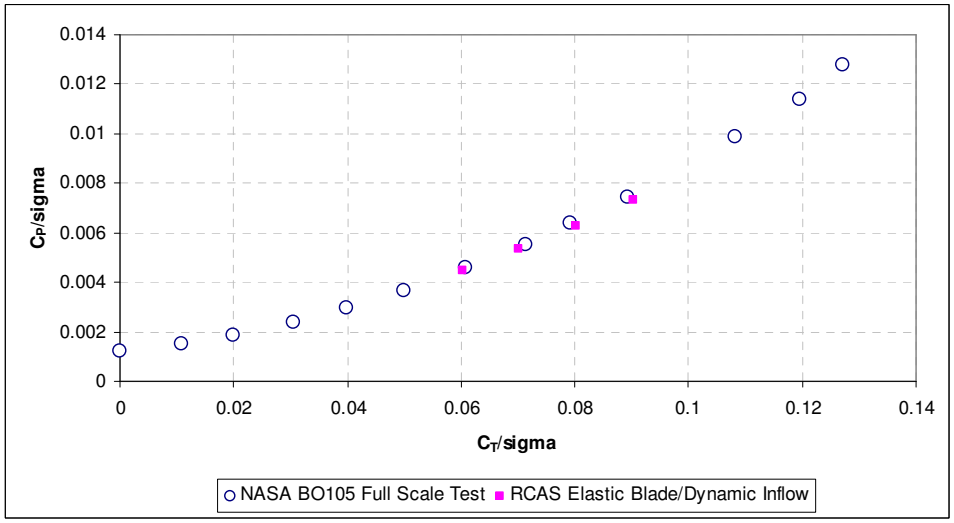

Figure 5-4: RCAS Elastic Blade Model Compared with Full Scale Test (Hover)

Experimental Data from NASA Full Scale BO-105 Rotor Test [93]

The high fidelity analysis shown in Figure 5-1 (b), is the same process used in Chapter 4 for the analysis of the point design optimum. However, in the research documented in this chapter, the process has been automated to be more useful as a design tool. The process that was automated is shown in Figure 5-5. Here again, a rotor geometry spreadsheet contains information that gets updated based on changes to design variables and/or flight condition parameters. This information is passed to RCAS for an elastic blade CSD analysis using the delta airloads algorithm shown in Figure 4-19. The CFD portion of that algorithm is performed by GT-HYBRID using a motion file created by RCAS and a grid file created by GT-GRIDGEN. Finally, after a specified number of coupled CFD/CSD runs (typically 7 for this research), the final blade surface geometry and pressures output from GT-HYBRID are given to PSU-WOPWOP for aeroacoustic analysis. Validation of this process for the HART-II baseline was performed and the results were very similar to those presented in Figure 4-20 and Figure 4-21 as expected since there are only small differences between the HART-I and HART-II rotors.

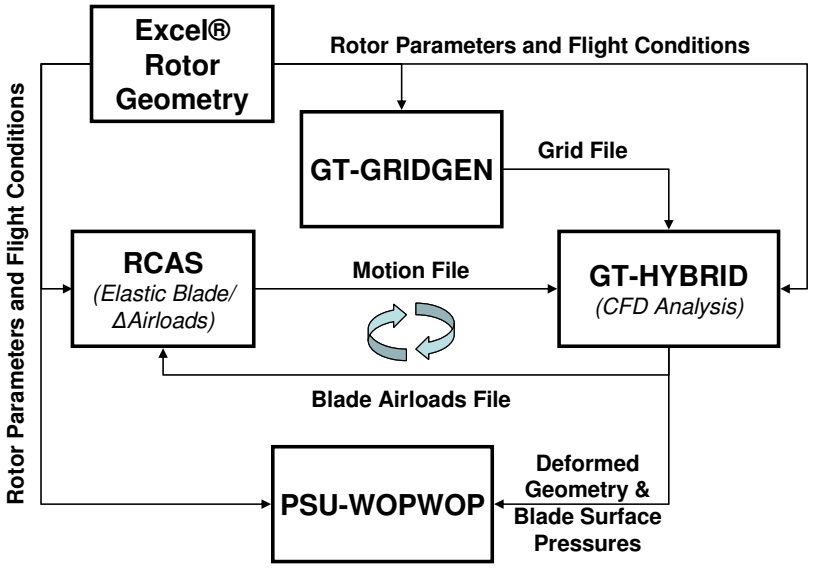

Figure 5-5: GT-HYBRID/RCAS Elastic Blade to PSU-WOPWOP Process

To more completely automate the design process for both the low and high fidelity frameworks, ModelCenter® is again used. Figure 5-6 shows the frameworks as built in the ModelCenter® design framework. The low fidelity framework is designed to run each design and parse output created by RCAS and PSU-WOPWOP. This level of automation makes running a set of experiments simple, even though a complete run of a design which includes both the forward flight and hover analysis takes about an hour.

Those familiar with RCAS have probably analyzed output from RCAS interactively and are not accustomed to generating output files. This is required, however, for ModelCenter® to parse them. Fortunately, automated batch output from RCAS can be added to RCAS script files. An example of how this is done is shown in Appendix D. In order to utilize the combined analysis of RCAS and PSU-WOPWOP in ModelCenter®, the analysis must be made into a component within the design framework. A description of how this is done along with an example component "filewrapper" is given in Appendix E.

While the low fidelity framework of Figure 5-6 (a) contains an analysis of both forward flight and hover, the high fidelity framework of Figure 5-6 (b) is only used for forward flight analysis. This framework is also different in that it is mainly used to create all the required files to run a CFD/CSD/AA analysis for a given set of design parameters and submit this job to a cluster of compute nodes. Parsing of the ouput is also done using ModelCenter®, but only after the user knows the run is complete and requests the results to be parsed. Even still, this level of automation and ability to utilize multiple processors is a large reason why this research is successful in applying high fidelity simulation tools to the design of a rotor blade, as will be described later.

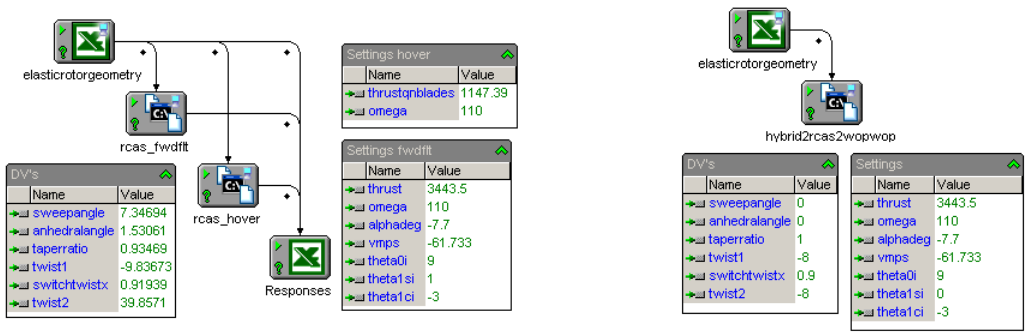

(a) (b)

Figure 5-6: Low (a) and High (b) Fidelity Process Implementation in ModelCenter®

5.3 Revisiting the Optimums of Section 4.3.3

As a first design study check, the high fidelity GT-HYBRID/RCAS/PSU-WOPWOP framework of Figure 5-5 and Figure 5-6 (b) is called upon to analyze the Pareto Anchor designs documented in Section 4.3.3. Each design is analyzed and the power and noise metrics (J_{PF} and J_{NF}) are calculated. The results are given in Table 5-2. Only these eight designs are compared and only forward flight characteristics are compared even though the designs themselves are Pareto anchors in metrics of both forward flight and hover. That being stated, some interesting information can still be gained from this analysis. The design found to have minimum forward flight power required is a low fidelity Pareto Anchor in the dimension of forward flight power. The design found to have minimum forward flight noise is a low fidelity surrogate Pareto Anchor in the dimension of forward flight noise.

Table 5-2: High Fidelity Forward Flight Analysis of Section 4.3.3 Optimums

	c/4 Sweep Angle	Anhedral Angle	Taper Ratio	Twist1	SwitchTwistx	Twist2	JPF	JNF
Pareto Anchors Found Using 4th Order RSE								
Minimum J_PF	15	1	0.76	-17	0.95	36	0.0042451	106.028
Minumum J_PH	0	15	0.6	-18	0.95	6	0.0043879	105.047
Minumum J_NF	0	11	0.6	-8	0.9	-18	0.0042581	**104.738**
Minimum J_NH	0	15	0.6	-18	0.85	-18	0.0044398	105.086
Pareto Anchors of Low Fidelity DATA								
Minimum J_PF	15	3.7	0.8	-17	0.95	45	**0.0042191**	105.763
Minumum J_PH	15	0	0.6	-18	0.95	45	0.004297	105.955
Minumum J_NF	0	0	0.6	-8	0.9	-8	0.004297	105.554
Minimum J_NH	0	15	0.6	-18	0.85	-18	0.0044398	105.086

The results does not mean that these particular designs are the forward flight power and noise minima in the high fidelity domain as the comparison is made against too small a sampling of designs. However, the result does add some credibility to the answers given by the rigid blade low fidelity model used in the research of Parts I and II.

In the next section, a process is proposed that will utilize the high fidelity and low fidelity frameworks together to optimize a rotor blade.

5.4 A Process of Low/High Fidelity Optimization

The method proposed will be a process of intelligently using high fidelity simulation tools in concert with lower fidelity analysis to optimize a rotor configuration having a number of design variables. This process is depicted in Figure 5-7. The process begins with the assumption that a low and high fidelity rotor simulation are available or have been developed. It is also assumed that both simulations are parametric; meaning that a set of design variables can be changed for the purpose of examining the design space. In this thesis, these simulations are developed from existing tools currently in use within the rotorcraft industry as discussed previously in Section 5.2.

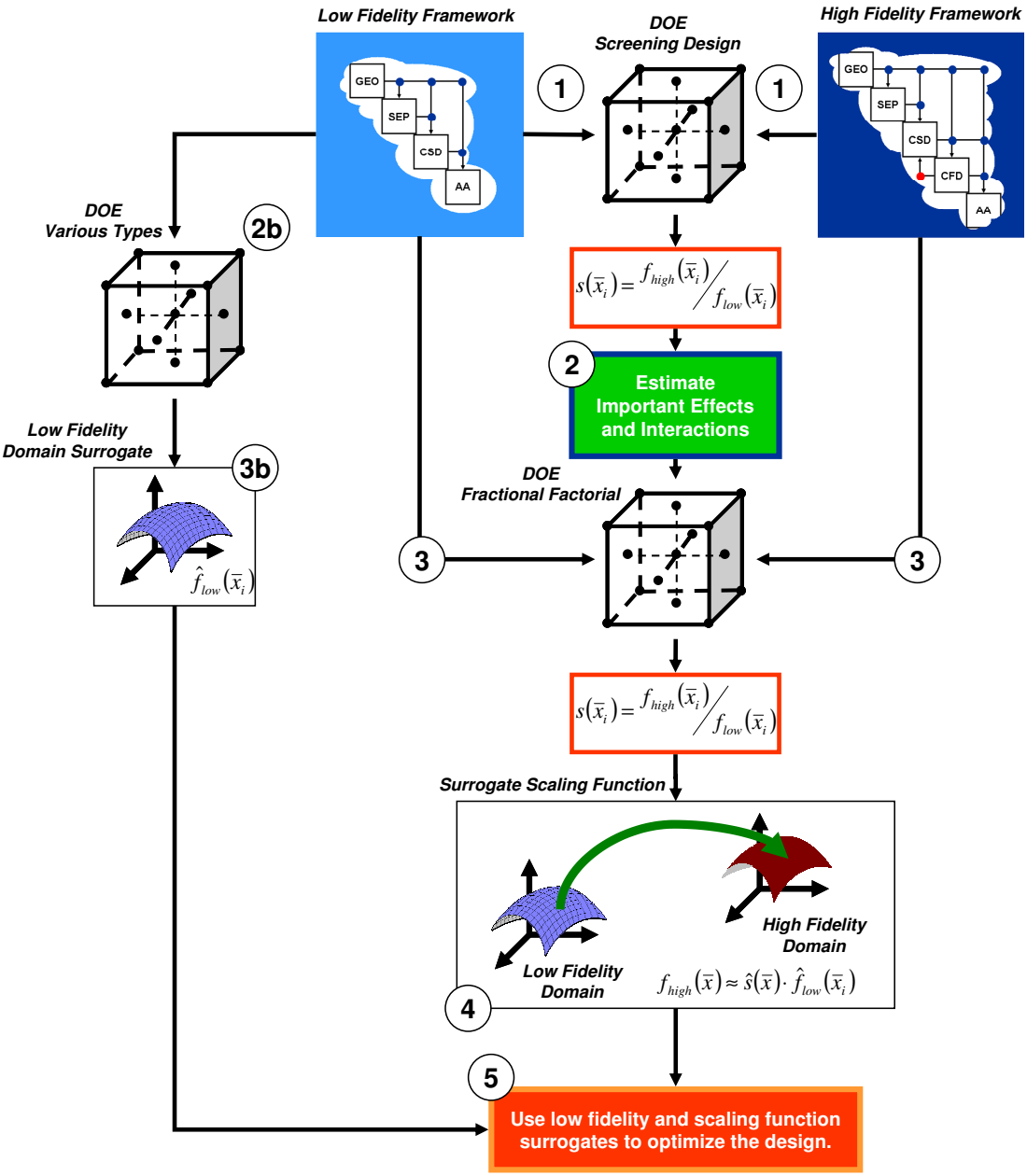

Figure 5-7: New Method of Rotor Design Using Low and High Fidelity Analysis

To begin the process, Step 1, both low and high fidelity simulations are used in a small size DOE. The purpose of this DOE is to determine the relative importance of each design variable as well as the importance of any interactions that may exist between the design variables. The objectives being tracked are not the parameter values themselves, but rather the value of some type of scaling parameter used to map low fidelity values to

high fidelity values. It is desired to create a scaling function for each parameter that will provide an approximation to high fidelity results, given the design variable settings and the value of the low fidelity result. For example, equation 5-1 shows a scaling parameter $s(\bar{x}_i)$ that is the ratio of high and low fidelity values of the parameter $f(\bar{x}_i)$ which stands for a generic parameter of interest. This parameter is very similar to the $\beta(x)$ parameter of Reference [67].

$$s(\bar{x}_i) = f_{high}(\bar{x}_i) \Big/ f_{low}(\bar{x}_i) \qquad \textbf{5-1}$$

In Step 2, the results of the "screening" DOE are analyzed to determine the effects and interactions of importance. This part of the process allows a fractional factorial DOE to be created for the purpose of projecting power into the dimensions found to be important. In Step 3 of the process, this DOE is performed using both low and high fidelity simulations and again capturing the values of $s(\bar{x}_i)$ for each run. These results are used in Step 4 to create a surrogate model for $s(\bar{x})$ called $\tilde{s}(\bar{x})$. In parallel, if possible, Steps 2b and 3b involve making surrogate models of low fidelity output parameters using a variety of DOE's. This surrogate model is an approximation to $f_{low}(\bar{x})$ called $\tilde{f}_{low}(\bar{x})$. These steps assume that the low fidelity simulation is efficient enough to perform hundreds of analysis runs in a reasonable amount of time. The idea is to use surrogate model of the scaling function $\tilde{s}(\bar{x})$ along with the surrogate model of the low fidelity metric $\tilde{f}_{low}(\bar{x})$ to calculate approximate values for the high fidelity results. This high fidelity approximation is calculated by equation 5-2.

$$f_{high}(\bar{x}_i) \approx \tilde{s}(x) \cdot \tilde{f}_{low}(\bar{x}_i) \qquad \textbf{5-2}$$

Finally, in Step 5, using equations similar to 5-2 for objectives and constraints, optimization is performed using approximations to high fidelity results to arrive at a better design. This better design can then be examined with the actual high fidelity simulation to see if indeed it has merit.

5.5 Testing the Process – A Case Study

To test the process, the updated low and high fidelity frameworks will be used to build approximation models for two specific high fidelity forward flight metrics; one for rotor efficiency and one for vibration. The HART-II rotor is the baseline and the same design variables used throughout this thesis will be used again here. The approximations will be used to generate designs on the rotor efficiency and vibration Pareto Frontier using a series of constrained optimization problems.

The rotor efficiency metric is the lift to equivalent drag ratio of the rotor and is given by equation 5-3. This parameter is commonly used when comparing various designs for efficiency in forward flight. It is a better parameter than simply looking at forward flight power required as done in Chapter 4 because each design may trim to a slightly different thrust in RCAS. This thrust difference, though small, may account for part of any difference in power required. Here, thrust is included in the equation as the hub z-force value, F_Z.

$$L/D_e(\bar{x}) = \frac{F_Z(\bar{x})}{\left(F_X(\bar{x}) + \frac{M_Z(\bar{x})\Omega}{V_\infty}\right)} \qquad \textbf{5-3}$$

The form of the vibration metric used is given by equation 5-4. This metric is derived from Lim and Chopra [71]. All force and moment quantities under the square root (i.e. $F_{\_H}^{4P}$ or $M_{\_H}^{4P}$) are functions of the design variable vector $\bar{x}$. Each quantity is obtained from a harmonic breakdown of the rotor hub forces and moments. Specifically, these quantities are those related to the 4th harmonic since this is a four bladed rotor. Each quantity (i.e. $F_{\_H}^{4P}$ or $M_{\_H}^{4P}$) is the peak-to-peak value of the 4th harmonic for that particular hub force or moment. Because a true harmonic breakdown yields cosine and sine components, this peak-to-peak value is obtained using a square root of the sum of squares of these components (i.e. $F_{xH}^{4P} = \sqrt{\left(F_{xH\ \sin e}^{4P}\right)^2 + \left(F_{xH\ \cos ine}^{4P}\right)^2}$).

$$Vi(\bar{x}) = \sqrt{\left(F_{xH}^{4P}\right)^2 + \left(F_{yH}^{4P}\right)^2 + \left(F_{zH}^{4P}\right)^2} + \sqrt{\left(M_{xH}^{4P}\right)^2 + \left(M_{yH}^{4P}\right)^2 + \left(M_{zH}^{4P}\right)^2} \qquad \textbf{5-4}$$

To begin, a screening Design of Experiments is performed in both the low and high fidelity to understand the importance of the various design variables as they relate to the metrics given above. Results of the screening experiments can hopefully be used to identify the form of the approximation models. However, this is not a guarantee and more experiments will most likely be required. Nonetheless, it is desired to only perform the minimum number of high fidelity experiments to create a reasonably accurate model.

5.5.1 **Screening Design of Experiments**

The screening design chosen for this study is one developed by Cotter [99] that is designed to segregate important factors when the model under study has a large number of significant factors and interactions. Hereafter this design will be called the Cotter Screening Design. Nixon [100] used this design in a Systematic Process for Adaptive Concept Exploration. The Cotter Screening Design is a systematic fractional replicate design and requires *2n+2* experimental trials where *n* is the number of design variables

(or factors). The first trial – called trial *0* – is one in which all factors are set to their lowest setting. The next *n* trials have each factor switched to its highest setting while all other factors remain at the lowest setting. The next *n* trials have each factor switched to its lowest setting while all other factors remain at the highest setting. The *2n+2* trial is one in which all factors are set to their highest setting. A Cotter Screening Design for six design variables (or factors) is presented in Table 5-3 with low and high settings represented by -1 and 1 respectively. The values -1 and 1 represent the minimum and maximum design space values of a design variable respectively. In this particular problem, these minimum and maximum values are given according to Table 4-2.

Table 5-3: Screening Design for Factorial Experiments with Interactions

Trial	Factors						*Response*
	1	2	3	4	5	6	*y*
0	-1	-1	-1	-1	-1	-1	*y0*
1	1	-1	-1	-1	-1	-1	*y1*
2	-1	1	-1	-1	-1	-1	*y2*
3	-1	-1	1	-1	-1	-1	*y3*
4	-1	-1	-1	1	-1	-1	*y4*
5	-1	-1	-1	-1	1	-1	*y5*
6	-1	-1	-1	-1	-1	1	*y6*
7	-1	1	1	1	1	1	*y7*
8	1	-1	1	1	1	1	*y8*
9	1	1	-1	1	1	1	*y9*
10	1	1	1	-1	1	1	*y10*
11	1	1	1	1	-1	1	*y11*
12	1	1	1	1	1	-1	*y12*
13	1	1	1	1	1	1	*y13*

A small screening design is desired since the cost of running the high fidelity experiments makes running a large number of experiments very difficult. The idea here is not to use the results of the *2n+2* trials to build a surrogate model since there are most likely not enough trials to do this. The screening design is meant to identify the important factors and possible interactions so that a separate set of experiments can be designed to better capture these significant factors and interactions.

5.5.2 **Identification of Important Factors and Interactions**

To help identify which factors and interactions may be important, an analysis of the results from the Cotter Screening Design is performed. One way of doing this is to examine the contrasts of the combined effects for each factor as defined in Cotter's paper [99]. These contrasts are given by equation 5-5 for the odd factor interactions and equation 5-6 for the even factor interactions.

$$C_o(j) = \frac{1}{4}\left\{\left(y_{2n+1} - y_{n+j}\right) + \left(y_j - y_0\right)\right\} \qquad \textbf{5-5}$$

$$C_e(j) = \frac{1}{4}\left\{\left(y_{2n+1} - y_{n+j}\right) - \left(y_j - y_0\right)\right\} \qquad \textbf{5-6}$$

where $j = 1 \ldots n$

For example, if there were four factors: A, B, C, and D; then the contrasts for factor A would have the expected values $E\{C_o(A)\} = \alpha_A + \alpha_{ABC} + \alpha_{ABD} + \alpha_{ACD}$ and $E\{C_e(A)\} = \alpha_{AB} + \alpha_{AC} + \alpha_{AD} + \alpha_{ABCD}$ where α_A represents the effect of factor A, α_{AB} represents the effect of the interaction of factors A and B, α_{ABC} represents the effect due to the interaction of factors A, B, and C, and so on.

The response, *y*, could be any output parameter of interest. In this part of the work, two responses are being investigated, rotor equivalent lift to drag and vibration. These metrics are given by equations 5-3 and 5-4. Specifically, the metric being investigated is the scaling parameter of low and high fidelity results, as given generically by equation 5-1. The calculation of this scaling parameter for L/D_e^* is given by equation 5-7. The calculation of the scaling parameter for Vi^* is done in a similar manner. The asterisk superscript signifies that the parameter is normalized by dividing the parameter by the baseline (HART-II model) value.

$$s\left\{L/D_e^{\,*}(\bar{x}_i)\right\} = \left\{L/D_e^{\,*}(\bar{x}_i)\right\}_{high} \Big/ \left\{L/D_e^{\,*}(\bar{x}_i)\right\}_{low} \qquad \textbf{5-7}$$

The results of the Cotter Screening DOE are given in Table 5-4. The first row contains the design variable settings and responses for the baseline HART-II rotor. The remaining rows contain the results of the Cotter Screening trials from both low and high fidelity analysis, along with the scaling parameters calculated from these results combined.

Table 5-4: Cotter Screening Design Results

trials	sweepangle	anhedralangle	taperratio	twist1	switchtwistx	twist2	L/De* Low Fidelity	L/De* High Fidelity	S(L/De*)	Vi* Low Fidelity	Vi* High Fidelity	S(Vi*)
baseline	0	0	1	-8	0.9	-8	1	1	1	1	1	1
0	0	0	0.6	-18	0.85	-18	0.9909	0.7762	0.7833	2.2909	2.6445	1.1544
1	15	0	0.6	-18	0.85	-18	0.9884	0.7945	0.8039	2.2316	2.4938	1.1175
2	0	15	0.6	-18	0.85	-18	0.9086	0.7441	0.8189	2.3826	2.6124	1.0964
3	0	0	1	-18	0.85	-18	0.9857	0.7760	0.7872	2.2035	2.4667	1.1195
4	0	0	0.6	-8	0.85	-18	1.0203	0.9667	0.9475	1.3279	1.3354	1.0056
5	0	0	0.6	-18	0.95	-18	0.9909	0.7762	0.7833	2.2909	2.6445	1.1544
6	0	0	0.6	-18	0.85	45	0.8340	0.9597	1.1508	0.9283	1.2821	1.3811
7	0	15	1	-8	0.95	45	0.9254	0.9706	1.0488	0.9361	0.8841	0.9445
8	15	0	1	-8	0.95	45	0.9923	1.0266	1.0346	1.0216	0.8639	0.8456
9	15	15	0.6	-8	0.95	45	0.8956	0.9230	1.0307	0.7042	0.9517	1.3515
10	15	15	1	-18	0.95	45	0.9039	0.7847	0.8682	1.3122	2.1794	1.6609
11	15	15	1	-8	0.85	45	0.6558	0.8248	1.2578	1.0070	0.4372	0.4342
12	15	15	1	-8	0.95	-18	0.9337	0.9393	1.0060	0.6736	1.0092	1.4982
13	15	15	1	-8	0.95	45	0.8703	0.9365	1.0760	0.6944	0.9456	1.3618

The contrasts as calculated using equations 5-5 and 5-6 for the two scaling parameters are given in Table 5-5. Another way of identifying the important interactions is to use the software JMP®. JMP® is also capable of calculating contrasts but has more capabilities in terms of its ability to calculate the contrasts of specific effects and

interactions. These JMP® calculated contrasts are shown in Figure 5-8 (a) and (b) for $s\{L/D_e^*(\bar{x}_i)\}$ and $s\{Vi^*(\bar{x}_i)\}$ respectively.

Table 5-5: Cotter Screening Design Contrast Results

	S(L/De*)		S(Vi*)	
	Co	Ce	Co	Ce
sweepangle	0.0119	0.0017	0.0951	0.1136
anhedralangle	0.0193	0.0015	0.1146	0.1435
taperratio	0.0123	0.0104	-0.0061	0.0113
twist1	0.0930	0.0109	-0.1120	-0.0376
switchtwistx	-0.0454	-0.0454	0.2319	0.2319
twist2	0.1094	-0.0744	0.0226	-0.0908

Comparing the results in Table 5-5 with those shown in Figure 5-8, both seem to be saying similar things but JMP® is better at distinguishing the specific interactions of importance.

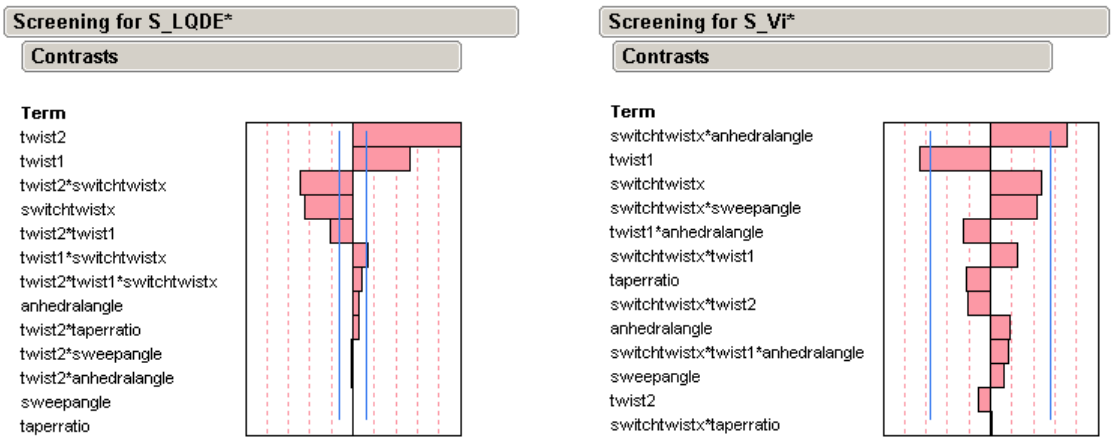

(a) (b)

Figure 5-8: JMP® Calculated Contrasts using Cotter Screening Design Results

The effects listed in Figure 5-8 for both of these responses are a great first guess as to which terms should be included in a surrogate model for them. The next step is to perform another set of experiments to gain data that can be used to build surrogate

models of these two scaling parameters to an accuracy that is suitable for use in an optimization problem.

5.5.3 **Fractional Factorial Design of Experiments**

The type of fractional factorial Design of Experiments performed is very dependent on the amount of time available for analysis and the number of separate cases that can be examined within that time. In this research, it was reasonable to assume that approximately 50 different high fidelity experiments could be performed in the time available. Constrained by this, it was decided to combine a Resolution IV and a Resolution VI fractional factorial DOE. Both of which are designed for six, 2-level factors. Due to their size, these DOE's are given in Appendix G. The 16 run Resolution IV design is one in which no main effect is aliased with any other main effect or two-factor interactions but two-factor interactions are aliased with each other. The 32 run Resolution VI design is one in which no main effect or two-factor interaction is aliased with any other main effect or two-factor interactions but three-factor interactions are aliased with each other. In these DOE's, the experiments also have each design variable taking either its minimum (-1) or maximum (1) design space value. One experiment has all design variables set to 0. This means each design variable is set to its median design space value.

The union of these two DOE's contained 41 unique designs. Utilizing the automated high fidelity framework for high fidelity forward flight design framework, the creation of the models and analysis of these designs took just under 13 days. Four designs failed and two designs had previously been done for the Cotter Screening Design. So counting only the 35 completed runs, this makes for an average of about 9 hours per design. This is very fast considering that each design analysis includes 7 separate CFD runs during the loose CFD/CSD coupling. Each CFD run used 12 processors.

5.5.4 **Surrogate Scaling Function**

Surrogate Models of the scaling functions were built assuming models that used the important factors and interactions estimated from the Cotter Screening Design Analysis in JMP®. The data used when fitting to these models was that which was gathered in the Res IV and Res VI experiments along with the data gathered in the Cotter Screening Design for a total of 50 cases. A good fit of the data was made for the model of $\tilde{s}\left\{L/D_e^{\,*}(\bar{x})\right\}$ when created in JMP®. However, fitting the model guess for $\tilde{s}\left\{V_i^{\,*}(\bar{x})\right\}$ from the Cotter Screening Design analysis using the 50 runs created a fit with an R^2 value of 0.57 which was considered insufficient. A new guess for the form of the model needed to be made.

Using the same functionality within JMP® used to analyze the contrasts for the data collected in the Cotter Screening Design runs and select model factors and interactions, the same contrast analysis was performed for the data collected in the Res IV and Res VI experiments. This new guess for the $\tilde{s}\left\{V_i^{\,*}(\bar{x})\right\}$ model contained a number of three factor interactions. Using the 50 runs to fit the model, an acceptable fit was found. The actual versus predicted plots for both scaling functions can be seen in Figure 5-10.

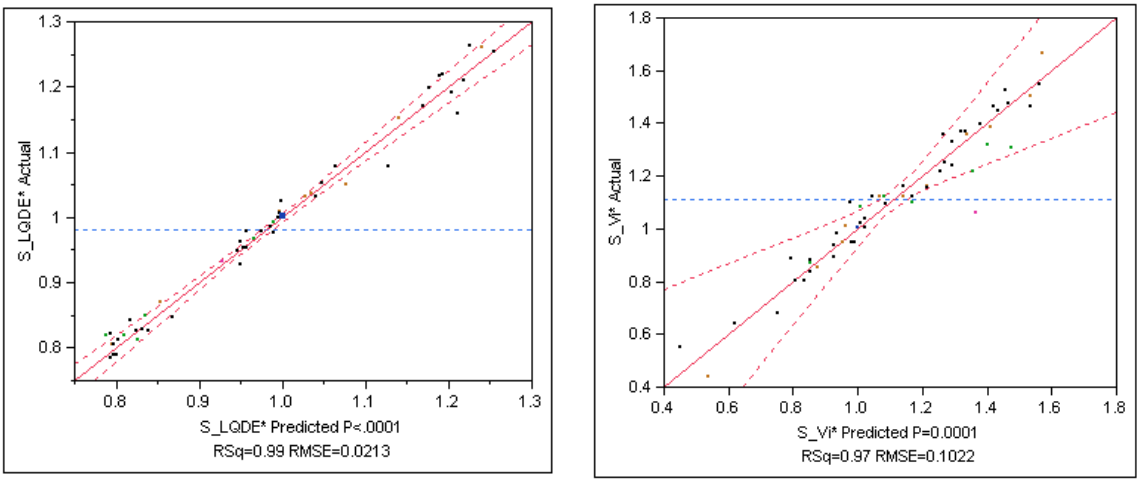

(a) (b)

Figure 5-9: Actual vs. Predicted Plots for Surrogate Models of Scaling Functions

Now that surrogates of the scaling functions had been built, it was time to make surrogate models for the low fidelity functions themselves and then later, combine the low fidelity and scaling surrogates to generate designs on the approximate high fidelity Pareto Frontier.

5.5.5 **Surrogate Modeling of Low Fidelity Model**

The parallel process of creating surrogates for the low fidelity framework is shown by itself in Figure 5-10. There are various types of surrogate models that can be applied to a data set. For instance, in Figure 5-10, Kriging, RSE, and Neural Net surrogate modeling is depicted. These are all valid and tested ways of employing surrogates. In this work, however, only the RSE is used. Specifically stepwise regression is performed to calculate the estimates of a 4^{th} Order RSE surrogate model.

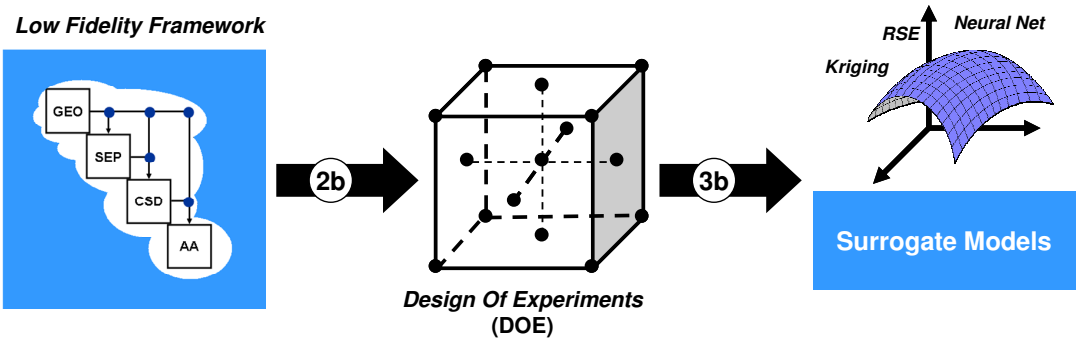

Figure 5-10: Low Fidelity Surrogate Modeling

A varied selection of experimental designs is chosen to gather the data required from the low fidelity model to create the surrogate models of specific parameters. Table 5-6 lists the various experiments performed with the low fidelity model. A total of 412 experiments were performed. The data from 331 experiments was used in the building of the surrogate models. The remaining 81 experiments were used to check the model representation error of each surrogate.

Table 5-6: Experimental Designs Used to Build RSE's

Test Description	# Runs	*Modeling*
Baseline	1	*Use to Build 4th Order RSE's*
Central Composite Design*	77	
Latin Hypercube*	62	
Latin Hypercube**	50	
Sphere Packing**	50	
Minimum Potential**	50	
Res IV and VI Designs	41	
Cotter Screening	14	*Use to Check Model Representation Error*
Latin Hypercube*	50	
Other Cases	17	
** DOE built in ModelCenter®*		
*** DOE built in JMP®*		

Statistical analysis of the data using stepwise regression was performed using an automated RSE generator that works with MATLAB® called STARS [96]. STARS is unique in that it allows the user to select the order of the surrogate model being created

and see instantly through fit information plots how well the model fits the data used to create it (Model Fit Error – MFE) as well as how well the model fits data not used to create it (Model Representation Error – MRE). Information about the surrogate model fits for both $\left\{L/D_e^{\ *}(\bar{x})\right\}_{low\ fideltiy}$ and $\left\{Vi^{*}(\bar{x})\right\}_{low\ fideltiy}$ can be seen in Figure 5-11 and Figure 5-12 respectively. Nice model fits are obtained for both parameters.

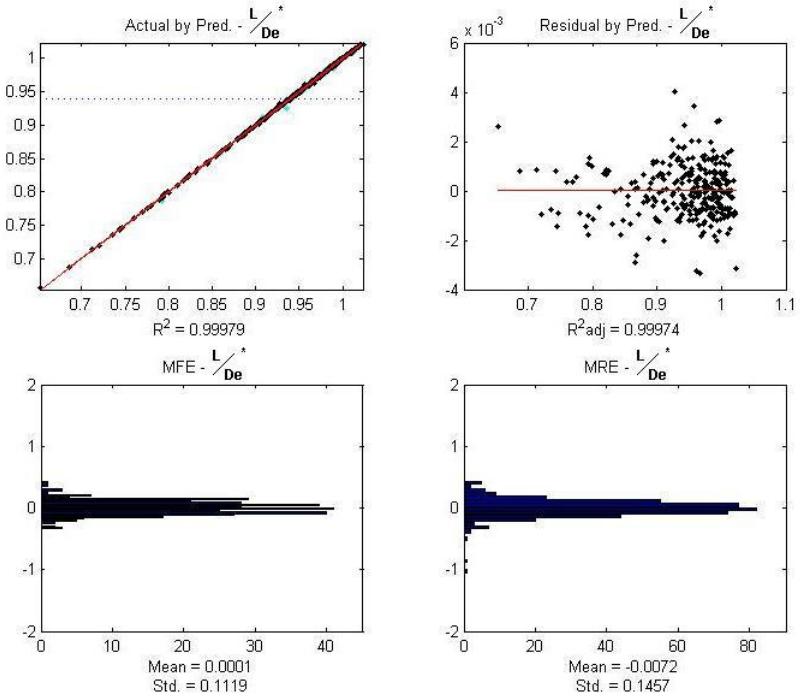

Figure 5-11: Surrogate Model Fit Information for Low Fidelity L/De*

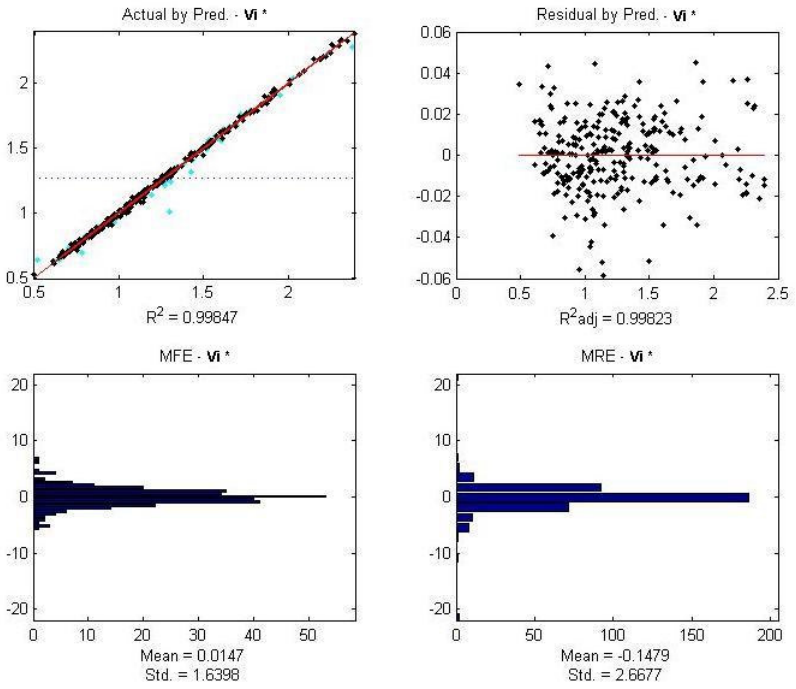

Figure 5-12: Surrogate Model Fit Information for Low Fidelity Vi*

Now that the process has been used to create surrogate models of the low fidelity metrics and also surrogate models of the low to high fidelity scaling functions, it is now time to use these various surrogates to generate designs on the L/D_e^* and Vi^* Pareto Frontier.

5.5.6 **Pareto Frontier Generation**

This test case has been built around the multi-objective optimization problem of increasing rotor efficiency as represented by rotor lift to effective drag while reducing the vibration level. This problem is stated in equations 5-8 – 5-10 . The goal is to minimize the negative of the lift to drag and minimize the vibration index. Equation 5-8 puts this into standard multi-objective optimization form. Again, this is accomplished by varying the six design variables shown in Figure 4-5. This optimization problem, as stated earlier, yields not a single optimum but many optimums that make up the Pareto Frontier.

$$\text{Minimize: } \begin{bmatrix} F_1 \\ F_2 \end{bmatrix} \qquad \text{objective function} \qquad \textbf{5-8}$$

where:

$$F_1 = -\left\{ L/D_e{}^{*}(\bar{x}) \right\}_{high\ fidelity} \qquad \text{Maximize L/De} \qquad \textbf{5-9}$$

$$F_2 = \left\{ Vi^{*}(\bar{x}) \right\}_{high\ fidelity} \qquad \text{Minimize Vibration} \qquad \textbf{5-10}$$

by changing:

$$\bar{x} = (x_1, x_2, ..., x_6) \qquad \text{design variables}$$

Because surrogate models are being used, the number of function calls required to perform this optimization task is not really important. Multi-Starting Point Gradient Based Optimization (see Figure 4-31) is used to find local optimums from every corner of the design space. For six design variables at high and low settings, this makes $2^6 = 64$ starting locations. From the 64 optimums, a global optimum is selected.

Minimizing both F_1 and F_2 separately, the Pareto anchor designs are found. The resulting Pareto anchors found in each objective are given in Table 5-7. The values of L/D_e and *Vi* given for each design are the actual high fidelity values calculated using the GT-HYBRID/RCAS/PSU-WOPWOP framework. For the maximum L/D_e design, the L/D_e has been increased by 3.4%. The historical Brequet range equation states that $R \propto L/D$ which means the rotor could potentially have an increased range of ~3%. The minimum *Vi* design shows a reduction in the vibration index from the baseline of almost 50%. More discussion of the best rotor efficiency and low vibration designs is given in Section 5.5.7.

Table 5-7: High Fidelity Pareto Anchors Found Using Surrogate Models

	c/4 Sweep Angle	Anhedral Angle	Taper Ratio	Twist1	SwitchTwistx	Twist2	L/De	Vi
Baseline HART-II	0	0	1	-8	0.90	-8	2.97	196.62
Maximum L/De	15	0	1	-8	0.91	24.96	3.07	156.84
Minimum Vi	3.98	10.13	1	-8	0.85	27.17	2.87	98.83
Note: Values for L/De and Vi are Calculated in High Fidelity GT-HYBRID/RCAS Framework								

In the remainder of this section, designs located on the L/D_e and *Vi* Pareto Frontier are generated using four different methods. All methods use a sequence of optimizations to find points on the frontier. A notional description of each technique is described in Appendix H. In this section, all Pareto Frontier charts will have the same axes, F_1 and F_2 described by equations 5-9 and 5-10. The values of F_1 and F_2 are determined using the high fidelity surrogate approximations.

Each optimization required by the methods used was performed using `fmincon` within MATLAB® using Multi-Starting Point Gradient Based Optimization. All Pareto Frontier charts will show the anchor designs (minimums in each objective) depicted by solid circles. In addition, the number of designs found on the frontier is restricted to 33 to show how well each of the methods performs at finding an even distribution of designs on the frontier. The Pareto Anchors in each figure are the same anchor designs given in Table 5-7.

The first method used to generate the Pareto Frontier was the Weighted Sum of Objectives approach. This can be seen in Figure 5-13 (a). Each design on the frontier was determined by minimizing a weighted sum of both objectives. For every unique combination of weights, a different design on the Pareto Frontier will be found. However, an even distribution of weights does not guarantee an even distribution of designs on the frontier.

The second approach used was the was ε-Constraint method developed by Marglin [55] and further described in Reference [56]. This can be seen in Figure 5-13 (b). In this method, a sequence of constrained optimizations is performed. In each optimization, the goal is to minimize F_2 while maintaining a constraint that says $\{F_1 \leq \varepsilon(i) \quad i = 1 \ldots n\}$ where n is the number of points being generated and ε is the distance in the F_1 direction between each point found. As seen in the Figure 5-13 (b), the evenness of the distribution of points found on the frontier is better than when using the weighted sum approach. However, improvement can certainly be made.

The third approach used follows the Normal Constraint Method, also described in Reference [56]. The results of using this method can be seen in Figure 5-13 (c). In this method, a line is drawn between the anchor points and is called the utopia line. Next, and even distribution of lines are defined which are normal to the utopia line. In succession, each of these lines that is normal to the utopia line is used as a constraint while F_2 is minimized in a constrained optimization problem. The even spread of designs using this method is better than that produced by the ε-Constraint method.

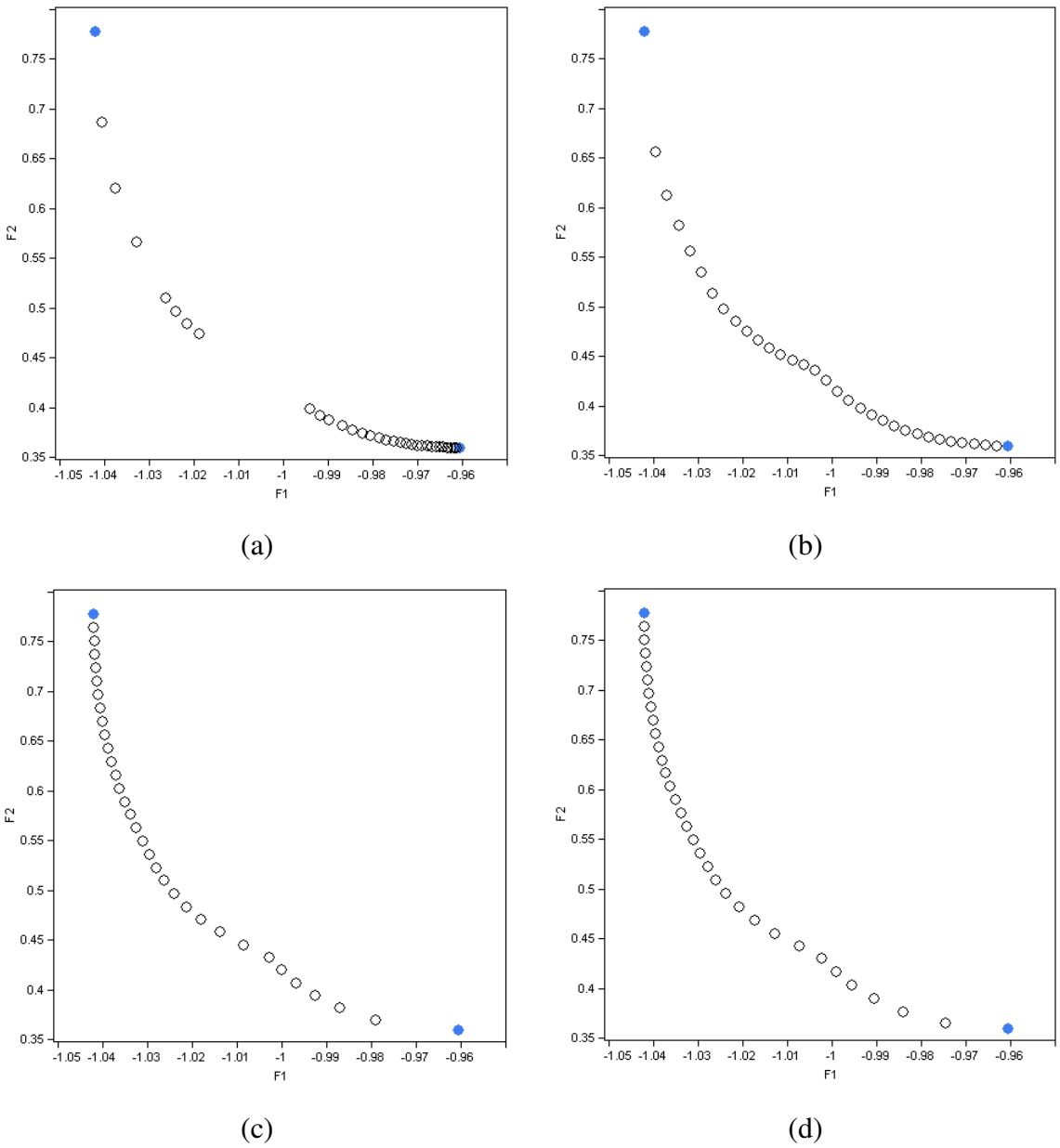

Figure 5-13: Pareto Frontier Generated using Various Methods

(a) Weighted Sum of Objectives (b) ε-Constraint (c) Normal Constraint and (d) Modified Normal Constraint

In this work, a modification was made to the normal constraint method and used as the fourth approach. The results of using this Modified Normal Constraint method can be seen in Figure 5-13 (d). To begin, the utopia line is drawn between the anchor points. Next, a single normal constraint is used and is located at the midpoint of the utopia line. A constrained optimization problem is performed to find a third point on the frontier

located approximately midway between the anchor points. Next, a line is drawn between one of the anchor points and this third point just found. A line normal to this line is drawn located at its midpoint. Using this normal line as a constraint, another constrained optimization is performed to find a fourth point. Then a line is drawn between the other anchor point and the third point. Again, at the midpoint, a line is drawn normal to this line and used in constrained optimization to find a fifth point. This process is continued until a desired number of designs are found.

As seen in Figure 5-13 (d), this method produces a distribution of designs that is slightly more even than the unmodified Normal Constraint method of Figure 5-13 (c). In both (a) and (c) of Figure 5-13, it appears there is a lack of evenness near the minimum F_2 anchor. However, some of this appearance is due to the fact that the scaling of the F_1 and F_2 axes are not the same. To show the difference, the Pareto Frontiers generated using the unmodified and modified Normal Constraint methods are redrawn in Figure 5-14 (a) and (b) respectively with both axes drawn to the same scale. This shows that both produce even distributions of designs along the frontier. However, the modified method does a slightly better job. This is expected since the successive constraints used do not have to be parallel to each other.

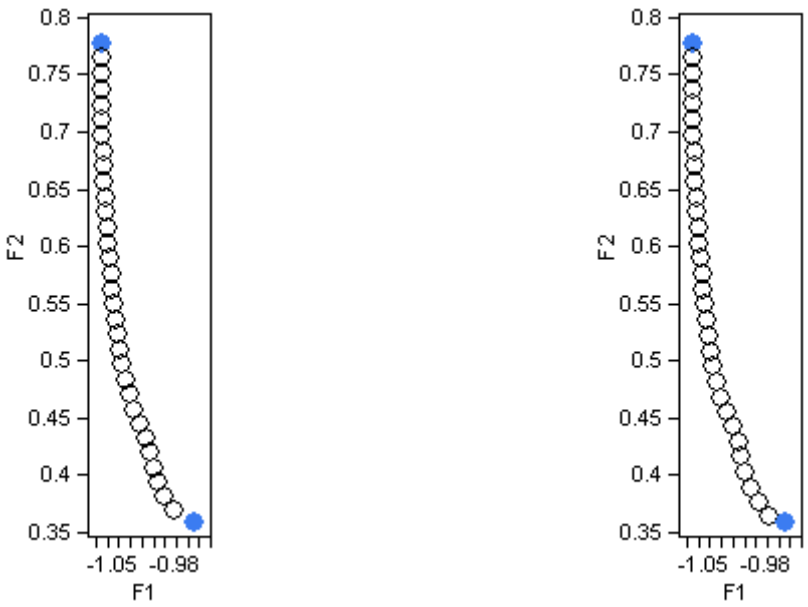

(a) (b)

Figure 5-14: Pareto Frontier Generated using the Normal Constraint Methods

(a) Unmodified and (b) Modified

5.5.7 **High Fidelity Simulation of Pareto Anchor Designs**

To check just how good the Pareto Anchor designs given in Table 5-7 are, they are tested in the high fidelity GT-HYBRID/RCAS/PSU-WOPWOP framework and added back to the database of high fidelity analyzed designs. The top three max L/D_e designs from the database are given in Table 5-8. The design having the highest L/D_e is the same design found using the high fidelity surrogate approximation. This fact gives more confidence that the high fidelity surrogate function for L/D_e^* is capable of pointing to the optimums in the high fidelity domain despite the fact that these surrogate scaling functions were built using less than fifty high fidelity runs.

Table 5-8: Top Three Maximum L/De Designs from High Fidelity Data

	c/4 Sweep Angle	Anhedral Angle	Taper Ratio	Twist1	SwitchTwistx	Twist2	L/De	Vi	Same Picked by Surrogates?
1st	15	0	1	-8	0.91	24.961	3.07	156.84	yes
2nd	15	0	0.6	-8	0.95	45.00	3.06	170.54	no
3rd	15	0	1	-8	0.95	45.00	3.05	169.85	no

Note: Values for L/De and Vi are Calculated in High Fidelity GT-HYBRID/RCAS Framework

The top three minimum *Vi* designs from the high fidelity database are shown in Table 5-9. Here the design picked by the high fidelity approximation has the third lowest value of the vibration metric. While not the same result as obtained above with L/D_e, this is still very good, especially since the trend of the design variables seems to match the top two performers. The reason the high fidelity approximation did not find the 1st design of Table 5-9 lies in the fact that the fit for the scaling function for $\tilde{s}\left\{V_i^*(\bar{x})\right\}$ was deemed acceptable, but was not great as shown previously in Figure 5-9 (b).

Table 5-9: Top Three Minimum Vi Designs from High Fidelity Data

	c/4 Sweep Angle	Anhedral Angle	Taper Ratio	Twist1	SwitchTwistx	Twist2	L/De	Vi	Same Picked by Surrogates?
1st	15	15	1	-8	0.85	45	2.45	85.96	no
2nd	15	0	1	-8	0.85	45	2.75	94.26	no
3rd	3.98056	10.13398	1	-8	0.85	27.17	2.87	98.83	yes

Note: Values for L/De and Vi are Calculated in High Fidelity GT-HYBRID/RCAS Framework

The top design from both Table 5-8 and Table 5-9 are shown in Figure 5-15. These two designs represent the maximum L/D_e design (a) and minimum *Vi* design (b) from the 50+ different designs investigated using the high fidelity framework.

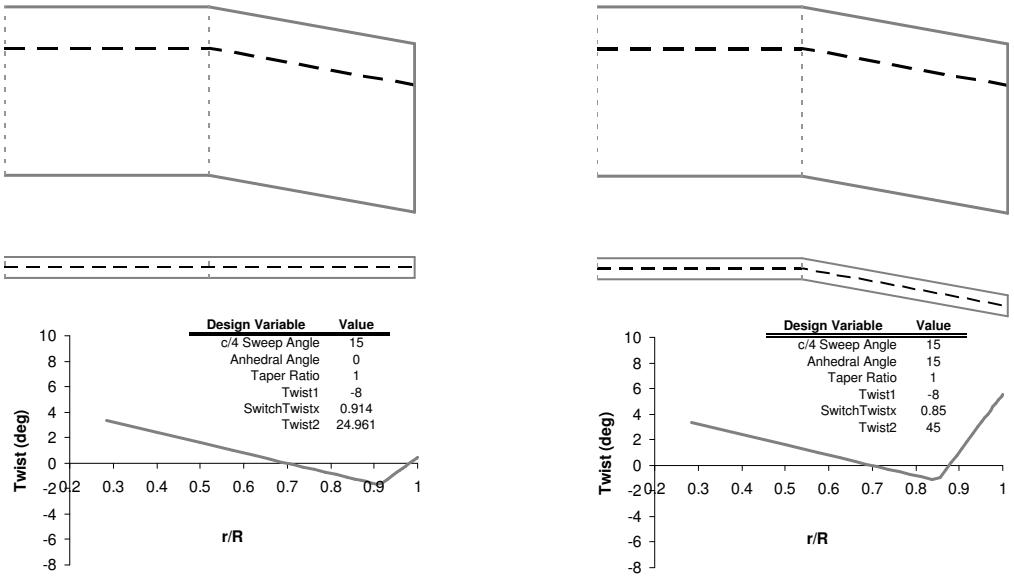

(a) (b)

Figure 5-15: Top High Fidelity Designs for Max L/De (a) and Min Vi (b)

The top L/D_e designs exhibit similar traits in most design variables. All have the maximum 15 degrees of sweep, no anhedral, the least negative -8 degree inboard twist rate, and a positive outboard twist rate. To understand the cause of the L/D_e improvement when compared to the baseline, the parameters of the L/D_e equation given in equation 5-3 are compared in Table 5-10. The largest parameter change occurs for F_X. This means that the amount of force acting in the direction of thrust is increased for the optimum L/D_e design. Figure 5-16 shows a contour plot of the difference between the baseline and optimum L/D_e design in airloads acting in the x direction. In this plot, the value is negative where the optimum L/D_e design has improvement over the baseline. The plot indicates the optimum L/D_e is reducing the drag on the tip of the retreating side as well as on the inboard advancing side. The effect of tip sweep alone can not explain the benefit since it appears that more drag is created on the advancing side due to the higher angle of attack created by the positive outboard twist rate.

Table 5-10: Components of L/De Metric for Baseline and Max L/De Designs

	Baseline	Max L/De	%change
Fz (N)	3342.44	3351.22	0.26%
Fx (N)	-139.62	-174.84	25.22%
Mz (N.m)	709.51	711.08	0.22%
L (N)	3342.44	3351.22	0.26%
De (N)	1124.70	1092.27	-2.88%

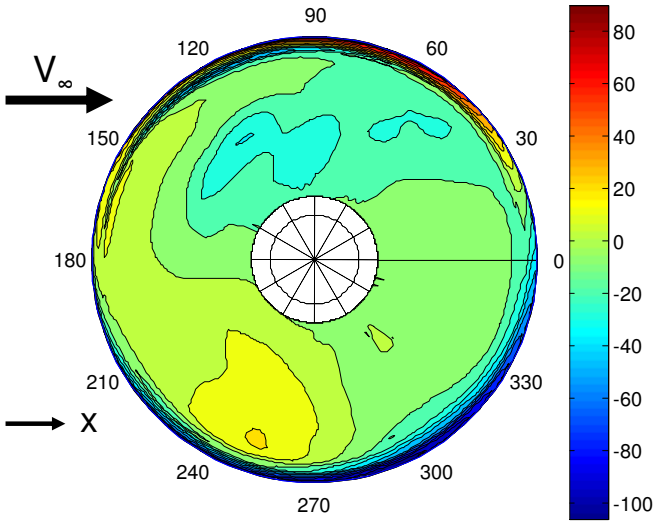

Figure 5-16: Difference in Local Fx Force Between Max L/De and Baseline Designs

The top *Vi* designs also exhibit similar traits. All have some sweep while the top two designs have the maximum. Two of the designs have anhedral while the second place design had none. However, the design with minimum *Vi* had the maximum anhedral and had a vibration index 9% smaller than the second place design. All designs had no taper and the least negative inboard twist rate of -8 degrees. All also had a positive outboard twist rate with the top two designs having the maximum of 45 degrees. Table 5-11compares the components that make up the vibration index between the baseline and the minimum vibration design. The minimum *Vi* design has a reduction in every 4 per rev force or moment harmonic with the exception of main rotor torque harmonic, M_{zH}^{4P}. This is expected since the overall value of the main rotor torque is large in comparison to

the other forces and moments. The design variables are changing the airloads in such a way that cause the rotor to be trimmed to a low state of vibration. This can be seen in Figure 5-17 which shows the change in pitching moment ($C_m M^2$) with azimuth angle (Ψ) or $dC_m M^2 / d\Psi$. This plot highlights pitching moment fluctuations which can be a source of vibration. In general, the plot for the design for minimum Vi in Figure 5-17 (b) has fewer ripples when compared to the baseline in Figure 5-17 (a). The exact reason for the reduced vibration is difficult to pinpoint as it is probably due to a combination of tip sweep and positive twist rate.

Table 5-11: Components of Vi Metric for Baseline and Min Vi Designs

	Baseline	Min Vi	%change
Fx_4P (N)	102.5	41.7	-59.32%
Fy_4P (N)	97.6	35.4	-63.73%
Fz_4P (N)	58.0	23.7	-59.14%
Mx_4P (N.m)	27.9	14.3	-48.75%
My_4P (N.m)	27.7	8.1	-70.76%
Mz_4P (N.m)	19.0	20.5	7.89%

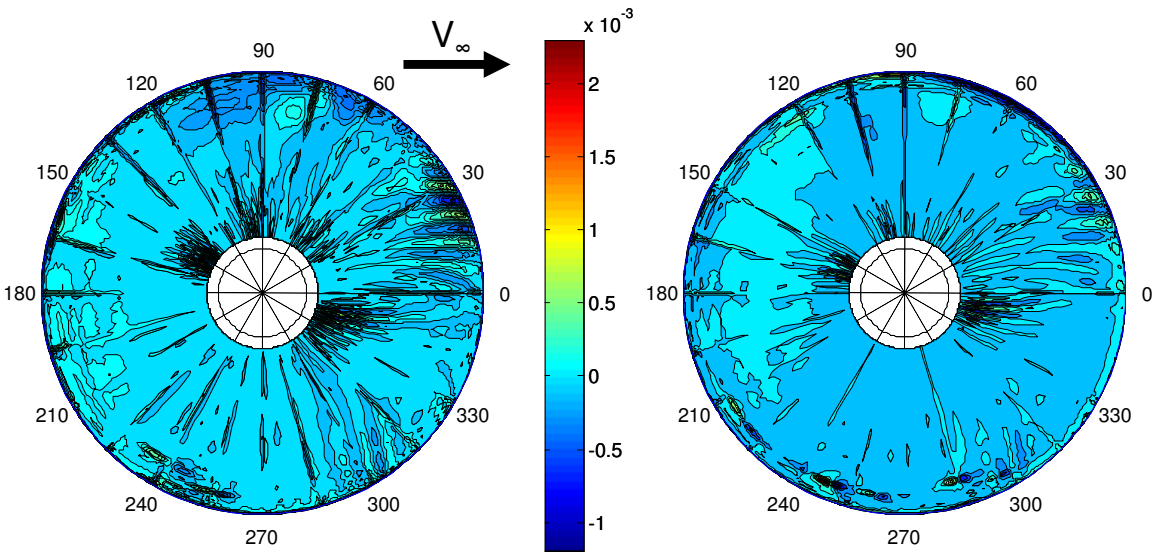

(a) (b)

Figure 5-17: $d(C_m M^2)/d(\psi)$ for Baseline (a) and Minimum Vi (b) Designs

Regardless of the exact mechanisms producing the lower vibration, a look at the histories of all six hub forces and moments shows the reduction in peak-to-peak vibration levels. Figure 5-18 shows plots of these histories. The histories of the moments shown in Figure 5-18 (b, d, & f) have the means removed.

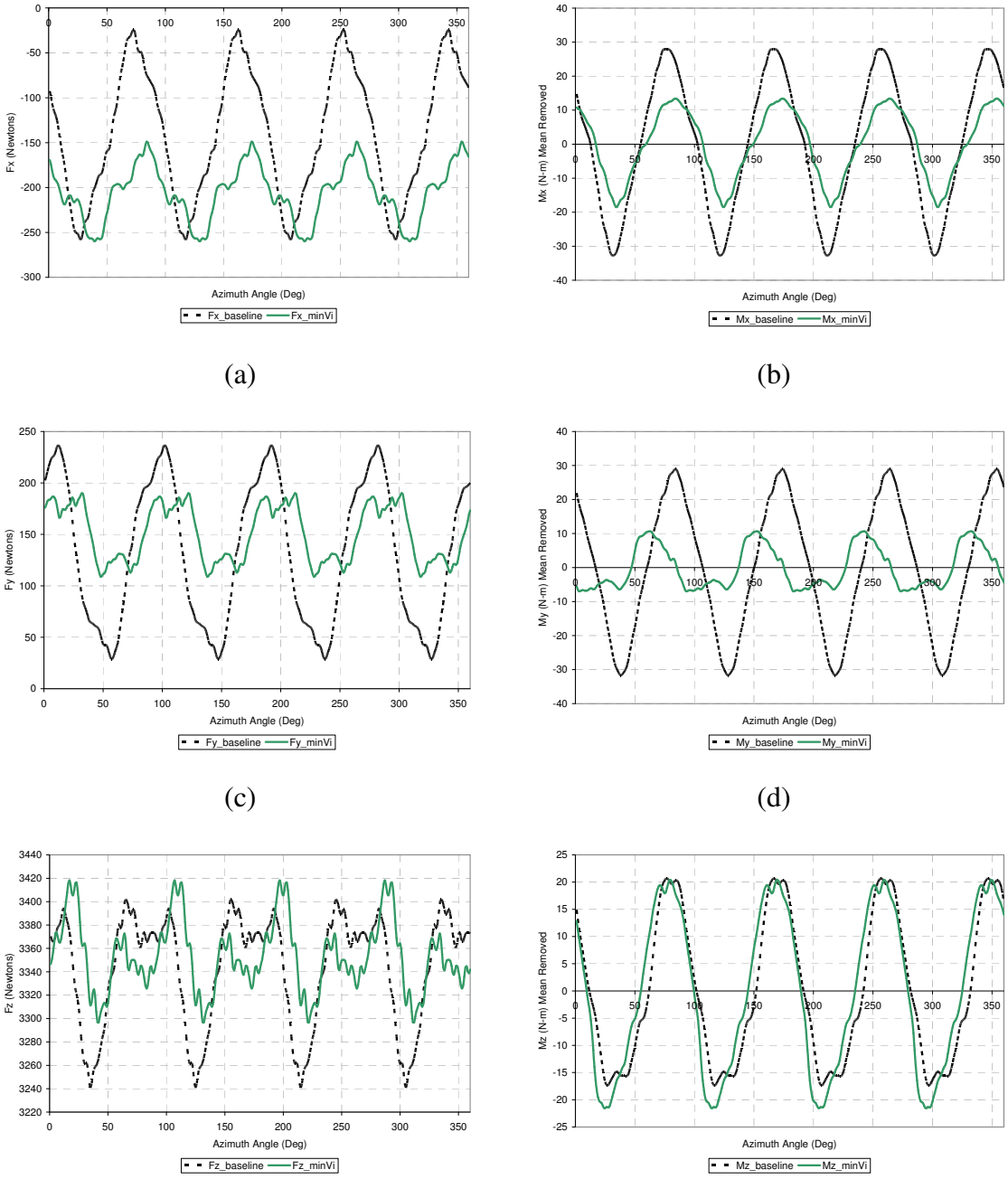

Figure 5-18: Minimum Vi Hub Force and Moment Histories

Force and Moment Histories (Moments Shown with Means Removed): (a) Fx (b) Mx (c) Fy (d) My (e) Fz and (f) Mz

Both maximum L/D_e and minimum Vi optimums shown in Figure 5-15 were found to have less vibration than the baseline. A comparison of the vibratory characteristics of both the maximum L/D_e and minimum Vi designs can be seen in Figure 5-19. For comparison, this is the same chart previously shown in Figure 4-23 when the optimum found during preliminary research was examined with high fidelity tools and shown to have more vibration than the baseline.

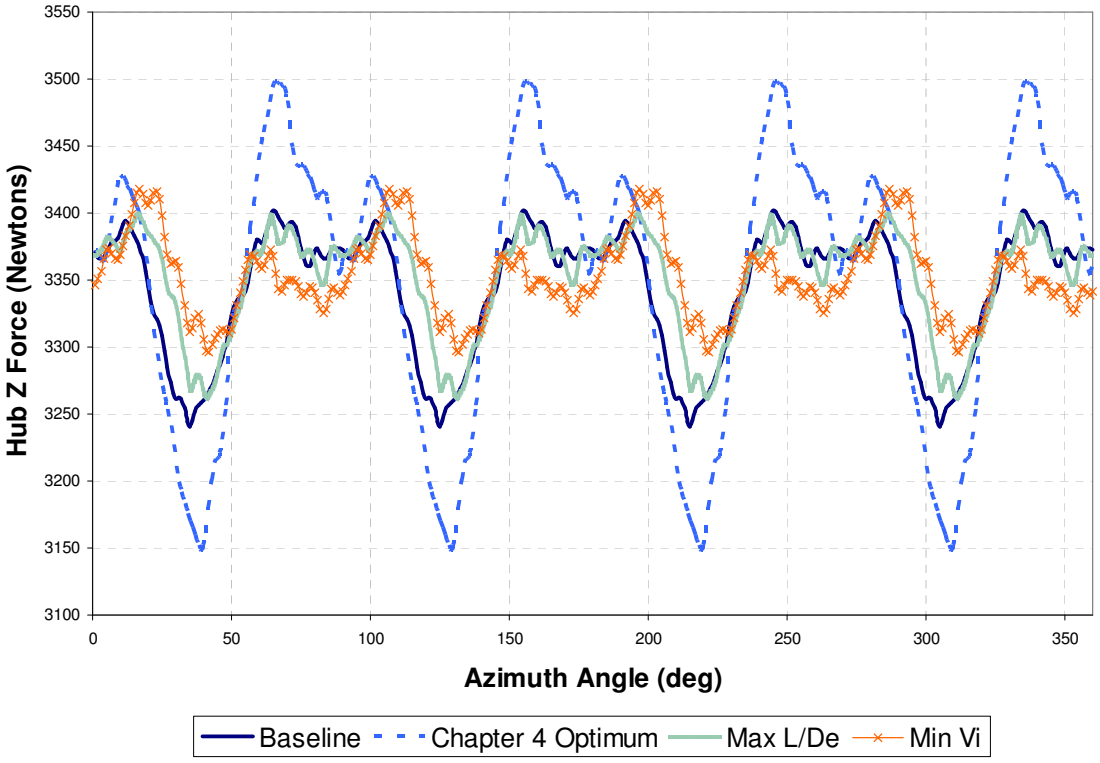

Figure 5-19: Hub Z-Force History for High Fidelity Max L/De and Min Vi Designs

In this test case, noise was not used as a metric during the optimization. However, the noise characteristics for both of these designs can be investigated since the framework already performs an aeroacoustic analysis. This investigation for the optimum rotor blades shown in Figure 5-15 is given in Table 5-12. The two rotors being compared with the baseline were not designed specifically to reduce the noise metric. The max L/D_e

design performed slightly better than the baseline acoustically; whereas the min *Vi* design was louder by about 1.5 dB.

Table 5-12: Acoustic Metric Comparison of Max L/De and Min Vi Designs

Forward Flight	GTHYBRID/RCAS/PSU-WOPWOP Baseline	Max L/De	Min Vi	
J_{NF}	106.02	105.79	107.56	dB
Pt 1	106.48	105.82	109.21	dB
Pt 2	106.91	105.93	108.62	dB
Pt 3	105.48	104.83	108.31	dB
Pt 4	104.03	104.17	108.17	dB
Pt 5	109.25	108.80	111.21	dB
Pt 6	109.12	108.39	108.92	dB
Pt 7	103.94	103.02	105.43	dB
Pt 8	103.72	104.45	108.32	dB
Pt 9	109.96	109.63	111.66	dB
Pt 10	111.48	111.26	111.43	dB
Pt 11	104.00	102.70	97.34	dB
Pt 12	96.94	98.72	103.98	dB
Pt 13	108.06	107.79	108.55	dB
Pt 14	109.37	109.55	110.63	dB
Pt 15	108.12	108.42	109.80	dB
Pt 16	99.51	99.10	99.41	dB

Louder than Baseline

Quieter than Baseline

So questions remain on what low fidelity "options" create the best balance of simplifying assumptions and essential physics. Prescribed wake may be better than dynamic inflow at predicting the trends of the metrics under consideration. Or, one option may be better for one metric but not another. These questions are not trivial to answer and require many experiments. In any case, there is considerable research that could be done in determining which models should be used in various situations. That being said, the research performed here has shown that despite the fact the low fidelity models may not predict the physics of the high fidelity domain with complete accuracy, a method of performing a limited number of experiments with both low and high fidelity analysis can allow the creation of scaling functions to map low fidelity results to the high fidelity

domain. Surrogate models of both low fidelity metrics such as L/D_e and Vi and their scaling functions can be used in an optimization problem to find designs that appear to be optimum in the true high fidelity domain. And while the test case shown only used rotor efficiency and vibration in forward flight as metrics under consideration, the method could be applied to other metrics and other flight conditions as well.

5.6 Chapter Summary

The methods and results presented in this chapter report on the work done to answer the questions driving the research. One, "What disciplinary analysis elements can be combined to form an efficient high fidelity CFD/CSD/AA simulation for application to rotary wing optimization?" And two, "In what way can low and high fidelity rotary wing simulations be used together in a process of rotary wing design?" Both low and high fidelity frameworks for rotary wing simulation were developed from integrating a variety of industry standard disciplinary analysis tools. Together, these automated low and high fidelity frameworks were used in a synergistic process of rotary wing optimization; solving the same problem.

The method and results covered in this chapter pull elements from preliminary research of Chapter 4 and inject new elements to meet the objectives and make novel contributions to the field of rotary wing design research. The low fidelity model is updated with elastic blades and assumed to have a dynamic inflow and 2-D table look-up aerodynamics. The high fidelity forward flight CFD/CSD/AA framework is automated so as to be able to perform a Design of Experiments. As a test, the high fidelity framework is used to examine the optimums given in Section 4.3.3.

Next, a process is developed where both low and high fidelity frameworks can be used together to solve a common rotor optimization problem. The process begins by performing a screening DOE using both low and high fidelity frameworks. A scaling parameter equal to the ratio of a high to low fidelity parameter value of interest is used as

a response. The importance of the effects of the design variables and their interactions on the scaling parameter is estimated, leading to an estimate of the form of the RSE of the scaling parameter. An additional fractional factorial DOE is performed by both low and high fidelity frameworks to add more data to fit the estimated RSE model. In parallel, the process calls for performing a number of experiments with the low fidelity model alone to build RSE's of the parameter value of interest. An approximation of the high fidelity parameter value can then be obtained by multiplying the RSE for the scaling function to the RSE for the low fidelity parameter value. The surrogate models can then be used in an optimization process to arrive at an estimate for an optimum in the high fidelity domain.

This process is tested using the HART-II rotor in forward flight for objectives of both rotor efficiency and vibration. Both low and high fidelity frameworks are used in a screening DOE and subsequent fractional factorial DOE. A total of 50+ experiments were performed. The results of these experiments are used to build a surrogate model of a scaling function to map the low fidelity objective and constraint values to the high fidelity domain. In parallel, separate DOE's are performed by the low fidelity model alone and surrogate models of the objective and constraint are built. The surrogates of low fidelity parameters and their scaling functions are used to find optimum values of the design variables to maximize lift to drag while constraining vibration. In addition, the surrogates are used to generate designs on the Pareto Frontier. Optimums found are tested in the high fidelity framework and found to be feasible in terms of vibration and also to have the highest rotor efficiency when compared to the 50+ designs previously analyzed. The frameworks and methods developed show that various enabling technologies can be exploited to allow high fidelity tools to become integral elements of optimization studies.

Chapter 6

Concluding Remarks

6.1 Overview

The research documented in this thesis has been driven by two research questions. The first question – "What disciplinary analysis elements can be combined to form an efficient high fidelity CFD/CSD/AA simulation for application to rotary wing optimization?" – stems from the desire to utilize high fidelity, state-of-the-art rotorcraft analysis tools in preliminary design stage optimization which is currently dominated by lower fidelity tools. The second question – "In what way can low and high fidelity rotary wing simulations be used together in a process of rotary wing design?" – stems from the desire to exploit the ideas related to multi-fidelity optimization in the rotorcraft discipline.

The research performed to answer the research questions has achieved four separate objectives. The core objective of this research is to create an integrated and automated high fidelity framework for rotary wing simulation for use in design and optimization studies. A second objective is to also develop an integrated and automated low fidelity framework for rotary wing simulation for use in design and optimization studies. The third objective is to combine both frameworks together in a process of rotary wing optimization to solve the same problem. A final objective is to test these various frameworks and processes and document the findings in this thesis.

The methods and results documented in this thesis provide evidence that the objectives have been met. In the next section of this chapter, key findings will be discussed. This is followed by a list of the major contributions from this work. Lastly, a section is devoted to the avenues for future work.

6.2 Key Findings

The following are four key findings from the research. They are listed here and then a discussion follows.

1) Design Frameworks and Parallel Computing are the key enabling technologies for preliminary design stage optimization to be performed using high fidelity rotorcraft analysis tools.

2) Utilizing high fidelity tools in preliminary rotorcraft design is a perfect application for Design of Experiments (DOE) and Surrogate Modeling.

3) Pareto Frontier generation methods that use a sequence of constrained optimization problems are more effective at finding the frontier than more random methods like Monte Carlo Simulation.

4) Combining DOE, surrogate modeling, and concepts from multi-fidelity optimization can allow low and high fidelity rotorcraft simulation tools to create approximations of the high fidelity domain which can be used in various optimization tasks.

A design framework such as ModelCenter® is very effective at allowing the analysis tools from multiple rotorcraft disciplines to be combined into a single simulation framework. The ability of the framework to make custom input files based on a generic template for a particular analysis is very useful in parameterization. The ability of the framework to utilize components on different computers within a network – whether Windows or Linux based – allows flexibility in the types of disciplinary analysis tools that can be used. This also makes it easy to make components from analyses located on a computer cluster, giving access to those high fidelity tools which can be run in parallel.

Access to parallel computing is on the rise. This means that for high fidelity simulation tools properly coded to utilize multiple processors, great time savings can be made per analysis. For the designer, this also means that it is possible to analyze numerous design configurations simultaneously. This impacts the strategies used to utilize these tools in optimization problems. Strategies that involve experiments that can be analyzed in parallel will dominate. Parallel strategies include domain spanning methods of optimization like Grid Search, Genetic Algorithm, and Monte Carlo Simulation. These methods still however could require hundreds of analysis runs depending on the number of design variables being investigated. This can take days even when low fidelity rotorcraft simulations are used. In addition, by their nature, these parallel strategies alone however do not guarantee that the true global optimum will be found. Thus serial approaches like gradient based optimization are still desired. This makes this application perfect for use of a surrogate model to approximate results.

The surrogate model can be created from data collected in a DOE. The experiments in the DOE are defined ahead of time and can therefore be executed in parallel, which makes efficient use of parallel computing. Once the surrogate model is created, it can be executed in less than a second. This removes the issue of worrying about the number of function calls for a particular optimization strategy since it really isn't an issue. In addition, it is reusable, meaning it can be used in a gradient based optimization for one study, then Monte Carlo Simulation, grid search, or genetic algorithm for another.

In Chapter 4, a Monte Carlo Simulation was performed using surrogate models of objectives to analyze four million possible rotor blade configurations. It was shown that while it was hoped that this large number of points would begin to define the Pareto Frontier, a test to find the anchor designs using a Genetic Algorithm proved otherwise. Solving an optimization problem found a much better design than simply selecting the best design from the Monte Carlo Simulation. This showed that methods of generating

points on the Pareto Frontier that solve a sequence of constrained optimization problem would find points much closer to the actual Pareto Frontier than through a random process like Monte Carlo Simulation.

These findings are a few of the many things learned in the process of performing the research documented in this thesis. The specific novel contributions made are described next.

6.3 Contributions

The novel contributions presented in this thesis include simulation frameworks and method that have been successfully developed and demonstrated to allow for an efficient process to improve rotor blade designs in terms of a selected choice of objectives. With improvements in the low and high fidelity prediction components that will certainly occur, this framework could become a powerful tool for future rotorcraft design work. A summary of the specific contributions is given below.

1) An automated high fidelity CFD based forward flight simulation framework has been built for use in preliminary design stage optimization. The framework was built around an integrated, parallel processor capable CFD/CSD/AA process.

2) A novel method of building approximate models of high fidelity parameters has been developed. The method uses a combination of low and high fidelity results and combines Design of Experiments, statistical effects analysis, surrogate modeling, and aspects of approximation model management.

3) Determination of rotor blade shape variables through optimization using CFD based analysis in forward flight has been performed. This was done using the high fidelity CFD/CSD/AA framework and method mentioned above.

6.4 Recommendations for Future Work

This thesis work has advanced the state-of-the-art in terms of methods that allow high fidelity rotorcraft simulation tools to be applied to preliminary design stage optimization. But the book is by no means closed on this. There are a number of avenues for future work. A few of those are listed below.

1) Use the methods developed in this thesis to perform optimization studies of importance to the industry.

2) Experiment with other forms of non-CFD based low fidelity models to document which low fidelity model options work best when acquiring a particular parameter of interest. In other words, attempt to answer which options provide results closest to the high fidelity answers.

3) Integrate technologies related to Arbitrary Shape Deformation (ASD) to investigate the impact of arbitrary shape changes to a rotor blade's tip region for improvements in efficiency, noise, and vibration.

4) Perhaps there are different types of scaling parameters that could be used in the methodology of Figure 5-7. In addition, there could be other types of screening DOE's that may work better under certain conditions. Following the screening, there may be better DOE's to gather data for surrogate modeling of the scaling function that those used here. Or perhaps adaptive methods could be devised to build a model of the high fidelity approximation on the fly. These types of investigations are left for future work.

6.5 Final Remarks

In closing, the work represented in this dissertation has unlocked a large potential for future design studies in rotorcraft. The ability to utilize efficient, high fidelity tools to

solve real world problems will certainly be of interest to designers of rotorcraft. The example used throughout was the optimization of a 40% scale BO-105 rotor blade using design variables of tip geometry and spanwise twist distribution. This example is indicative of the types of problems real world rotorcraft designers are trying to solve. And throughout this thesis, various "optimized" configurations have been revealed. However, the design variables settings for these optimums are not as important as the frameworks and methods used to derive them. The methods developed in this thesis and future modifications to them will certainly by appreciated by those working in this field.

Appendix A

RCAS Rigid Blade Model

The preliminary research reported in Chapter 4 used a rigid blade RCAS model of the HART-I rotor as the baseline for the low fidelity simulations. This appendix lists some of the more detailed information about this model. Basic parameters of the HART-I rotor are given in Table A-1. Each rigid blade had structural members A-M and Aerodynamic segments 1-29 as shown in Figure A-1.

Table A-1: Basic Parameters of HART-I Baseline

Description	Value
Radius	2 m
Chord	0.121 m
Nominal Rotational Speed	110 rad/sec
Linear Twist Rate	-8 deg
Zero Twist Span %	0.7

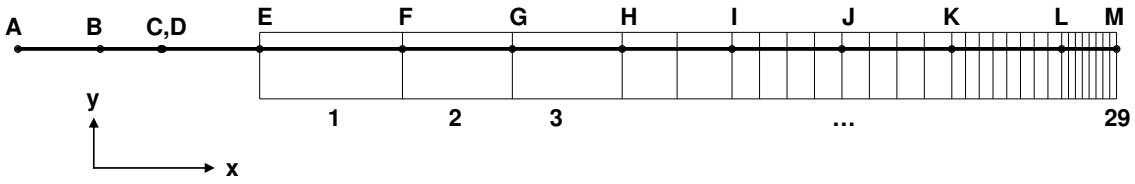

Figure A-1: RCAS Rigid Blade HART-I Model

(Structural Nodes A thru M and Aerodynamic Segments 1 thru 29)

The structural nodes A-M are located at the x and y locations given in Table A-2. Mechanical hinges for pitch, flap, and lag are located at nodes B, C, and D respectively. A torsion node is located at node D also, but is assumed to be outboard of the lag node by being listed second in the RCAS file. The flap hinge has a spring of stiffness 610.7 N.m/rad. The lag hinge has a spring of stiffness 7552.5 N.m/rad and a damper constant

equal to 2.4084 N.m.s/rad. The torsion spring had a stiffness of 359.8 N.m/rad. The rigid bars connecting the nodes and hinges have length and mass given in Table A-3.

Table A-2: Structural Nodes of RCAS Rigid Blade HART-I Baseline

Node	x/R	y/R	
A	0	0	Root
B	0.075	0	Pitch Hinge
C	0.13	0	Flap Hinge
D	0.1318	0	Lag, Torsion Hinges
E	0.22	0	Blade Start
F	0.35	0	
G	0.45	0	
H	0.55	0	
I	0.65	0	
J	0.75	0	
K	0.85	0	
L	0.95	0	
M	1	0	Blade Tip

Table A-3: Rigid Bars of RCAS Rigid Blade HART-I Baseline

Start	End	Length (m)	Mass (kg)
A	B	0.15	0.45504
B	C	0.11	0.177408
C	D	0.0036	0.0058061
D	E	0.1764	0.169344
E	F	0.26	0.2496
F	G	0.2	0.192
G	H	0.2	0.192
H	I	0.2	0.192
I	J	0.2	0.192
J	K	0.2	0.192
K	L	0.2	0.192
L	M	0.1	0.096

The aerodynamic segments 1-29 are all composed of NACA 23012 airfoil sections. The center of each segment is located at the ¼ chordline in the middle of the segment's width. The location of each segment center, along with the segment width, is listed in Table A-4. The rotating frequencies of the rigid blade model are compared with

the rotating frequencies of the actual HART-I blade in Table A-5. The frequencies of the HART-I blade are taken from Reference [4].

Table A-4: Aerodynamic Segment Locations of RCAS Rigid Blade HART-I Baseline

	Segment Center		Width
Segment	x/R	y/R	dx/R
1	0.285	0	0.13
2	0.4	0	0.1
3	0.5	0	0.1
4	0.575	0	0.05
5	0.625	0	0.05
6	0.6625	0	0.025
7	0.6875	0	0.025
8	0.7125	0	0.025
9	0.7375	0	0.025
10	0.7625	0	0.025
11	0.7875	0	0.025
12	0.8125	0	0.025
13	0.8375	0	0.025
14	0.85625	0	0.0125
15	0.86875	0	0.0125
16	0.88125	0	0.0125
17	0.89375	0	0.0125
18	0.90625	0	0.0125
19	0.91875	0	0.0125
20	0.93125	0	0.0125
21	0.94375	0	0.0125
22	0.953125	0	0.00625
23	0.959375	0	0.00625
24	0.965625	0	0.00625
25	0.971875	0	0.00625
26	0.978125	0	0.00625
27	0.984375	0	0.00625
28	0.990625	0	0.00625
29	0.996875	0	0.00625

Note: Segment Center on quarter chord line at middle of width and thickness

Table A-5: HART-I Rotating Natural Frequencies Compared with RCAS Rigid Blade

Hz	RCAS	HART-I
Flap	19.42	20.00
Lag	13.426	11.50
Torsion	58.087	67.5

A prescribed wake inflow model was used for both hover and forward flight conditions. In hover, the Landgrebe model from maximum bound circulation was used. In forward flight, the Classical helix wake with no distortion was used. In both cases, 32 time steps per revolution were used.

Appendix B

RCAS Elastic Blade Model

The research reported in Chapter 4 and Chapter 5 made use of an elastic blade RCAS model of both the HART-I and HART-II rotors. This model was used in both low and high fidelity simulations. This appendix lists some of the more detailed information about this model. Basic parameters of the HART-I and HART-II rotors are given in Table B-1. Each elastic blade had structural members A-R and Aerodynamic segments 1-29 as shown in Figure B-1.

Table B-1: Basic Parameters of the HART-I & II Baseline

Description	Value
Radius	2 m
Chord	0.121 m
Nominal Rotational Speed	110 rad/sec
Linear Twist Rate	-8 deg
Effective Flap Hinge %	0.13
Zero Twist Span % (HART-I)	0.7
Zero Twist Span % (HART-II)	0.75

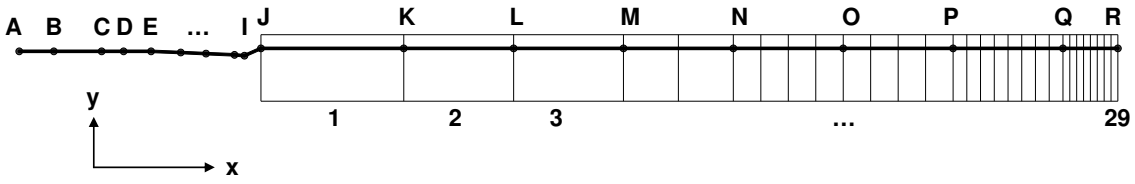

Figure B-1: RCAS Elastic Blade HART-I & II Model

(Structural Nodes A thru R and Aerodynamic Segments 1 thru 29)

The structural nodes A-R are located at the x and y locations given in Table B-2. Each of these nodes is connected by a nonlinear beam element. The RCAS models used for the HART-I and HART-II differed in two aspects: 1) The location of zero twist and

2) The nonlinear beam properties. The differences in the location of zero twist can be seen in Table B-1.The nonlinear beam properties can be found for the HART-I in Reference [4] and for the HART-II in Reference [98].

Table B-2: Structural Nodes of RCAS Elastic Blade HART-I & II Baseline

Node	x/R	y/R	
A	0	0	Root
B	0.0315	0	
C	0.075	0	Pitch Hinge
D	0.095	0	
E	0.12	0	
F	0.147	-0.00106	
G	0.17	-0.00207	
H	0.195	-0.00313	
I	0.205	-0.00397	
J	0.22	0.00268	Blade Start
K	0.35	0.00268	
L	0.45	0.00268	
M	0.55	0.00268	
N	0.65	0.00268	
O	0.75	0.00268	
P	0.85	0.00268	
Q	0.95	0.00268	
R	1	0.00268	Blade Tip

The aerodynamic segments 1-29 are all composed of NACA 23012 airfoil sections. The center of each segment is located at the ¼ chordline in the middle of the segment's width. The location of each segment center, along with the segment width, is listed in Table B-3. The rotating frequencies of the HART-I elastic blade model are compared with the rotating frequencies of the actual HART-I blade in Table B-4. The frequencies of the HART-I blade are taken from Reference [4]. The rotating frequencies of the HART-II elastic blade model are compared with the rotating frequencies of the actual HART-II blade in Table B-5. The frequencies of the HART-II blade are taken from Reference [98].

Table B-3: Aerodynamic Segment Locations of RCAS Elastic Blade Model

Same Aerodynamic Segment Locations Used for both HART-I & II RCAS Models

	Segment Center		Width
Segment	x/R	y/R	dx/R
1	0.285	0	0.13
2	0.4	0	0.1
3	0.5	0	0.1
4	0.575	0	0.05
5	0.625	0	0.05
6	0.6625	0	0.025
7	0.6875	0	0.025
8	0.7125	0	0.025
9	0.7375	0	0.025
10	0.7625	0	0.025
11	0.7875	0	0.025
12	0.8125	0	0.025
13	0.8375	0	0.025
14	0.85625	0	0.0125
15	0.86875	0	0.0125
16	0.88125	0	0.0125
17	0.89375	0	0.0125
18	0.90625	0	0.0125
19	0.91875	0	0.0125
20	0.93125	0	0.0125
21	0.94375	0	0.0125
22	0.953125	0	0.00625
23	0.959375	0	0.00625
24	0.965625	0	0.00625
25	0.971875	0	0.00625
26	0.978125	0	0.00625
27	0.984375	0	0.00625
28	0.990625	0	0.00625
29	0.996875	0	0.00625

Note: Segment Center on quarter chord line at middle of width and thickness

Table B-4: HART-I Rotating Natural Frequencies

Experimental Compared with RCAS HART-I Elastic Blade Model

Hz	RCAS	HART-I
Lag	10.34	11.50
Flap	18.74	20.00
Flap	46.88	46.00
Torsion	64.60	67.50
Lag	76.20	78.50
Flap	81.89	82.50

Table B-5: HART-II Rotating Natural Frequencies

Experimental Compared with RCAS HART-II Elastic Blade Model

Hz	RCAS	HART-II
Lag	13.09	13.55
Flap	17.09	19.49
Flap	46.10	49.11
Torsion	75.55	66.61
Lag	79.02	79.55
Flap	85.47	89.53

The elastic blade model used in Chapter 5 for low fidelity simulations used a dynamic inflow model for inflow. Aerodynamic forces were calculated using a 2-D table look-up of aerodynamic coefficients with 72 time steps per revolution. When used with CFD in CFD/CSD coupling, the RCAS model used uniform inflow plus delta airloads for post CFD trim with 360 time steps per revolution.

Appendix C

GT-HYBRID Blade Model

GT-HYBRID is 3-D compressible Reynolds Averaged Navier-Stokes (RANS) flow SOLVER. The methodology is hybrid in the sense that it doesn't use Navier-Stokes to capture the far, wake which can extend up to 4-6 rotor radii. Instead it uses a wake model (Figure C-1) which is basically a collection of linear segments of vorticity whose strengths are based on the loading on the blade. The downwash from this wake is introduced as a boundary condition on the computational domain. The use of hybrid methodology has 2 main advantages: 1) It is computationally very efficient since you do not need massive grids. And 2) We can avoid numerical dissipation which is otherwise a problem if we try to use coarse grids to capture the far wake.

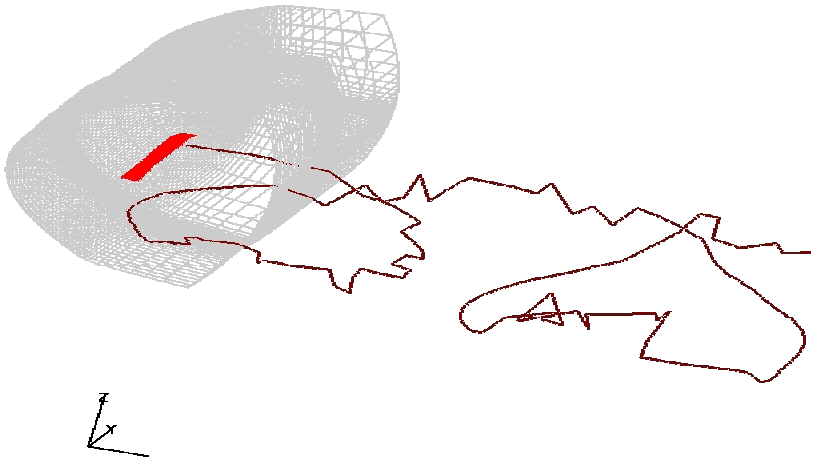

Figure C-1: GT-HYBRID Single Blade Grid and Free-Wake Model

The computational grid is based on the C-H grid topology as shown in Figure C-2. This allows flexibility with grid density near surface, along with better orthogonality and smoothness of grid lines near the blunt leading edge typical of rotor blade airfoils. The far

field boundary is located at 8-10 chords from surface. The grid has a size of 131x65x45 or roughly half a million node points. For aerolelastic studies, the grid can be deformed based on a user-supplied table of elastic deformations.

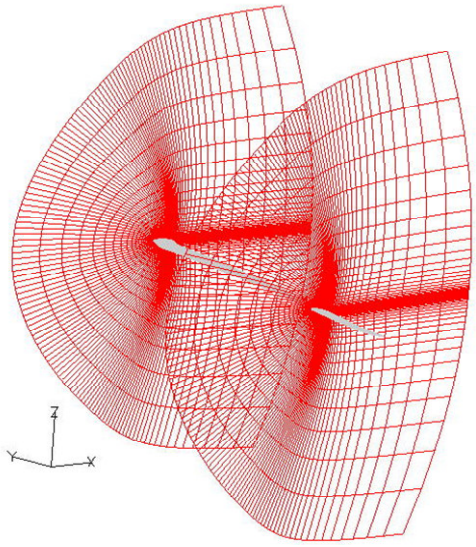

Figure C-2: GT-HYBRID CH Grid

For the CFD/CSD experiments performed in this research, GT-HYBRID version 3.2 was used. The following are some of the computational details of the solver. GT-Hybrid uses a node centered finite volume implementation of the RANS equations. It uses first order LU-SGS (Lower Upper Symmetric Gauss-Siedel) time stepping. Newton sub-iterations were available but not used. It uses the Roe's Flux differencing scheme for the inviscid fluxes with 3rd / 5^{th} Order MUSCL (Monotone Upstream entered Scheme for Conservation Laws) for flux reconstruction. 3r Order was used in this research. The solver has three turbulence models: Baldwin Lomax, Spalart - Allmaras DES, and K-ω SST. K-ω SST was used in this research. 1/20 degree time step is used for all the simulations. The solver has a single tip vortex and full span wake model, 4 revs of the wake information is stored and the wake geometry is updated every 5 deg. The single tip vortex model was used in this research.

The Lagrangian free wake model used in this research is based on single tip vortex assumption as shown in Figure C-3. The tip vortex is a collection of piecewise linear trailed vorticities. Strength of the vortex elements is set to be equal to the peak bound circulation at time of shedding. The vortex shedding point is based on centroid of trailed circulation between the tip and location of peak bound circulation. The vortex is trailed at discrete azimuthal intervals. Each vortex segment uses a Vatistas viscous core model [101] to desingularize the velocity profile near the core radius.

The number of time steps used for each simulation of GT-HYBRID during CFD/CSD coupling can be seen in Table C-1. 28,800 time steps were used for the first iteration without restart. This is equal to four revolutions. The subsequent iterations used two revolutions or 14,400 time steps per simulation with restart.

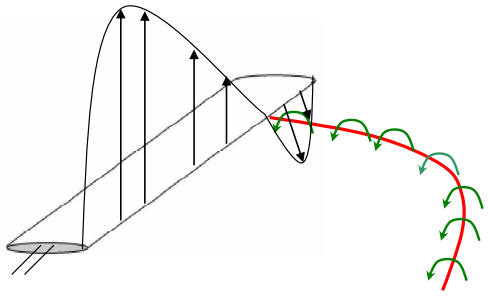

Figure C-3: GT-HYBRID Single Tip Vortex Model

Table C-1: Number of Time Steps Used In CFD/CSD Coupling

Iter	#_steps	restart	total_steps
0	28800	no	28800
1	14400	yes	43200
2	14400	yes	57600
3	14400	yes	72000
4	14400	yes	86400
5	14400	yes	100800
6	14400	yes	115200

Appendix D

Example of RCAS Batch Output

When examining RCAS outputs manually, the settings within a specific TUTOR menu can be saved to a file. The contents of the file can be placed at the end of the .rcas and executed at the end of the analysis automatically. A screen available in RCAS is called BATCHOUTPUT. Within this screen, a list of the scripts to be executed is made and each is given an ID as shown below. In this example, the batch output runs three scripts to create reports of hub forces in the x, y, and z directions.

```
S BATCHOUTPUT
!  Row              Output
!  ID               Filename
!  --          -------------------------
a    1            forcex.topr
a    2            forcey.topr
a    3            forcez.topr
```

An example of one of these .topr scripts is given below. It generates a report with the results of a harmonic analysis of the hub force in the x direction. Four harmonics are reported in a report named frc_x.rep. The scripts forcey.topr and forcez.topr are very similar and thus are not printed here. The great thing about this setup is that it commands RCAS to create reports or data that you need to parse. It does this automatically. This is helpful when integrating a .rcas file into ModelCenter®.

```
***begin-RCAS-file: forcex.topr ***
oilsdrv
ANALYS   TRIM
JOBCAS   TESTING_00.01
LODTYP   FRC
AXIS     X
NODESEL  MROTOR_HUB_HUBNODE
REFNODE  MROTOR_HUB_HUBNODE
HARMFLG  Y
NUMHARM  4
MCFLAG   NODS
```

```
COMPVAR  NONE
XRANGE   0
XRANGE   0
XRANGE   0
YRANGE   0
YRANGE   0
YRANGE   0
SCALE    1
SCALE    1
LABEL    INTERNAL LOADS
DATADEST NO
PLOTDEST NO
REPTDEST frc_x.rep
REPSIZ   80
REPSIZ   60
*****end-RCAS-file: forcex.topr ***
```

Appendix E

Elastic Blade RCAS to PSU-WOPWOP Component

Contributing analyses are made into ModelCenter® components using what are called filewrappers. The filewrapper below was built to create the required input files to run RCAS and subsequently PSU-WOPWOP. The input files are created in the RunCommands section using generate commands. Each generate command refers to a separate RowFieldInputFile section of the filewrapper. The run "./newhart.tcsh" command runs the script newhart.tcsh which is also given in this appendix after this filewrapper. In general, the newhart.tcsh script runs RCAS, GT-GRIDGEN, GT-HYBRID (for deformed geometry only, no CFD), and finally PSU-WOPWO. In addition, it also calls other executable "converters" required in the process. After the script newhart.tcsh is complete, the analysis is finished and the parse commands are used to parse output files created by RCAS and PSU-WOPWOP. RCAS output reports and/or data are generated using the BATCHOUTPUT screen as described in Appendix D.

```
# @author: kyle collins
# @version: 1.0
# @description: File wrapper to create files required to perform an
RCAS elastic blade analysis using dynamic inflow model followed by an
aeroacoustic analysis via wopwop using compact blade loads only.
#

RunCommands
{
   generate rcasinputFile
   generate gridgeninputFile
   generate wopwop1inputFile
   generate wopwop2inputFile
   run "./newhart.tcsh"
   parse frcx
   parse frcy
   parse frcz
   parse momx
   parse momy
   parse momz
   parse pwr
   parse trim
```

```
   parse flap
   parse noise
   parse sigma
   parse converged
}

RowFieldInputFile rcasinputFile
{
 templateFile:       rdi_hart_ff.rcas.template
 fileToGenerate:     newhart.rcas

 setDelimiters "= ,"

 #         name   type        row   field
 #-------------------------------------------------
   setGroup "rcasinput"
   markAsBeginning "S TRIMVAR"
   variable: thrustqnblades   double   3    6
   clearMarks

   markAsBeginning "S ROTORPARAM"
   variable: omega   double   3    2
   clearMarks

   markAsBeginning "S INITCOND"
   variable: theta0i    double   4    2
   variable: theta1si   double   4    3
   variable: theta1ci   double   4    4
   variable: alpharad   double   9    6
   clearMarks

   markAsBeginning "S CONSTWIND"
   variable: vmps   double   5    2
   clearMarks

   markAsBeginning "S AEROSTATCONST"
   variable: rho   double   4    5
   clearMarks

   markAsBeginning "S AEROSTATCONST"
   variable: speedsound   double   4    6
   clearMarks

   markAsBeginning "S FENODE"
   array: fenode   double   6:25   3:5 numDimensions=2
   clearMarks

   markAsBeginning "S AERONODE"
   array: aeronode   double   4:33   3:5 numDimensions=2
   clearMarks

   markAsBeginning "S AEROSEG"
   array: aeroseg_chord   double   4:32   5:5
   array: aeroseg_twist   double   4:32   8:8
   clearMarks

   markAsBeginning "M BSTRUCTW"
```

```
   array: bstructw   double   2:23   1:2 numDimensions=2
   clearMarks

   markAsBeginning "M BMPL"
   array: bmpl       double   2:23   1:2 numDimensions=2
   clearMarks
}

RowFieldInputFile gridgeninputFile
{
 templateFile:       gridgen_hart.inp.template
 fileToGenerate:     gridgen_newhart.inp

 setDelimiters " "

 #         name   type        row   field
 #-------------------------------------------------
   setGroup "gridgeninput"
   markAsBeginning "ZS(K) XL YL CHORD THICK TWIST NEWSEC"
   array: station01   double   2:2   1:7
   clearMarks

   markAsBeginning "ZS(K) XL YL CHORD THICK TWIST NEWSEC" occurrence=2
   array: station02   double   2:2   1:7
   clearMarks

   markAsBeginning "ZS(K) XL YL CHORD THICK TWIST NEWSEC" occurrence=3
   array: station03   double   2:2   1:7
   clearMarks

   markAsBeginning "ZS(K) XL YL CHORD THICK TWIST NEWSEC" occurrence=4
   array: station04   double   2:2   1:7
   clearMarks

   markAsBeginning "ZS(K) XL YL CHORD THICK TWIST NEWSEC" occurrence=5
   array: station05   double   2:2   1:7
   clearMarks

   markAsBeginning "ZS(K) XL YL CHORD THICK TWIST NEWSEC" occurrence=6
   array: station06   double   2:2   1:7
   clearMarks

   markAsBeginning "ZS(K) XL YL CHORD THICK TWIST NEWSEC" occurrence=7
   array: station07   double   2:2   1:7
   clearMarks

   markAsBeginning "ZS(K) XL YL CHORD THICK TWIST NEWSEC" occurrence=8
   array: station08   double   2:2   1:7
   clearMarks

   markAsBeginning "ZS(K) XL YL CHORD THICK TWIST NEWSEC" occurrence=9
   array: station09   double   2:2   1:7
   clearMarks

   markAsBeginning "ZS(K) XL YL CHORD THICK TWIST NEWSEC" occurrence=10
   array: station10   double   2:2   1:7
   clearMarks
```

```
   markAsBeginning "ZS(K) XL YL CHORD THICK TWIST NEWSEC" occurrence=11
   array: station11   double   2:2   1:7
   clearMarks

   markAsBeginning "ZS(K) XL YL CHORD THICK TWIST NEWSEC" occurrence=12
   array: station12   double   2:2   1:7
   clearMarks
}

RowFieldInputFile wopwop1inputFile
{
 templateFile:       rcas2wopwop.inp.template
 fileToGenerate:     rcas2wopwop.inp

 setDelimiters "= ,;"

 #         name   type        row   field
 #-------------------------------------------------
   setGroup "wopwopconverterinput"
   markAsBeginning "omega"
   variable: omega   double   1      2
   clearMarks

   markAsBeginning "c"
   variable: speedsound   double   1      2
   clearMarks

   markAsBeginning "rho"
   variable: rho   double   1      2
   clearMarks

   markAsBeginning "chord"
   variable: chord   double   1      2
   clearMarks

}

RowFieldInputFile wopwop2inputFile
{
 templateFile:       namelist.nam.rcas.template
 fileToGenerate:     namelist.nam

 setDelimiters "= ,;"

 #         name   type        row   field
 #-------------------------------------------------
   setGroup "wopwopnamelistinput"
   markAsBeginning "&EnvironmentConstants"
   variable: speedsound   double   2      2
   variable: rho          double   3      2
   clearMarks

   markAsBeginning "Flight Velocity"
   variable: obsvel   double   3      2
   clearMarks
```

```
   markAsBeginning "Flight Velocity" occurrence=2
   variable: acvel   double   3      2
   clearMarks

   markAsBeginning "Shaft Tilt"
   variable: shafttilt   double   5      2
   clearMarks
}

RowFieldOutputFile frcx
{
 fileToParse: newhart00/frc_x001.rep
 setDelimiters "= "
   variable: Fx   double   10    2
   variable: Fx4pc   double   14    2
   variable: Fx4ps  double   14    3
}

RowFieldOutputFile frcy
{
 fileToParse: newhart00/frc_y001.rep
 setDelimiters "= "
   variable: Fy   double   10    2
   variable: Fy4pc   double   14    2
   variable: Fy4ps  double   14    3
}

RowFieldOutputFile frcz
{
 fileToParse: newhart00/frc_z001.rep
 setDelimiters "= "
   variable: Fz   double   10    2
   variable: Fz4pc   double   14    2
   variable: Fz4ps  double   14    3
}

RowFieldOutputFile momx
{
 fileToParse: newhart00/mom_x001.rep
 setDelimiters "= "
   variable: Mx   double   10    2
   variable: Mx4pc   double   14    2
   variable: Mx4ps  double   14    3
}

RowFieldOutputFile momY
{
 fileToParse: newhart00/mom_y001.rep
 setDelimiters "= "
   variable: My   double   10    2
   variable: My4pc   double   14    2
   variable: My4ps  double   14    3
}

RowFieldOutputFile momz
{
 fileToParse: newhart00/mom_z001.rep
```

```
 setDelimiters "= "
   variable: Mz   double   10    2
   variable: Mz4pc   double   14    2
   variable: Mz4ps  double   14    3
}

RowFieldOutputFile pwr
{
 fileToParse: newhart00/power001.rep
 setDelimiters "= "
   variable: CTqsigma_final   double   9    1
   variable: CPqsigma_final   double   9    2
}

RowFieldOutputFile trim
{
 fileToParse: newhart00/trimcontrols.dat
 setDelimiters "= "
   variable: theta0  double   15    1 units="deg"
   variable: thetas  double   17    1 units="deg"
   variable: thetac  double   19    1 units="deg"
}

RowFieldOutputFile flap
{
 fileToParse: newhart00/flapping.dat
 setDelimiters "= "
   variable: beta0  double   15    1 units="rad"
   variable: betas  double   17    1 units="rad"
   variable: betac  double   19    1 units="rad"
}

RowFieldOutputFile noise
{
 fileToParse: wopwop3/Results/OASPLdB.fn
 setDelimiters "= "
   array: obslocs_thickness  double   18:33    1
   array: obslocs_loading    double   34:49    1
   array: obslocs_total      double   50:65    1
}

RowFieldOutputFile sigma
{
 fileToParse: newhart00/sigma.dat
 setDelimiters "= "
   variable: sigmaperblade   double   13    1
}

RowFieldOutputFile converged
{
 fileToParse: newhart00/rcasmaster001.log
 setDelimiters "= "
 markAsEnd "Saving outputs in the RDB"
   variable: trim    integer  -2   1
}
```

The script below – newhart.tcsh – is a HERE document written to run RCAS. It is run from the filewrapper given above. The script then runs the executable motionSAV2TXT72 to convert the motion.sav file created by RCAS into a motion.txt file that can converted using rcas2hybird72 to be read into GT-HYBRID. Here GT-HYBRID is used solely for the purpose of creating the deformed grid geometry that will be read into PSU-WOPWOP. No CFD calculations are performed in this analysis. The converter rcas2wopwop turns the created blade surface .xyz files and the compact loading data files into the binary files required by PSU-WOPWOP. Finally, PSU-WOPWOP is run using the executable wopwop3.

```
#! /bin/tcsh
touch zstart
source rcas-linux-setup
rm -rf newhart00
rm -fr wopwop3
rcas <<LIMITSTRING
exec newhart
batch
m
1
r
e
e
e
y
LIMITSTRING
./motionSAV2TXT72
./gridgen < gridgen_newhart.inp
./rcas2hybrid72
./hybrid3.2 < hybrid.namelist
rm blade_vol*
cp namelist.nam rcas2wopwop.inp wopwop3start
cp -fr wopwop3start/ wopwop3/
cp newhart00/compactloads00* wopwop3/
mv blade_surf* wopwop3/
cd wopwop3/
./renamebladesurf
./rcas2wopwop
./wopwop3
touch ../zfinish
```

Appendix F

CFD/CSD/AA Coupling Script

The following shell script is submitted to the cluster of compute nodes for each design case. It functions to run RCAS in the background and then run the coupling script mpijob.script which is written in Perl.

```
#!/bin/sh
#
#$ -N case001
#
# Use current working directory
#$ -cwd
#
# Join stdout and stderr
#$ -j y
#
# Run job through tcsh shell
#$ -S /bin/tcsh
#

source rcas-linux-setup
echo "$rbin/rcasbatchrun newhart.rcas newhart.log" | at -qd now
./mpijob.script >> mpijob.log
```

The Perl script mpijob.script is presented next. The essence of this Perl script is to wait for the CSD program (RCAS in this case) to generate the first motion file using uniform inflow (iteration=0). It knows that this is complete when RCAS creates a file called rcas_motion_data_is_ready. RCAS continues to run in the background waiting for the CFD airloads file. The motion file is then converted to the form required by the CFD code (GT-HYBRID in this case). This requires a separate converter executable. Then the CFD code can run using iteration=0 motions. After completion, the airloads results from GT-HYBRID are converted into what is required by RCAS. This too requires a separate converter code. RCAS is informed that the CFD airloads file is ready by the existence of a file named cfd_airloads_data_is_ready. The CSD code runs using delta airloads

calculated as shown in Figure 4-19 and results in another motion file. The iteration number is incremented by +1 and the process continues. After a preset number of iterations, the CFD/CSD coupling is complete. This script also executes the converters required to generate the data files needed by the AA code (PSU-WOPWOP in this case) and finally, to run the AA code. While this particular coupling script uses the codes GT-HYBRID, RCAS, and PSU-WOPWOP for CFD, CSD, and AA respectively; it can be customized to work with the analysis tools available.

In the code that follows, some lines must be broken into two lines. When this occurs, a combination of characters (**cont**) is used.

```
#!/usr/bin/perl -w
use strict;
use Cwd;

$| = 1;                          # unbuffer output

# User defined constants
my $dir = '';
my $restartiter = 0;
my $casenumber = 106;
my $mainfolder = "/.";
my $final_iteration = 6;
my $max_iterations = 7;
my $rcas_sleep_period = 60;
my $hybrid_sleep_period = 120;
my @mpi_copy_list = qw(
                  fort.16
                  fort.71
                  hybrid.namelist
                  mpihybrid3.2
                  mpihybridjob
                  hybrid2rcas
                  );
# Local variables
my $result = '';               # command execution results
my $rcas_job = 0;              # job number of RCAS job
my $hybrid_job = 0;            # job number of Hybrid job
my $mpi_iter_pfolder = '';     # built in the code (prev. iter. folder)
my $mpi_iter_folder = '';      # built in the code
my $mpi_iter_vis = '';         # built in the code
my $airloads_file_name = '';   # name of file rotor_1.onerev.txt.0#
my $motion_file_name = '';     # name of file motion.txt.0#
my $casefolder = '';           # built in the code
my $rcas_folder = '';
my $mpi_folder = '';
```

```
# Update names of folders
$casefolder = sprintf("%s/case%03d",$mainfolder,$casenumber);
$rcas_folder = "$casefolder";
my $wopwop_folder = "$casefolder/wopwop3";
my $rcas_data_ready = "$rcas_folder/rcas_motion_data_is_ready";
my $rcas_go = "$rcas_folder/cfd_airloads_data_is_ready";
$mpi_folder = "$casefolder";

# Remove any sentinal files
unlink $rcas_data_ready;
unlink $rcas_go;

$dir = getcwd;
print "Current Working Directory is $dir\n";
unlink $dir;

# Begin the job loop
my $iteration = 0;            # current iteration number

# Start the RCAS program
# Normally goes here since it sleeps
# Taken out and put into qsub job script.
# Same effect since it runs somewhat in
# the background.

# Main execution loop
while ($iteration < $max_iterations) {

  # Wait for the RCAS data ready flag to appear - polling loop
  print "RCAS polling loop: looking for $rcas_data_ready\n";
  while(1) {
    last if -e "$rcas_data_ready";
    print ".";
    sleep $rcas_sleep_period;
  }
  print "\n";

  # Copy motion.txt file to motion.txt.#
  $motion_file_name = sprintf("motion.txt.0%01d",$iteration);
  my $cmd = qq[cp **cont**
       $rcas_folder/motion.txt $rcas_folder/$motion_file_name];
  print "For iteration $iteration, copy: cmd=$cmd\n";
  qx[$cmd];

  # Delete the  RCAS data ready file
  unlink $rcas_data_ready;
  print "RCAS data is ready\n";

  # Create current and save previous iteration folder name
  $mpi_iter_pfolder = $mpi_iter_folder;
  $mpi_iter_folder = sprintf("%s/I%02d",$mpi_folder,$iteration);
  $mpi_iter_vis = "$mpi_iter_folder/vis";


  # Perform actions for iter > $restartiter
```

```
if (($iteration >= $restartiter) && ($iteration != 0)){

  # Make the iteration folder
  mkdir $mpi_iter_folder;
  mkdir $mpi_iter_vis;

  # Copy files from previous iteration directory
  foreach my $file (@mpi_copy_list) {
    my $cmd = qq[cp $mpi_iter_pfolder/$file $mpi_iter_folder/$file];
    print "Copy: cmd=$cmd\n";
    qx[$cmd];
  }

  # Rename fort.16 to fort.15
  my $cmd = qq[mv $mpi_iter_folder/fort.16 $mpi_iter_folder/fort.15];
  print "Rename: cmd=$cmd\n";
  qx[$cmd];

  # Change hybrid.namelist
  open(IN,"$mpi_iter_folder/hybrid.namelist") **cont**
     || die "Unable to open hybrid.namelist: $!";
  open(OUT,">$mpi_iter_folder/hybrid.namelist.new") **cont**
     || die "Unable to create hybrid.namelist.new: $!";
  my $newiterfolder=sprintf("I%02d",$iteration);
  while(<IN>) {
    if (m/^irstrt/) {
      s/0/1/;
    }
    if (m/^nstp/) {
      my @fields = m/(nstp=)([0-9]+)/;
      $fields[1] += 14400;
      print OUT  @fields;
      print OUT "\n";
    } else {
      print OUT;
    }
  }
  close(IN);
  close(OUT);
  unlink("$mpi_iter_folder/hybrid.namelist");
  rename "$mpi_iter_folder/hybrid.namelist.new",**cont**
     "$mpi_iter_folder/hybrid.namelist";

}

# Change motion.txt to fort.22 in rcas folder
$cmd = qq[./rcas2hybrid];
print "For iteration $iteration, run: cmd=$cmd\n";
qx[$cmd];

# Move fort.22 to mpi_iter_folder
$cmd = qq[mv $rcas_folder/fort.22 $mpi_iter_folder/fort.22];
print "For iteration $iteration, move: cmd=$cmd\n";
qx[$cmd];


# Change Directory to the iteration folder
```

```
chdir("$mpi_iter_folder") **cont**
     || die "Cannot change directory to $mpi_iter_folder ($!)";
print "Changed directory to $mpi_iter_folder\n";

$dir = getcwd;
print "Current Working Directory is $dir\n";
unlink $dir;

if ($iteration >= $restartiter) {
  # Start the hybrid program
  $cmd = qq[ssh gibbs 'cd $mpi_iter_folder;qsub mpihybridjob'];
  print "For iteration $iteration, run: cmd=$cmd\n";
  qx[$cmd];

  # Wait for the hybrid completion flag to appear - polling loop
  my $hybrid_finished = "$mpi_iter_folder/hybrid_is_finished";
  print "hybrid polling loop: looking for $hybrid_finished\n";
  while(1) {
    last if -e "$hybrid_finished";
    print ".";
    sleep $hybrid_sleep_period;
  }
  print "program works beeatch!!";
  print "\n";
}

# Make rotor_1.onerev.txt.0# and copy it to the rcas folder
# Change fort.56 to rotor_1.onerev.txt.0# in current iteration folder
$airloads_file_name = sprintf("rotor_1.onerev.txt.0%01d",$iteration);
$cmd = qq[./hybrid2rcas $airloads_file_name 1];
print "For iteration $iteration, run: cmd=$cmd\n";
qx[$cmd];

# Change directory back to main folder
chdir("$mpi_folder") **cont**
     || die "Cannot change directory to $mpi_folder ($!)";
print "Changed directory to $mpi_folder\n";

$dir = getcwd;
print "Current Working Directory is $dir\n";
unlink $dir;

# Copy the rotor_1.onerev.txt.0# file to RCAS folder
$cmd = qq[cp $mpi_iter_folder/$airloads_file_name **cont**
     $rcas_folder/$airloads_file_name];
print "For iteration $iteration, copy: cmd=$cmd\n";
qx[$cmd];

# Remove old rotor_1.onerev.txt and replace with new file
$cmd = qq[rm $rcas_folder/rotor_1.onerev.txt];
qx[$cmd];
print "For iteration $iteration, remove existing: cmd=$cmd\n";
$cmd = qq[cp $rcas_folder/$airloads_file_name **cont**
     $rcas_folder/rotor_1.onerev.txt];
print "For iteration $iteration, copy: cmd=$cmd\n";
qx[$cmd];
```

```
  # Signal RCAS that it can run again
  open(FILE,">$rcas_go") || die "Unable to create file: $!";;
  print FILE "\n";
  close(FILE);

  # Add code to run wopwop after the final iteration
  if ($iteration == $final_iteration) {
    # move blade .xyz and .q files from final iteration
    # vis folder to wopwop folder
    my $cmd = qq[mv $mpi_iter_vis/blade* $wopwop_folder];
    print "move: cmd=$cmd\n";
    qx[$cmd];

    # Change directory to wopwop folder
    chdir("$wopwop_folder") **cont**
       || die "Cannot change directory to $wopwop_folder ($!)";
    print "Changed directory to $wopwop_folder\n";

    $dir = getcwd;
    print "Current Working Directory is $dir\n";
    unlink $dir;

    # Run hybrid2wopwop converter
    $cmd = qq[./hybrid2wopwop];
    print "Convert Hybrid Data for Wopwop, run: cmd=$cmd\n";
    qx[$cmd];

    # Run wopwop3
    $cmd = qq[./wopwop3];
    print "Run PSU-WOPWOP, run: cmd=$cmd\n";
    qx[$cmd];

    # Change directory back to main folder
    chdir("$mpi_folder") **cont**
       || die "Cannot change directory to $mpi_folder ($!)";
    print "Changed directory to $mpi_folder\n";

    $dir = getcwd;
    print "Current Working Directory is $dir\n";
    unlink $dir;
  }

  # Update the iteration counter
  $iteration++;
  print "New iteration value=$iteration\n";
}
# Run script to generate hybrid hub loads
my $cmd = qq[./runhybhubloads];
print "Run runhybhubloads, run: cmd=$cmd\n";
qx[$cmd];
exit;

__END__
```

Appendix G

Fraction Factorial DOE's for Six Design Variables

Resolution IV Design of Experiment

trials	sweepangle	anhedralangle	taperratio	twist1	switchtwistx	twist2
1	-1	-1	-1	1	1	-1
2	1	-1	-1	-1	-1	1
3	-1	-1	1	1	-1	1
4	1	-1	1	-1	1	-1
5	1	1	-1	-1	1	-1
6	-1	1	-1	1	-1	1
7	-1	1	1	-1	-1	-1
8	-1	1	-1	-1	1	1
9	1	-1	-1	1	1	1
10	-1	-1	-1	-1	-1	-1
11	1	-1	1	1	-1	-1
12	1	1	-1	1	-1	-1
13	1	1	1	-1	-1	1
14	-1	1	1	1	1	-1
15	1	1	1	1	1	1
16	-1	-1	1	-1	1	1
center	0	0	0	0	0	0

Resolution VI Design of Experiment

trials	sweepangle	anhedralangle	taperratio	twist1	switchtwistx	twist2
1	1	1	-1	-1	1	1
2	-1	1	-1	-1	-1	1
3	-1	1	1	1	1	-1
4	1	1	1	1	1	1
5	-1	1	1	1	-1	1
6	-1	-1	-1	1	-1	1
7	-1	-1	1	1	1	1
8	1	-1	-1	1	1	1
9	1	1	-1	1	1	-1
10	-1	1	-1	1	1	1
11	1	-1	1	-1	-1	-1
12	1	1	1	-1	-1	1
13	1	-1	1	1	-1	1
14	-1	1	1	-1	1	1
15	1	1	1	1	-1	-1
16	1	-1	1	-1	1	1
17	1	-1	-1	1	-1	-1
18	-1	-1	1	-1	-1	1
19	-1	-1	-1	-1	1	1
20	-1	1	-1	1	-1	-1
21	1	-1	-1	-1	1	-1
22	1	1	1	-1	1	-1
23	-1	-1	1	1	-1	-1
24	1	1	-1	-1	-1	-1
25	1	-1	-1	-1	-1	1
26	-1	1	-1	-1	1	-1
27	1	1	-1	1	-1	1
28	-1	-1	-1	-1	-1	-1
29	1	-1	1	1	1	-1
30	-1	1	1	-1	-1	-1
31	-1	-1	-1	1	1	-1
32	-1	-1	1	-1	1	-1

Appendix H

Pareto Frontier Generation

In this appendix, four methods of generating points on the Pareto Frontier are defined with illustrations. The first three methods are well documented in the literature. The final method was devised in this thesis work and is a simple modification to one of the first three methods. All methods share a common aspect in that each design on the frontier is generated through an optimization process. The also all share the fact that the minimums in each objective are the same regardless of the method used. These points are called the Pareto anchor points as shown by P_1 and P_2 in Figure H-4. P_1 is found using an optimization to minimize F_1. Likewise, P_2 is found by minimizing F_2. The purpose of each of the methods to be mentioned is to generate a distribution of points between P_1 and P_1 that lie on or very close to the Pareto Frontier.

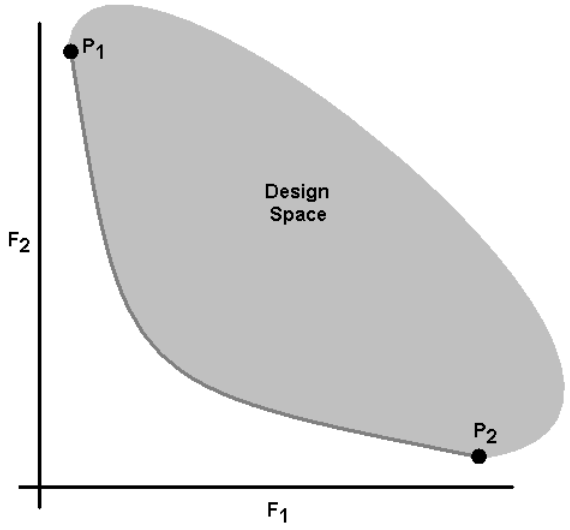

Figure H-4: General Pareto Frontier Example for the Bi-Objective Case

Method of Minimized Weighted Sum of Objectives

Perhaps the easiest method to program to generate designs on the Pareto Frontier is the Weighted Sum of Objectives approach. Each design on the frontier is determined by minimizing a weighted sum of both objectives as given in equation H-1. This method finds points on the Pareto Frontier. However, it does not produce an even distribution of points. Every unique combination of α and β finds a different point on the frontier. If one of these weights is set to zero, an anchor point is found.

Minimize: $J = \alpha F_1(\bar{x}) + \beta F_2(\bar{x})$ objective function **H-1**

where: $\alpha + \beta = 1$

by changing: $\bar{x} = (x_1, x_2, ..., x_n)$ design variables

ε-Constraint Method

The second approach illustrated is the ε-Constraint method developed by Marglin [55] and further described in Reference [56]. In this method, a sequence of constrained optimizations is performed. In each optimization, the goal is to minimize F_2 while maintaining a constraint that says $\{F_1 \le \varepsilon(i) \quad i = 1 \ldots n\}$ where n is the number of points being generated and ε is the distance in the F_1 direction between each point found. A description of this method is pictured in Figure H-5.

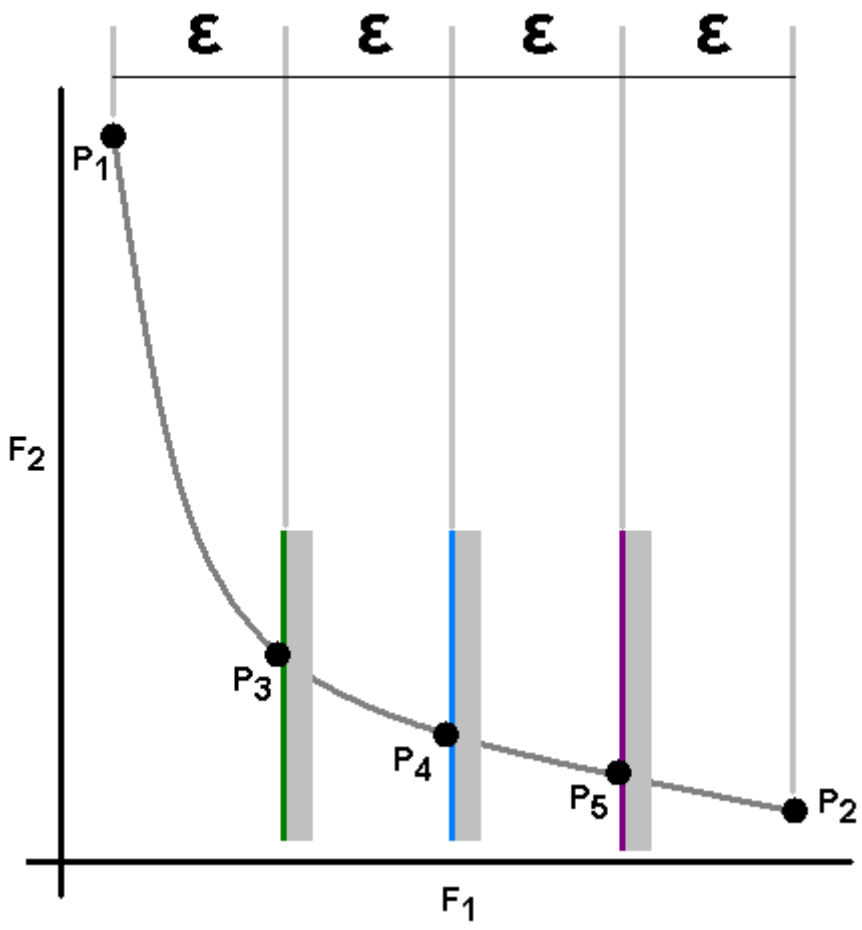

Figure H-5: Pareto Set Generation Using the ε-Constraint Method

Normal Constraint Method

The Normal Constraint Method is also described in Reference [56]. In this method, a line is drawn between the anchor points, P_1 and P_2 and is called the utopia line. Next, and even distribution of lines are defined which are normal to the utopia line. In succession, each of these lines that is normal to the utopia line is used as a constraint while F_2 is minimized in a constrained optimization problem. An illustration of this method can be seen in Figure H-6.

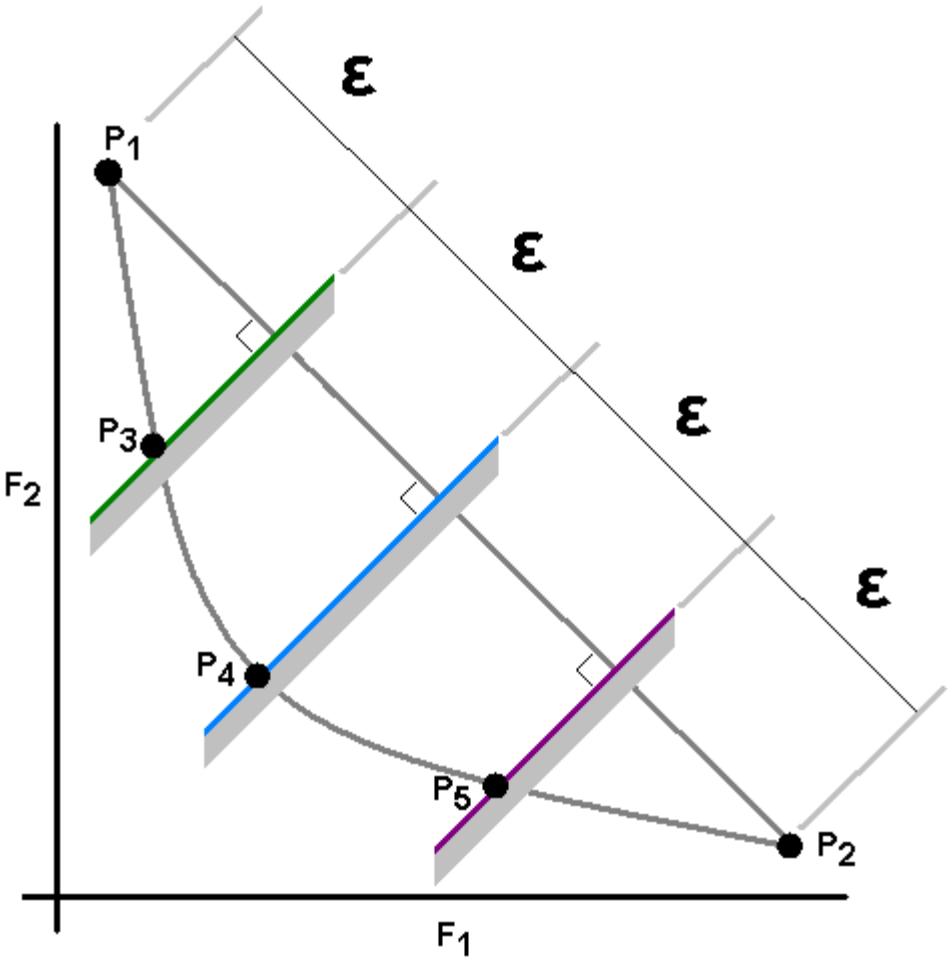

Figure H-6: Pareto Set Generation Using the Normal Constraint Method

Modified Normal Constraint Method

In this work, a modification was made to the normal constraint method. To begin, the utopia line is drawn between the anchor points P_1 and P_2. Next, a single normal constraint is used and is located at the midpoint of the utopia line. A constrained optimization problem is performed to find a third point, P_3 on the frontier located approximately midway between the anchor points as shown in Figure H-7 (a). Next, a line is drawn between P_1 and P_3. A line normal to this line is drawn located at its midpoint. Using this normal line as a constraint, another constrained optimization is

performed to find a fourth point, P_4. Then a line is drawn between P_3 and the other anchor point, P_2. Again, at the midpoint, a line is drawn normal to this line and used in constrained optimization to find a fifth point, P_5. This process is depicted in Figure H-7 (b) and would be continued until a desired number of designs are found. Each time, a line between neighboring points is drawn and then a normal line at its midpoint becomes a constraint to find another Pareto point between the two.

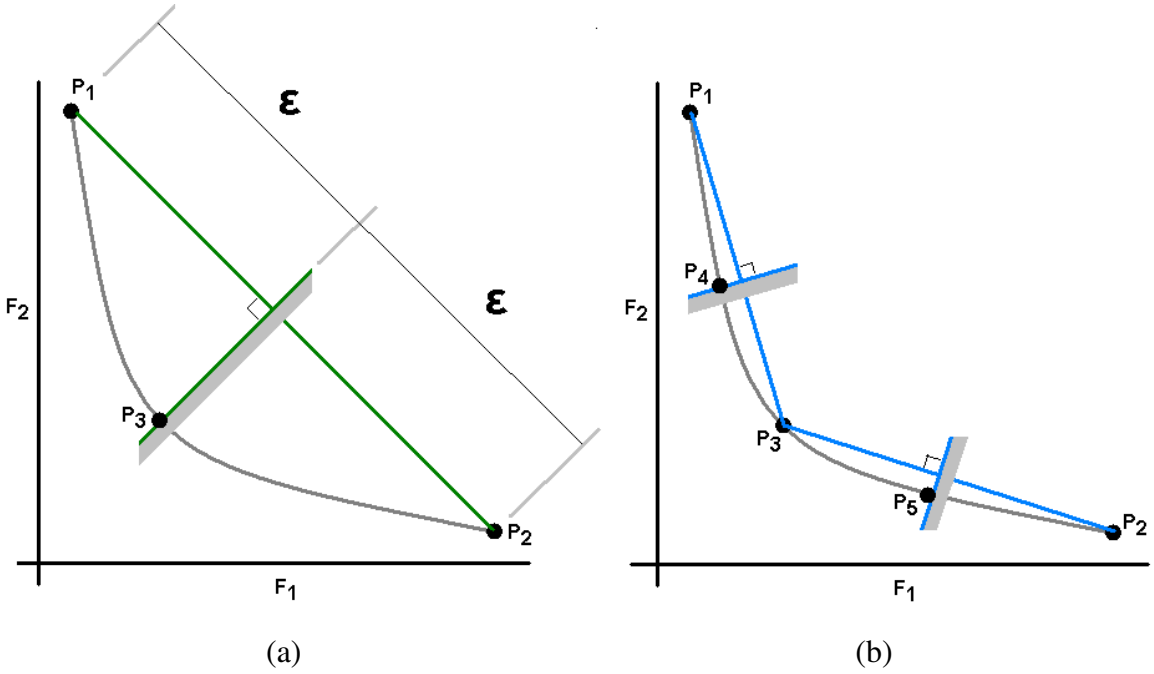

Figure H-7: Pareto Set Generation Using a Modified Normal Constraint Method

References

1. Celi, R. *Recent Applications of Design Optimization to Rotorcraft - A Survey*. in *Proceedings of the 55th Annual Forum of the American Helicopter Society*. 1999. Montreal, Canada,.

2. Ganguli, R., *Survey of Recent Developments in Rotorcraft Design Optimization.* Journal of Aircraft, 2004. **41**(3): p. 493-510.

3. Kunz, D.L. *Comprehensive Rotorcraft Analysis- Past, Present, and Future*. in *Proceedings of the 46th AIAA/ASME/ASCE/AHS/ASC Structures, Structural Dynamics, and Materials Conference*. 2005.

4. Splettstoesser, W.R., R. Kube, U. Seelhorst, W. Wagner, A. Boutier, F. Micheli, E. Mercker, and K. Pengel, *Higher Harmonic Control Aeroacoustic Rotor Test (HART)-Test Documentation and Representative Results*, 1995

5. Leishman, J.G. and A. Bagai, *Challenges in Understanding the Vortex Dynamics of Helicopter Rotor Wakes.* AIAA Journal, 1998. **36**(7): p. 1130-1140.

6. Xue, S., B. Docker, J. Narramore, and Z.X. Han, *Integrated Aero-Acoustics Rotor Simulation and Design Optimization.* 12 th AIAA/CEAS Aeroacoustics Conference(27 th AIAA Aeroacoustics Conference), 2006.

7. Makinen, S., M. Hill, F. Gandhi, L. Long, R. Vasilescu, and L. Sankar. *A Study of the HART-I Rotor with Loose Computational Fluid/Structural Dynamic Coupling*. in *Proceedings of the 62nd Annual Forum of the American Helicopter Society*. 2006. Phoenix, AZ,.

8. Lim, J.W., T.A. Nygaard, R. Strawn, and M. Potsdam. *BVI Airloads Prediction Using CFD/CSD Loose Coupling*. in *Proceedings of the 4th American Helicopter Society Vertical Lift Aircraft Design Conference*. 2006. San Francisco, CA.

9. Duque, E.P.N., L.N. Sankar, S. Menon, O. Bauchau, S. Ruffin, M. Smith, K. Ahuja, K.S. Brentner, L.N. Long, and P.J. Morris. *Revolutionary Physics-Based Design Tools for Quiet Helicopters*. in *Proceedings of the 44th AIAA Aerospace Sciences Meeting & Exhibit*. 2006. Reno, NV.

10. Tarzanin, F. and D.K. Young, *Boeing Rotorcraft Experience with Rotor Design and Optimization.* AIAA Paper, 1998: p. 98-4733.

11. Baeder, J.D. *Passive Design for Reduction of High-speed Impulsive Rotor Noise*. in *Proceedings of the 52nd Annual Forum of the American Helicopter Society*. 1996. Washington, DC.

12. Zhao, Q.-J. and G.-H. Xu, *A Study on Aerodynamic and Acoustic Characteristics of Advanced Tip-Shape Rotors.* Journal of the American Helicopter Society, 2007. **52**(3): p. 201-213.

13. Le Pape, A. and P. Beaumier, *Numerical Optimization of Helicopter Rotor Aerodynamic Performance in Hover.* Aerospace Science and Technology, 2005. **9**(3): p. 191-201.

14. Lee, S.W. and O.J. Kwon, *Aerodynamic Shape Optimization of Hovering Rotor Blades in Transonic Flow Using Unstructured Meshes.* AIAA Journal, 2006. **44**(8): p. 1816-1825.

15. Yang, C., T. Aoyama, S. Chae, K. Yee, S. Jeong, and S. Obayashi. *Blade Planform Optimization to Reduce HSI Noise of Helicopter in Hover*. in *Proceedings of the AHS International 64th Annual Forum & Technology Display*. 2008. Montréal, Canada: American Helicopter Society.

16. Askue, V., *Rotor Blade Design.* Air Medical Journal, 2004. **23**(3): p. 8-9.

17. Monteleone, R.A., *Blade for High Speed Helicopter*, USPTO, Editor. 1973, United Aircraft Corporation: United States.

18. Lowson, M.V., D.L. Hawkings, G.M. Byham, and F.J. Perry, *Helicopter Rotor Blades*, USPTO, Editor. 1978, Westland Aircraft Limited: United States.

19. Leishman, J.G., *Principles of Helicopter Aerodynamics*. 2nd ed. 2006: Cambridge University Press.

20. Hennes, C.C. and K.S. Brentner. *The Effect of Blade Deformation on Rotorcraft Acoustics*. in *Proceedings of the 31st European Rotorcraft Forum*. 2005. Florence.

21. Hennes, C.C. and K.S. Brentner, *The Effect of Blade Deformation on Rotorcraft Acoustics.* Journal of the American Helicopter Society, 2008. **53**(4): p. 398-411.

22. Cesnik, C.E.S. and D.H. Hodges, *VABS- A New Concept for Composite Rotor Blade Cross-sectional Modeling.* Journal of the American Helicopter Society, 1997. **42**(1): p. 27-38.

23. Ku, J., *A Hybrid Optimization Scheme for Helicopters with Composite Rotor Blades*, PhD Thesis, Georgia Institute of Technology, 2007

24. Johnson, W., *A Comprehensive Analytical Model of Rotorcraft Aerodynamics and Dynamics. Part 1: Analysis Development*. 1980, National Aeronautics and Space Administration.

25. Bauchau, O.A. and N.K. Kang, *A Multibody Formulation for Helicopter Structural Dynamic Analysis.* Journal of the American Helicopter Society, 1993. **38**(2): p. 3-14.

26. *RCAS User's Manual, Volume 1, Rotorcraft Comprehensive Analysis System Version 2.0*, 2003

27. He, C., *Development and Application of a Generalized Dynamic Wake Theory for Lifting Rotors*, Thesis, Georgia Institute of Technology, 1989

28. Landgrebe, A.J., *The Wake Geometry of a Hovering Helicopter Rotor and Its Influence on Rotor Performance.* Journal of the American Helicopter Society, 1972. **17**(4): p. 3-15.

29. Johnson, W., *Wake Model for Helicopter Rotors in High Speed Flight*. 1988.

30. Scully, M.P., *Computation of Helicopter Rotor Wake Geometry and its Influence on Rotor Harmonic Airloads*, in *ARSL TR 178-1*. 1975: Massachusetts Institute of Technology.

31. Srinivasan, G.R., J.D. Baeder, S. Obayashi, and W.J. McCroskey, *Flowfield of a Lifting Rotor in Hover: a Navier-Stokes Simulation.* AIAA Journal, 1992. **30**(10): p. 2371-2378.

32. Meakin, R.L. and A.M. Wissink. *Unsteady Aerodynamic Simulation of Static and Moving Bodies using Scalable Computers*. in *Proceedings of the 14th Computational Fluid Dynamics Conference*. 1999. Norfolf, VA: AIAA.

33. Cambier, L. and M. Gazaix. *elsA: An Efficient Object-oriented Solution to CFD Complexity. AIAA Paper 2002-0108*. in *Proceedings of the 40th AIAA Aerospace Sciences Meeting & Exhibit*. 2002. Reno, Nevada, USA: AIAA.

34. Srinivasan, G.R. and J.D. Baeder, *TURNS: a free-wake Euler/Navier-Stokes numerical method for helicopter rotors.* AIAA Journal, 1993. **31**(5): p. 959-962.

35. Berezin, C. and L. Sankar, *Improvements to a Tightly Coupled Viscous-inviscid Procedure for Three-dimensional Unsteady Transonic Flow.* Computers and Fluids, 1998. **27**(5): p. 689-694.

36. Yang, Z., *A Hybrid Flow Analysis for Rotors in Forward Flight*, PhD Thesis, Georgia Institute of Technology, 2000

37. Datta, A., M. Nixon, and I. Chopra, *Review of Rotor Loads Prediction with the Emergence of Rotorcraft CFD.* Journal of the American Helicopter Society, 2007. **52**(4): p. 287-317.

38. Nygaard, T.A., H. Saberi, R.A. Ormiston, R.C. Strawn, M. Potsdam, and W. Johnson, *Fluid Structure Interface for Rotorcraft Aeromechanic Computations*, 2005

39. Tung, C., F.X. Caradonna, and W.R. Johnson. *Prediction of Transonic Flows on Advancing Rotors*. in *Proceedings of the AHS International 40th Annual Forum & Technology Display*. 1986. Arlington, Va, USA: American Helicopter Society.

40. Tung, C., F.X. Caradonna, and W.R. Johnson, *Prediction of Transonic Flows on Advancing Rotors.* Journal of the American Helicopter Society, 1986. **31**(3): p. 389-399.

41. Lee, C., H. Saberi, and R. Ormiston. *Aerodynamic and Numerical Issues for Coupling CFD into Comprehensive Rotorcraft Analysis*. in *Proceedings of the AHS International 53th Annual Forum & Technology Display*. 1997. Virginia Beach, VA: American Helicopter Society.

42. Potsdam, M., H. Yeo, and W. Johnson. *Rotor Airloads Prediction Using Loose Aerodynamic/Structural Coupling*. in *Proceedings of the 60th Annual Forum of the American Helicopter Society*. 2004. Baltimore, MD: American Helicopter Society.

43. Potsdam, M., H. Yeo, and W. Johnson, *Rotor Airloads Prediction Using Loose Aerodynamic/Structural Coupling.* Journal of Aircraft, 2006. **43**(3): p. 732-742.

44. Rajmohan, N., O.A. Bauchau, S. Phanse, and L.N. Sankar. *An Efficient Tightly Coupled Fluid-Solid Interaction Approach with self-trim capability for Modeling Rotors in Forward Flight*. in *Proceedings of the 11th International Workshop on Rotorcraft Dynamics and Aeroelasticity*. 2005. Boca Raton, FL.

45. Phanse, S., L.N. Sankar, and B. Charles. *Efficient Coupled Fluid-Structure Interaction Approach for Analysis of Rotors in Forward Flight*. in *AHS Vertical Lift Aircraft Design Conference*. 2006. San Francisco: American Helicopter Society.

46. Brentner, K.S., G.A. Brès, G. Perez, and H.E. Jones. *Maneuvering Rotorcraft Noise Prediction: A New Code for a New Problem*. in *Proceedings of the American Helicopter Society's Aerodynamics, Acoustics, and Test Evaluation Technical Specialists Meeting*. 2002. San Francisco, CA.

47. Farassat, F. and G.P. Succi, *The Prediction of Helicopter Rotor Discrete Frequency Noise.* Vertica, 1983. **7**(4): p. 309-320.

48. Williams, J.E.F. and D.L. Hawkings, *Sound Generation by Turbulence and Surfaces in Arbitrary Motion.* Philosophical Transactions of the Royal Society of London. Series A, Mathematical and Physical Sciences, 1969. **264**(1151): p. 321-342.

49. Vanderplaats, G.N., *Numerical Optimization Techniques for Engineering Design: With Applications*. 1984: McGraw-Hill.

50. Keats, J., *John Koza Has Built an Invention Machine*, in *Popular Science*. 2006, Issue No. 5, p. 66-92.

51. Pareto, V. and C. Politique, *Cour d'economie Politique*. 1964 (first edition in 1896), Librarie Droz: Geneve.

52. Zadeh, L.A., *Optimality and non-scalar-valued performance criteria.* IEEE Transactions on Automatic Control 1963. **AC-8**: p. 59-60.

53. Koski, J., *Multicriteria Truss Optimization.* Multicriteria Optimization in Engineering and in the Sciences, 1988. **37**: p. 263–307.

54. Messac, A., *Physical programming- Effective Optimization for Computational Design.* AIAA Journal, 1996. **34**(1): p. 149-158.

55. Marglin, S., *Public Investment Criteria.* The MIT Press, 1967: p. 103.

56. Ismail-Yahaya, A. and A. Messac. *Effective Generation of the Pareto Frontier using the Normal Constraint Method*. in *Proceedings of the 40th AIAA Aerospace Sciences Meeting & Exhibit*. 2002. Reno, NV.

57. Messac, A., A. Ismail-Yahaya, and C.A. Mattson, *The Normalized Normal Constraint Method for Generating the Pareto Frontier.* Structural and Multidisciplinary Optimization, 2003. **25**(2): p. 86-98.

58. Messac, A. and C.A. Mattson, *Generating Well-Distributed Sets of Pareto Points for Engineering Design Using Physical Programming.* Optimization and Engineering, 2002. **3**(4): p. 431-450.

59. Das, I. and J.E. Dennis, *A Closer Look at Drawbacks of Minimizing Weighted Sums of Objectives for Pareto Set Generation in Multicriteria Optimization Problems.* Structural and Multidisciplinary Optimization, 1997. **14**(1): p. 63-69.

60. Rubinstein, R.Y., *Simulation and the Monte Carlo Method*. 1981: John Wiley & Sons, Inc. New York, NY, USA.

61. Montgomery, D.C., *Design and Analysis of Experiments*. 6th ed. 2005, New York: John Wiley & Sons, Inc.

62. Myers, R.H. and D.C. Montgomery, *Response Surface Methodology: Process and Product in Optimization Using Designed Experiments*. 1995: John Wiley & Sons, Inc. New York, NY, USA.

63. Matheron, G., *Principles of Geostatistics.* Economic Geology, 1963. **58**(8): p. 1246-1266.

64. Smith, M., *Neural Networks for Statistical Modeling*. 1993: Van Nostrand Reinhold. 235.

65. Jin, R., W. Chen, and T. Simpson. *Comparative Studies of Metamodeling Techniques under Multiple Criteria*. in *Proceedings of the 8th AIAA/USAF/NASA/ISSMO Symposium on Multidisciplinary Analysis and Optimization*. 2000. Long Beach, CA.

66. Wang, L., D. Beeson, G. Wiggs, and M. Rayasam. *A Comparison Of Meta-modeling Methods Using Practical Industry Requirements*. in *Proceedings of the 47th AIAA/ASME/ASCE/AHS/ASC Structures, Structural Dynamics, and Materials Conference*. 2006.

67. Alexandrov, N.M., C.R. Gumbert, L.L. Green, and P. Newman, *Approximation and Model Management in Aerodynamic Optimization with Variable-fidelity Models.* Journal of Aircraft, 2001. **38**(6): p. 1093-1101.

68. Alexandrov, N.M., E.J. Nielsen, R.M. Lewis, and W.K. Anderson, *First-Order Model Management With Variable-Fidelity Physics Applied to Multi-Element Airfoil Optimization.* 2000.

69. Robinson, T.D., M.S. Eldred, K.E. Willcox, and R. Haimes, *Strategies for Multifidelity Optimization with Variable Dimensional Hierarchical Models.* Proceedings of the 47th AIAA/ASME/ASCE/AHS/ASC Structures, Structural Dynamics, and Materials Conference, 2006: p. 1-19.

70. Alexandrov, N.M., J.E. Dennis, R.M. Lewis, and V. Torczon, *A Trust-region Framework for Managing the use of Approximation Models in Optimization.* Structural and Multidisciplinary Optimization, 1998. **15**(1): p. 16-23.

71. Lim, J.W. and I. Chopra. *Aeroelastic Optimization of a Helicopter Rotor*. in *Proceedings of the 44th Annual Forum of the American Helicopter Society*. 1988. Washington, DC.

72. Vanderplaats, G.N., *CONMIN-A FORTRAN Program for Constrained Function Minimization: User's Manual*. 1973.

73. Young, D.K. and F.J. Tarzanin, *Structural Optimization and Mach Scale Test Validation of a Low Vibration Rotor.* Journal of the American Helicopter Society, 1993. **38**(3): p. 83-92.

74. Ganguli, R., *Aeroelastic Optimization of a Helicopter Rotor with Composite Coupling.* Journal of Aircraft, 1995. **32**(6): p. 1326-1334.

75. Ganguli, R. and I. Chopra, *Aeroelastic Optimization of a Helicopter Rotor with Two-cell Composite Blades.* AIAA Journal, 1996. **34**(4): p. 835-841.

76. Paik, J., V.V. Volovoi, and D.H. Hodges, *Cross-Sectional Sizing and Optimization of Composite Blades*, in *AIAA 2002-1322*. 2002.

77. Chattopadhyay, A., J.L. Walsh, and M.F. Riley, *Integrated Aerodynamic/Dynamic Optimization of Helicopter Rotor Blades*. 1989.

78. Yuan, K.A. and P.P. Friedmann, *Aeroelasticity and Structural Optimization of Composite Helicopter Rotor Blades with Swept Tips*, NASA CR 4665, 1995

79. Yuan, K. and P. Friedmann. *Structural Optimization for Vibration Reduction of Composite Helicopter Rotor Blades with Advanced Geometry Tips Subject to Multidisciplinary Constraints*. in *Proceedings of the AHS International 51th Annual Forum & Technology Display*. 1995. Fort Worth, TX: American Helicopter Society.

80. Ganguli, R. and I. Chopra, *Aeroelastic Optimization of an Advanced Geometry Helicopter Rotor.* Journal of the American Helicopter Society, 1996. **41**(1): p. 18-28.

81. Jones, B.R., W.A. Crossley, and A.S. Lyrintzis, *Aerodynamic and Aeroacoustic Optimization of Rotorcraft Airfoils via a Parallel Genetic Algorithm.* Journal of Aircraft, 2000. **37**(6): p. 1088-1096.

82. Patt, D., L. Liu, and P.P. Friedmann. *Helicopter Noise Reduction By Actively Controlled Flaps*. in *Proceedings of the 11th AIAA/CEAS Aeroacoustics Conference (26th Aeroacoustics Conference)*. 2005.

83. Patt, D., L. Liu, and P.P. Friedmann, *Rotorcraft Vibration Reduction and Noise Prediction Using a Unified Aeroelastic Response Simulation.* Journal of the American Helicopter Society, 2005. **50**(1): p. 95-106.

84. Liu, L., P.P. Friedmann, I. Kim, and D.S. Bernstein, *Rotor Performance Enhancement and Vibration Reduction in Presence of Dynamic Stall Using Actively Controlled Flaps.* Journal of the American Helicopter Society, 2008. **53**(4): p. 338-350.

85. Harrison, R., S. Stacey, and B. Hansford. *BERP IV The Design DEvelopment and Testing of An Advanced Rotor Blade*. in *Proceedings of the AHS International 64th Annual Forum & Technology Display*. 2008. Montréal, Canada: American Helicopter Society.

86. *Research Opportunities in Aeronautics - (ROA 2006)*. 2006, National Aeronautics and Space Administration (NASA).

87. Truong, V.K. *Prediction of Helicopter Rotor Airloads Based on Physical Modeling of 3-D Unsteady Aerodynamics*. in *Proceedings of the 22nd European Rotorcraft Forum*. 1996. Brighton, United Kingdom.

88. *ModelCenter*. 2007, Phoenix Integration, Inc.: Wayne, PA, USA.

89. Collins, K., J. Bain, L. Sankar, T.A. Egolf, R.D. Janakiram, K. Brentner, and L. Lopes. *Pareto Frontier Method for Multi-Disciplinary Optimization of Helicopter Rotors*. in *Proceedings of the AHS Specialist's Conference on Aeromechanics*. 2008. San Francisco, CA: American Helicopter Society.

90. Collins, K., J. Bain, L. Sankar, and N. Rajmohan. *Toward a High-Fidelity Helicopter Rotor Redesign Framework*. in *Proceedings of the AHS International 64th Annual Forum & Technology Display*. 2008. Montréal, Canada: American Helicopter Society.

91. Prouty, R.W., *Helicopter Performance, Stability, and Control*. 1995: Krieger.

92. McVeigh, M.A. and F.J. McHugh. *Recent Advances in Rotor Technology at Boeing Vertol*. in *Proceedings of the 38th Annual Forum of the American Helicopter Society*. 1982. Anaheim, CA: American Helicopter Society.

93. Peterson, R., *Full-scale Hingeless Rotor Performance and Loads*, TM-110356, 1995

94. *JMP*. 2007, SAS Institute: Cary, NC, USA.

95. *MATLAB*. 2007, The Mathworks, Inc.: Natick, MA.

96. Barros, P. and M. Kirby, *Saving Time with Automated Response Surfaces (STARS)*. 2007: Atlanta. p. A matlab computer program that automatically generates response surface models using a data filled spreadsheet.

97. Yu, Y., C. Tung, B. van der Wall, H. Pausder, C. Burley, T. Brooks, P. Beaumier, Y. Delrieux, E. Mercker, and K. Pengel. *The HART-II test. Rotor Wakes and Aeroacoustics with Higher-Harmonic Pitch Control (HHC) inputs - The Joint German/French/Dutch/U. S. Project*. in *Proceedings of the 58th American Helicopter Society Annual Forum*. 2002. Montreal, Canada: American Helicopter Society.

98. van der Wall, B. and C. Burley, *2nd HHC Aeroacoustic Rotor Test (HART II) - Part I: Test Documentation*, DLR-IB 111-2003/31, 2003

99. Cotter, S.C., *A Screening Design for Factorial Experiments with Interactions.* Biometrika, 1979. **66**(2): p. 317-320.

100. Nixon, J., *A Systematic Process for Adaptive Concept Exploration*, PhD Thesis, Georgia Institute of Technology, 2006

101. Bhagwat, M., J. Leishman, and A. Center. *Generalized Viscous Vortex Model for Application to Free-Vortex Wake and Aeroacoustic Calculations*. in *Proceedings of the AHS International 58th Annual Forum & Technology Display*. 2002. Montreal, Canada.

Vita

Kyle Brian Collins

Kyle Collins was born on September 28, 1972 in Warm Springs, Georgia. He grew up with his parents, two brothers, and two sisters. He graduated from Flint River Academy high school in 1990 and was accepted to attend the Georgia Institute of Technology. He completed his undergraduate degree in Mechanical Engineering at Georgia Tech in March of 1995. Afterwards, he spent several years working in the aerodynamic decelerator industry as a parachute equipment designer in DeLand, Florida. It was during this time that he invented the "Parachute Release Apparatus and Method" which has improved the safety of sport parachute equipment. In addition to working in the industry, Kyle also competed on a world class competitive formation skydiving team, medaling in both national and world level competitions. Just prior to 2000, Kyle started Creative Development, a Computer Aided Design company aimed to assist small business owners in harnessing the power of CAD and rapid prototyping to develop their ideas into products. In July of 2001, Kyle married Jennifer Rice and they spent a year in Jacksonville, Florida. In the Fall 2002 term, Kyle was accepted into the graduate program at Georgia Tech in Aerospace Engineering. He completed his Master of Science in December of 2003. In February of 2007, Kyle earned his fixed wing private pilot rating. In December of 2008, Kyle completed his PhD. He and his wife plan to stay in Atlanta. Kyle plans to begin his academic career starting as a research engineer at Georgia Tech immediately upon graduation.